Analysis of platelet function and signalling in two experimental mouse models of abdominal aortic aneurysm formation

Inaugural-Dissertation

zur Erlangung des Doktorgrades
der Mathematisch-Naturwissenschaftlichen Fakultät
der Heinrich-Heine-Universität Düsseldorf

vorgelegt von

Agnes Bosbach geb. Ehrenberg
aus Gladbeck

Düsseldorf, Februar 2025

Aus der Arbeitsgruppe Experimentelle Vaskuläre Medizin
der Klinik für Gefäß- und Endovaskularchirurgie
des Universitätsklinikums der Heinrich-Heine-Universität Düsseldorf

Gedruckt mit der Genehmigung
der Mathematisch-Naturwissenschaftlichen Fakultät
der Heinrich-Heine-Universität Düsseldorf

Berichterstatter:

1. Prof. Dr. Margitta Elvers

2. Jun.- Prof. Dr. Wolfgang Hoyer

Tag der mündlichen Prüfung:

Table of content

List of Tables

List of Figures

List of Abbreviations

A	α-SMA	Alpha smooth muscle cell actin
	AAA	Abdominal aortic aneurysm
	ADP	Adenosine diphosphate
	AKT	Protein kinase B
	Ang II	Angiotensin II
	ANOVA	Analysis of variation of means
	APC	Allophycocyanin
	ApoE	Apolipoprotein E
	ApoER2	Apolipoprotein E receptor 2
	APP	Amyloid precursor protein
	ASA	Acetylsalicylic acid
	ATP	Adenosine triphosphate
B	BAPN	β-aminopropionitrile
C	Ca^{2+}	Calcium
	$CaCl_2$	Calcium chloride
	Casp 3	Caspase 3
	CCL	C-C motif chemokine ligand
	CD	Cluster of differentiation
	cm	centimeter
	CRP	Collagen-related peptide
	CT	Computed tomography
	CXCL	C-X-C motif chemokine ligand
	Cy5	Cyanine5
D	Dab-1	Disabled-1
	DAPI	4',6-Diamidino-2-phenylindol
	dH_2O	Distilled water
	DIC	Differential interference contrast
	DNA	Deoxyribonucleic acid
E	e.g.	Lat. e*xempli gratia*, engl. for example
	ECM	Extracellular matrix
	EGF	Epidermal growth factor
	ePPE	External porcine pancreatic elastase application
	ERK	Extracellular signal-regulated kinase

	EtOH	Ethanol
	EVAR	Endovascular aneurysm repair
F	FACS	Fluorescence-activated cell sorting
	FELASA	Federation of European Laboratory Animal Science Association
	Fig.	Figure
	FITC	Fluorescein-isothiocyanate
	FSC	Forward scatter
G	g	Gram
	GABA	Gamma-aminobutyric acid
	GDP	Guanosine diphosphate
	GMO	Genetically modified organism
	GP	Glycoprotein
	GPCR	G protein-coupled receptor
	GTP	Guanosine triphosphate
H	h	Hour
	H_2O_2	Hydrogen peroxide
	HCl	Hydrochloric acid
	H/E	Haematoxylin-eosin
	HEPES	2-[4-(2-hydroxyethyl)piperazin-1-yl] ethanesulfonic acid
I	ICAM-1	Intercellular adhesion molecule 1
	IgG	Immunglobulin G
	ILT	Intraluminal thrombus
K	kDA	Kilodalton
	Kg	Kilogram
L	L	Litre
	Ly6G	Lymphocyte antigen 6 complex locus G
M	mAb	Monoclonal antibody
	Mac	Macrophage
	mg	Milligram
	Mg^{2+}	Magnesium
	$MgCl_2$	Magnesium chloride
	Min	Minute
	mL	Millilitre
	mmHG	Millimetre of mercury

	MMP	Matrix metalloproteinase
	MPV	Mean platelet volume
	MRI	Magnetic resonance imaging
N	$NaCl_2$	Sodium chloride
	Nm	Nanometre
O	O^{2-}	Free superoxide radicals
	OR	Open repair
P	P^{5+}	Phosphor
	PAR4	Protease activated receptor 4
	PBS	Phosphate buffered saline
	PCT	Plateletcrit
	PDW	Platelet distribution width
	PE	Phycoerythrin
	PF4	Platelet factor 4
	PFA	Paraformaldehyde
	pH	*Potentia hydrogenii*
	PI3	Phosphatidylinositol 3
	PLC	Phospholipase C
	Plt	Platelet
	PPE	Porcine pancreatic elastase
	PS	Phosphatidylserine
R	Rac1	Ras-related C3 botulinum toxin substrate 1
	RELN	Reelin (gene)
	RhoA	Ras homolog family member A
	Rln	Reelin (protein)
	ROS	Reactive oxygen species
	RT	Room temperature
S	s.c.	Subcutaneous
	SFK	Src family kinase
	SSC	Sideward scatter
	SPF	Specific-pathogen free
	SYK	Spleen tyrosine kinase
T	t-PA	Tissue plasminogen activator
	TIMPs	Tissue inhibitors of metalloproteinases
	TXA_2	Thromboxane A_2

U	U46	U46619 (thromboxane A2 analogue)
	U/mL	Units per millilitre
	µg	Microgram
	µL	Microlitre
	µM	Micromolar
	µm	Micrometre
	USG	Ultrasonography
V	VCAM-1	Vascular cell adhesion molecule 1
	VLDLR	Very low-density lipoprotein receptor
	VSMC	Vascular smooth muscle cell
	vWF	von Willebrand factor
W	W	Watt
	WBC	White blood cell
	WT	Wild-type
Z	ZETT	Zentrale Einrichtung für Tierforschung und wissenschaftliche Tierschutzaufgaben

Zusammenfassung

Ein abdominales Aortenaneurysma (AAA) ist eine kardiovaskuläre Erkrankung, welche als progressive Erweiterung der infrarenalen Aorta mit einem Durchmesser von über 150 % definiert ist. Die wichtigsten pathophysiologischen Merkmale der AAA-Erkrankung sind die Inflammation, der Umbau der extrazellulären Matrix (EZM) und die Bildung eines intraluminalen Thrombus (ILT). Zu den wichtigsten Risikofaktoren dieser Erkrankung gehören neben dem Alter als Hauptrisikofaktor ebenfalls Rauchen, das männliche Geschlecht, sowie Bluthochdruck. Im Jahr 2021 war das AAA weltweit die zehnthäufigste Todesursache unter den kardiovaskulären Erkrankungen. Aktuell ist ein chirurgischer Eingriff die einzige Behandlungsmöglichkeit, denn bis heute steht keine medikamentöse Behandlung der AAA-Erkrankung zur Verfügung. Da Thrombozyten bekanntermaßen eine entscheidende Rolle bei der Entstehung und Progression von Herz-Kreislauf-Erkrankungen spielen, stellen diese ein vielversprechendes Ziel für die Entwicklung neuer medikamentöser Therapien zur Behandlung des AAA dar. Deswegen ist es entscheidend, die Thrombozyten-vermittelten Mechanismen, welche zur Entstehung und zum Fortschreiten des AAA beitragen, weiter zu untersuchen.

Aus diesem Grund wurde in dieser Arbeit die Funktion der Thrombozyten während der AAA-Progression anhand zweier verschiedener Mausmodelle zur experimentellen AAA-Induktion analysiert: dem PPE (*engl. porcine pancreatic elastase*) und dem ePPE (*engl. external porcine pancreatic elastase application*) Mausmodell. In beiden AAA-Mausmodellen zeigten die Thrombozyten ein verstärktes Aktivierungsprofil, eine erhöhte pro-koagulante Aktivität, sowie eine gesteigerte Inflammation, die durch die Bildung von Thrombozytenaggregaten mit inflammatorischen Zellen oder die Einwanderung von inflammatorischen Zellen in das aortale Gewebe nachgewiesen wurde. Darüber hinaus wurde ein verstärktes „*Shedding*“ von mindestens einem der beiden wichtigsten Glykoproteinrezeptoren (GP) auf der Thrombozytenoberfläche, GPIb und GPVI, beobachtet. Wie bereits erwähnt, ist ein pathophysiologisches Merkmal der AAA-Entwicklung die Bildung eines thrombozytenreichen ILT, welcher bei 75% aller AAA-Patienten vorhanden ist. Dennoch ist die genaue Rolle des ILT, der sowohl stabilisierende als auch ECM-abbauende Eigenschaften aufweist, im Zusammenhang mit der AAA-Entwicklung bis heute unklar. Daher wurde in dieser Arbeit das neue experimentelle ePPE-Mausmodell etabliert und charakterisiert, um den Prozess der ILT-Bildung *in vivo* analysieren zu können. Dabei konnte über einen Zeitraum von 28 Tagen nach Operation jedoch keine ILT-Bildung beobachtet werden.

Erst kürzlich konnte gezeigt werden, dass Thrombozyten während der AAA-Bildung eine Rolle bei der Inflammation und dem EZM-Umbau spielen. Dadurch stellt die gezielte Inhibierung von Thrombozytenrezeptoren und Signalwegen einen vielversprechenden Ansatz für die Entwicklung neuer medikamentöser AAA-Therapien dar. Das Glykoprotein Reelin, welches eine zentrale Rolle in der Gehirnentwicklung einnimmt, ist nachweislich ebenfalls an der Entstehung verschiedener Herz-Kreislauf-Erkrankungen beteiligt. Da Thrombozyten Reelin sowohl enthalten als auch über ihre Rezeptoren auf der Zelloberfläche binden können, was zur Folge intrazelluläre Signalwege auslöst, sollte die Rolle des von Thrombozyten stammenden Reelins im Rahmen dieser Arbeit in der AAA-Pathologie näher untersucht werden. Dabei konnten bei Reelin Knockout (Rln KO) Mäusen mit einer Thrombozyten-spezifischen genetischen Reelin-Defizienz im PPE-Mausmodell keine Auswirkungen auf die Entwicklung des Aortendurchmessers über einen Zeitraum von 28 Tagen beobachtet werden. Weiterhin konnte in den Thrombozyten von Rln KO Mäusen Reelin nachgewiesen werden, was auf eine Aufnahme des Reelins durch Thrombozyten aus der Zirkulation hindeutet. Dies ermöglicht keine genaue Analyse des von Thrombozyten stammenden Reelins in Rln KO Mäusen. Um die Auswirkung von globalem Reelin auf die Bildung der AAA-Erkrankung zu analysieren, könnten künftige Experimente in einem ersten translationalen Ansatz mit dem CR-50 Antikörper zur Hemmung der Reelin-Funktionalität durchgeführt werden.

Zusammenfassend unterstreichen die Ergebnisse dieser Arbeit, dass Thrombozyten eine entscheidende Rolle bei der Entstehung von AAA spielen. Dies konnte durch erhöhte Thrombozytenaktivierungsprofile, pro-koagulante Aktivität und Inflammation während der AAA-Progression gekennzeichnet werden. Um weiterhin zu analysieren, ob Reelin ein potenzielles Ziel für medikamentöse Therapien für AAA-Patienten sein könnte, könnten erste translationale Experimente mit dem CR-50 Antikörper in einem AAA Mausmodell durchgeführt werden. Zum Schluss zeigte das ePPE-Mausmodell keine ILT-Bildung über einen Zeitraum von 28 Tagen nach Eingriff, sodass die Verlängerung des Beobachtungszeitraums in Zukunft von Interesse sein könnte.

Abstract

An abdominal aortic aneurysm (AAA) is a cardiovascular disease (CVD) defined as the dilatation of the infrarenal part of the aorta with a diameter of more than 150%. Main pathophysiological features of the AAA pathology are the remodelling of the extracellular matrix (ECM), inflammation and intraluminal thrombus (ILT) formation. The major risk factors for this disease include age, smoking, male gender and hypertension. In 2021, AAA was the 10th leading cause of death in terms of CVDs worldwide. Since there is no drug-based therapy targeting AAA development to date, the only treatment option is a surgical intervention. As platelets are known to play a crucial role in CVDs, they represent a promising target for the development of new drug-based therapies for AAA treatment. For this reason, it is important to further investigate the underlying mechanisms of platelets contributing to the development and progression of AAA.

Therefore, platelet function in AAA progression was analysed in this thesis utilising two different mouse models for experimental AAA induction: the porcine pancreatic elastase (PPE) and external porcine pancreatic elastase application (ePPE) mouse model. Thereby, platelets showed an enhanced activation profile, pro-coagulant activity and inflammation, represented by the formation of platelet-aggregates with inflammatory cells or infiltration of inflammatory cells into the aortic tissue, in both AAA mouse models. In addition, enhanced shedding of at least one of the two major glycoprotein (GP) receptors on platelet surface, GPIb and GPVI, was observed. As previously mentioned, one pathophysiological hallmark of AAA development is the formation of a platelet-rich ILT, which is present in 75% of all AAA patients. Nevertheless, the role of the ILT in the context of AAA development, exhibiting both stabilising and ECM-degrading characteristics, remains unclear to date. Therefore, the novel experimental ePPE AAA mouse model was established and characterised to analyse the process of ILT formation in this thesis. However, no ILT formation could be observed over a time course of 28 days after surgery.

Recently, platelets were shown to play a role in the ECM remodelling and inflammation processes in AAA formation. Therefore, specifically targeting platelet receptors and signalling pathways represent a promising approach to develop novel drug-based AAA therapies. The glycoprotein reelin, which was identified to be crucial in brain development and maintenance, was shown to be involved in the progression of different CVDs as well. Since reelin is present in platelets, but also binds to platelet receptors on cell surface

and subsequently triggers intracellular signalling pathways, the role of platelet-derived reelin in AAA pathology should be investigated in detail within this thesis. Thereby, no effects on the aortic diameter progression could be observed in Reelin knockout (Rln KO) mice with a genetic reelin-deficiency in the PPE mouse model 28 days after surgery. Furthermore, reelin was still found in platelets of Rln KO mice. This indicates their ability to internalise the protein from the circulation. Thus, the specific analysis of platelet-derived reelin remains challenging. To analyse the effect of global reelin on AAA formation, future experiments could be performed in a first translational approach using the CR-50 antibody to inhibit reelin functionality.

In summary, the results of this thesis emphasise that platelets play a crucial role in the development of AAA, represented by enhanced platelet activation profiles, pro-coagulant activity and inflammation. To further analyse, whether reelin could be a potential target for drug-based therapies for AAA patients, first translational experiments using the CR-50 antibody in a mouse model of AAA formation could be performed. Finally, the ePPE mouse model showed no ILT formation over a time course of 28 days after surgery. Therefore, the extension of the analysis period would be of interest in future.

1 Introduction

1.1 Platelets

1.1.1 Physiology and function

Platelets are small discoid, anucleate cells circulating in the bloodstream and playing an important role in haemostasis, clot formation and thrombosis. In addition, they are involved in other physiological and pathological processes such as immune reactions, inflammation and wound healing [1, 2]. Originally, platelets were found by Giulio Bizzozero in 1882 by demonstrating their promoting role in thrombosis [3]. In human, produced by megakaryocytes with a size of 1 – 3 µm and a discoid shape, two thirds of platelets are circulating in the blood while the other one third is stored in spleen [1, 4]. Mouse platelets are much smaller, with a diameter of 0.5 µm [5]. When platelets remain inactivated, degradation proceeds after 5 – 9 days by phagocytosis in the liver or spleen. An average human has a platelet count of 150 – 400 x 10^3 platelets/µl blood [4]. In contrast, mice contain many more platelets with 1000 – 1500 x 10^3 platelets/µl blood. Therefore, these murine platelets have a shorter lifespan, which ranges between 3 to 4 days [5]. In case of activation, platelets change their shape in an actin-dependent process. This process includes the reorganisation of the platelet cytoskeleton as well as the organisation of new actin filaments. Following shape change, platelets can adhere to injured vessels, aggregate with other platelets and release their granule content [1]. In order to characterise platelets, various physiological parameters such as the platelet count, mean platelet volume (MPV), platelet distribution width (PDW) and the plateletcrit (PCT) are used. The MPV and PDW define the platelet size and its size variability, while the PCT indicates the volume covered by the platelets within the blood [6, 7].

1.1.2 Platelet receptors and granules

In order to become activated, platelets contain many different receptors on their surface. These receptors enable the binding of agonists and thereby trigger various signalling pathways within platelets. One of the main receptors involved in platelet activation is the glycoprotein (GP) Ib receptor. It is non-covalently linked with GPIX and GPV in a complex. This GPIb-IX-V complex serves as receptor for von Willebrand factor (vWF) proteins, being crucial for haemostasis [8]. The most abundant receptor is the GPIIb/IIIa, which is also termed integrin $\alpha_{IIb}\beta_3$ and mainly known as fibrinogen receptor [9, 10]. Human platelets express this receptor with around 80,000 copies on their surface, while mouse platelets even contain around 120,000 copies per platelet [11]. On resting circulating platelets this receptor has a low affinity for binding respective ligands. After

platelet activation, including conformational changes, this complex increases its ligand affinity [10]. The ligands for the integrin $\alpha_{IIb}\beta_3$ receptor are different adhesive proteins such as fibrinogen, vWF, fibronectin and vitronectin. Therefore, integrin $\alpha_{IIb}\beta_3$ plays a pivotal role in adhesion to site of vascular injury, platelet aggregation and outside-in signalling to amplify platelet activity [1, 12]. Other important receptors are the two major collagen receptors GPVI and $\alpha_2\beta_1$, which are crucial for platelets to adhere firmly to the injured vessel wall [13]. The two P2Y receptors, $P2Y_1$ and $P2Y_{12}$, are G protein-coupled receptors (GPCRs), which belong to the seven-transmembrane domain receptor family and are required for platelet aggregation after binding of adenosine diphosphate (ADP) [14, 15]. Further GPCRs with seven-transmembrane domains on the platelet surface are the thromboxane (TX)A_2- and the thrombin-binding PAR4-receptor, playing an important role in platelet activation and aggregation (**Figure 1**) [15-17].

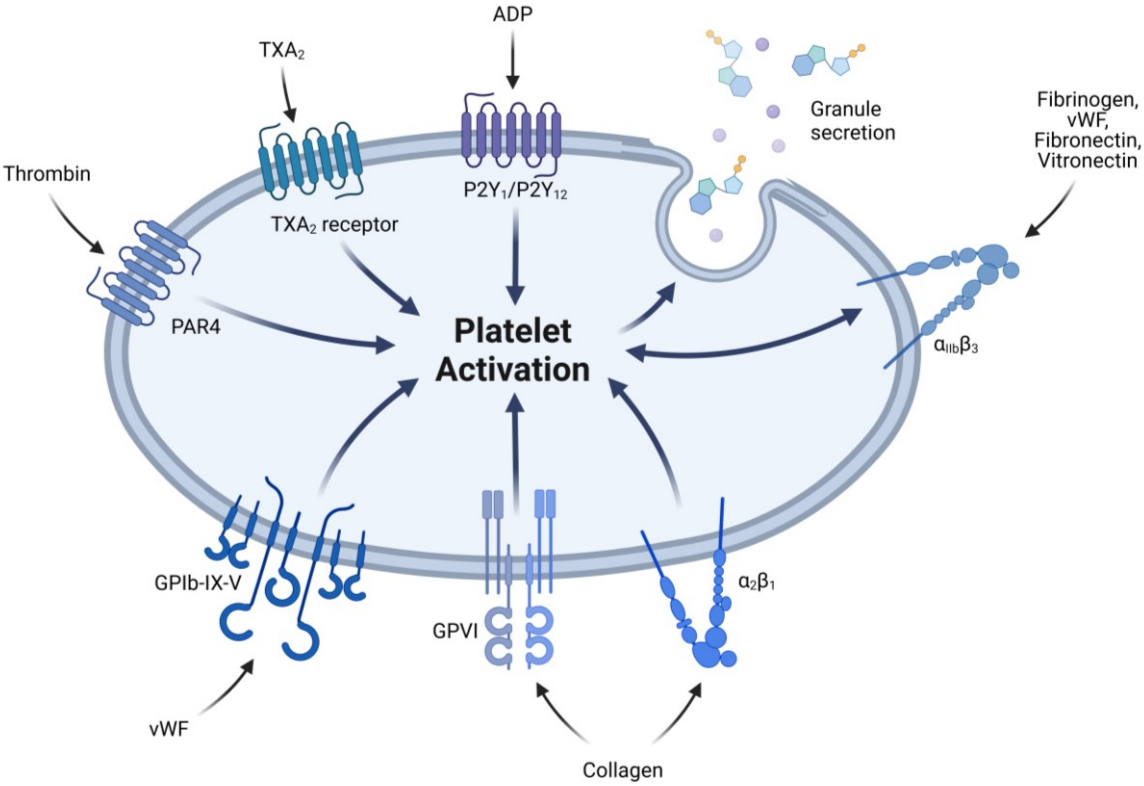

Figure 1. Main receptors on platelet surface along with their most important ligands. Platelets have various receptors on their surface. By binding of specific ligands to their respective receptors, platelets become activated. Collagen binds to the GPVI and integrin $\alpha_2\beta_1$ receptors, vWF to the GPIb-IX-V receptor complex and thrombin to the PAR4 receptor. In addition, the TXA_2 receptor is activated by TXA_2 and the $P2Y_1$ as well as $P2Y_{12}$ receptor by ADP. Ligands for the $\alpha_{IIb}\beta_3$ receptor are fibrinogen, vWF, fibronectin and vitronectin. The activation leads to changes in shape, the stimulation of various intracellular signalling pathways and degranulation. Created with BioRender.com.

Upon activation, platelets release the content of their granules. Thereby, platelets contain three different kinds of granules: α-granules, δ-granules, and lysosomes. In these granules haemostatic mediators and surface molecules are stored that are released into the bloodstream or transported to and translocated on the platelet surface after activation (**Table 1**). The most abundant granules are the α-granules with around 50 to 80 per platelet. These exhibit a diameter of 200 – 500 nm and contain different molecules, including adhesion molecules, chemokines, growth factors, fibrinolysis and coagulation proteins [1, 18]. The δ-granules occur in a significantly lower quantity with 5 to 8 per platelet, revealing a high content of ADP and serotonin as well as magnesium, calcium, and nucleotides [19, 20]. The few lysosomes contain e.g. cathepsins and acid hydrolases [21]. However, granule secretion not only induces the translocation of adhesion receptors to the cell surface and the release of agonists and mediators into the bloodstream. Moreover, granule secretion also activates intracellular signalling pathways and causes conformational changes in surface receptors, leading to new binding affinities [1].

Table 1. Content of platelet granules.

Platelets contain three types of granules with different contents. PF4 = platelet factor 4; CCL = C-C motif chemokine ligand; CXCL = C-X-C motif chemokine ligand; Ca^{2+} = calcium; Mg^{2+} = magnesium; P^{5+} = phosphor; ATP = adenosine triphosphate; GTP = guanosine triphosphate; ADP = adenosine diphosphate; GDP = guanosine diphosphate; vWF = von Willebrand factor (Table adapted from Reed *et al*. [21]).

Granules	Content
α-granules	Adhesion molecules (P-selectin, vWF, fibrinogen, fibronectin, $\alpha_{IIb}\beta_3$, etc.), chemokines (PF4, CCL3, CCL5, CXCL5, CXCL8, etc.), coagulation proteins, fibrinolysis proteins, growth factors, immunologic molecules and other proteins
δ-granules	Ions (Ca^{2+}, Mg^{2+}, P^{5+}, pyrophosphate), nucleotides (ATP, GTP, ADP, GDP), membrane proteins, serotonin
Lysosomes	Acid hydrolases, cathepsins

1.1.3 Inside-out and outside-in signalling

Several integrin receptors are expressed on platelet surface including the $\alpha_{IIb}\beta_3$ (fibrinogen receptor), $\alpha_v\beta_3$ (vitronectin receptor), $\alpha_2\beta_1$ (collagen receptor), $\alpha_5\beta_1$ (fibronectin receptor), and $\alpha_6\beta_1$ (laminin receptor) [22, 23]. After vascular injury, integrins

are able to mediate platelet activation, adhesion, following aggregation and thrombus formation by a bi-directional signal transduction. The ‘inside-out signalling’ describes the integrin activation by ligand-binding to different receptors on platelet surface [9]. As previously mentioned, the $\alpha_{IIb}\beta_3$ receptor is the most abundant integrin on platelets with about 80,000/120,000 copies per cell and is crucial for stable platelet adhesion and aggregation [9, 10]. Under resting conditions, the receptor is in an inactive conformation. Upon platelet activation via other receptors such as the GPVI receptor the integrin $\alpha_{IIb}\beta_3$ undergoes a conformational change and is externalised in a higher number from α-granules to the platelet surface [10, 18, 21]. This process is called ‘inside-out signalling’. The conformational change switches the affinity for fibrinogen and collagen-bound vWF from a low to a high state. Following ligand binding to the activated integrin $\alpha_{IIb}\beta_3$ then promotes ‘outside-in signalling’. Outside-in signalling induces and increases cellular processes to regulate major platelet functions including platelet spreading, thrombus stabilisation mediated by fibrin and the control of platelet aggregation via fibrinogen binding [24].

1.1.4 Physiology of primary and secondary haemostasis

Haemostasis describes the process of thrombus formation at site of vascular injury to stop bleeding. This process is divided into primary and secondary haemostasis. Within primary haemostasis, blood platelets are recruited from circulation to form a haemostatic plug in order to occlude the injured vessel (**Figure 2**). Under physiological conditions, platelets are circulating in a resting state within the bloodstream without interacting with the vessel wall. In case of a vascular injury, components of the subendothelial extracellular matrix (ECM) such as collagen, laminin and vitronectin are exposed. The uncovered collagen of the ECM binds soluble vWF from circulation. Subsequently, the membrane-bound GPIb-IX-V complex on platelets binds to the collagen-bound vWF, resulting in the deceleration of platelets from the bloodstream. This leads to an unstable temporary adhesion of platelets to the vessel wall and is known as “tethering”. The tethering facilitates binding of the platelet GPVI receptor to exposed collagen, leading to the activation of various intracellular signalling pathways. Subsequently, this induction of various intracellular signalling pathways contributes to platelet activation, including the release of α- and δ-granules and the regulation of surface receptor activation. Through the following degranulation second wave mediators as ADP and TXA_2 are released [25]. All these processes support the recruitment and adhesion of additional platelets from the bloodstream into the growing thrombus. For the interaction and aggregation of platelets, fibrinogen binding to activated integrin $\alpha_{IIb}\beta_3$ is crucial. Since this binding is only a weak connection between platelets, the initial thrombus is unstable. Therefore, the secondary

haemostasis is necessary for stabilising the newly formed thrombus by the incorporation and cross-linkage of fibrin [25-27].

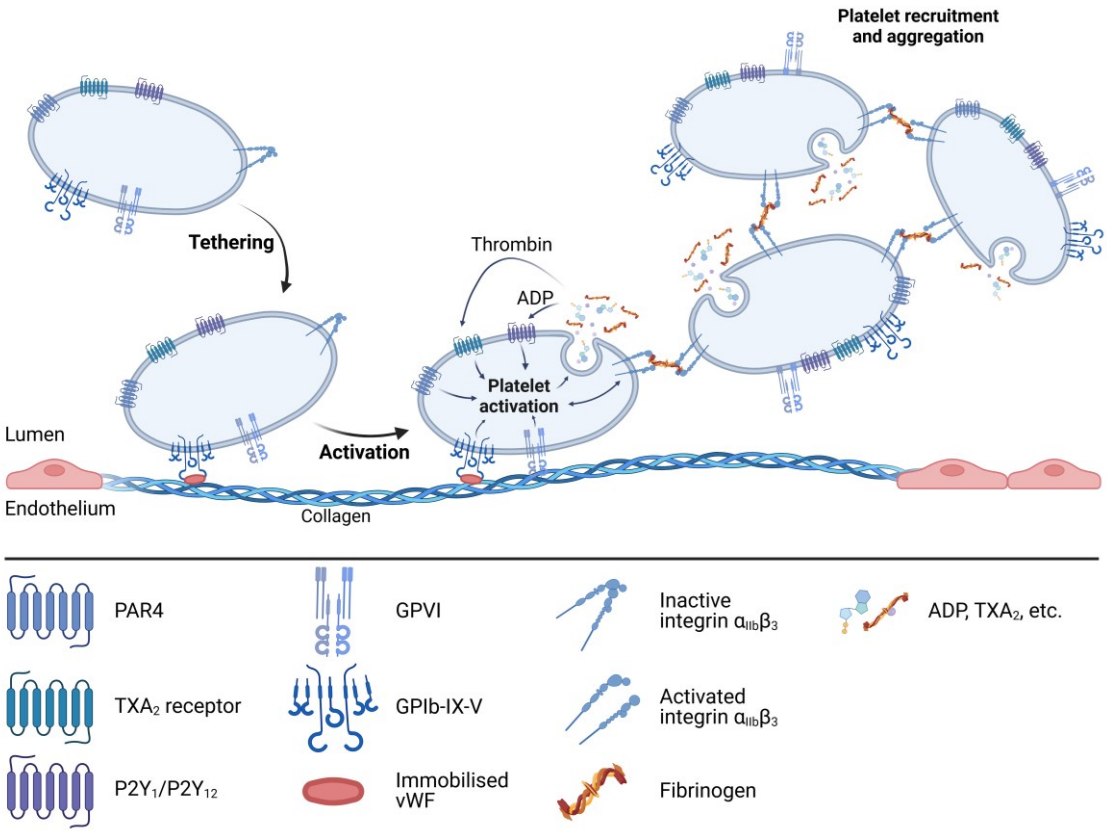

Figure 2. Primary haemostasis. The injury of the vessel wall exposes the subendothelial extracellular matrix. As a result, uncovered collagen binds soluble vWF from circulation. The immobilised vWF can be recognised and bound by the GPIb-IX-V complex on platelet surface. This process is known as “tethering”. After platelet deceleration, the GPVI receptor binds to exposed collagen, which triggers various signalling pathways including platelet activation, degranulation, and receptor conformation. The release from second wave mediators from granules, such as ADP and TXA_2, trigger the recruitment, activation and aggregation of further platelets, which leads to the formation of a thrombus. ADP = adenosine diphosphate; GP = glycoprotein; TXA_2 = thromboxane A_2; vWF = von Willebrand factor. Created with BioRender.com.

In the secondary haemostasis the coagulation cascade is activated, resulting in the cleavage of pro-thrombin to thrombin by factor Xa. Subsequently, thrombin mediates fibrinogen cleavage to fibrin. The cross-linking of fibrin finally leads to the stabilisation of the haemostatic plug build in the primary haemostasis under recruitment of further platelets [27]. Platelets itself also contribute to thrombin generation supporting secondary haemostasis by the externalisation of phosphatidylserine (PS) on the platelet surface upon platelet activation. Through the formation of pro-thrombinase complexes for thrombin formation, this platelet activation also stabilises the thrombus via fibrin formation [28, 29].

1.1.5 Platelets in cardiovascular diseases

As already mentioned, platelets play a pivotal role not only in physiological processes but also under pathological conditions in cardiovascular diseases (CVDs), such as atherosclerosis, arterial thrombus and aneurysm formation (see chapter **1.3.5**). These pathologic events can be caused by altered platelet compositions and reactivity resulting from increased pro-aggregatory or decreased anti-aggregatory stimuli. Furthermore, platelet surface receptors and molecules stored in the platelet granules can facilitate the crosstalk of activated platelets with inflammatory cells during vascular inflammation. Thus, platelets can contribute to development and progression of atherosclerosis [30, 31]. Since platelets are a driving force in the development of CVDs, they are primary targets for prevention of these diseases. For this reason, platelet activation can be inhibited with anti-platelet agents such as aspirin or $P2Y_{12}$ inhibitors (e.g. clopidogrel) [32].

1.2 Reelin

1.2.1 Function

The extracellular matrix protein reelin was first found to be synthesised and secreted by Cajal-Retzius neurons, which are formed in early brain development within the marginal zone [33, 34]. Reelin is essential for the migration and positioning of neurons during the development of the neocortex and cerebellar cortex of the brain [35]. The way reelin achieves its function is described in various hypotheses. These are: reelin attracts neurons, it can be a rejecting molecule, or it disturbs the connection between migrating neurons and radial glia [36]. Although 95% of the Cajal-Retzius neurons degenerate within weeks after birth, reelin can also be found in adult humans' brain tissue [37, 38]. In these reelin is produced by some cortical gamma-aminobutyric acid (GABA)-ergic and hippocampal interneurons, as well as by cerebellar granule cells. Since the prenatally brain development is finished, reelin provides other functions in adult humans. Postnatally, it is involved in synaptogenesis, neurotransmission, or the regulation of synaptic plasticity, which is important for learning and memory functions. As a result, disrupted reelin signalling is associated with human neurological disorders such as autism, Alzheimer's disease, and schizophrenia [38]. In addition, it was shown that reelin is also present in several adult pituitary pars intermedia, blood, liver, and adrenal chromaffin cells [39]. Non-neurological functions of reelin implicate its role in coagulation dysfunctions, cancer progression, and endothelial disorders in chronic inflammatory diseases [40]. In 1951, Falconer first described a mouse with a spontaneous autosomal recessive mutation in the reelin gene, the reeler mouse [41]. However, this mutated gene

in the reeler mouse was first mapped and named in 1995 [35]. A comparison of amino acids (94.2%) and nucleotide sequences (87.2%) between mice and humans revealed a high homology [42]. Effects of the genetic variants in mice were neuroanatomical impairments as reduced size of the cerebellum, lack of folding pattern and disturbed organisation of distinct brain layers [43]. Due to the typical reeling gait the mice got their name. This reeling gait goes along with tremor, ataxia and hypotonia [41].

1.2.2 Structure of the reelin protein

Reelin is a large glycoprotein with a molecular weight of 388 kDa and 3461 amino acids, which gene is highly conserved in many vertebrates, including humans [35, 42]. The glycosylated status of the protein has around 450 kDa [44]. In the early nineties the RELN gene location (7q22) could be identified by DeSilva *et al*. and was described in 1997 [42]. Meanwhile, D'Arcangelo *et al*. published in 1995 the partly identified protein structure of reelin [35]. Structurally, the reelin protein is composed of a signal peptide with a following F-spondin homology domain and a unique region. The main part consists of eight repeated reelin-specific sequences (R1 to R8 with 350 – 390 amino acids each) containing two sub-repeats (A and B) that are flanking an epidermal growth factor (EGF)-like motif (30 amino acids) [35]. Near to the N-terminus a hinge region containing a CR-50 epitope can be found, being crucial for signalling processes by inhibiting reelin oligomerisation [45]. At the positively charged C-terminal end (33 amino acids) a highly conserved sequence is located that is identical among mammalian species [38, 46]. After secretion of the reelin protein it can be cleaved by metalloproteases at two different cleaving sites [47, 48]. These are the N-terminal cleavage between repeats 2 and 3 and the C-terminal cleavage between repeats 6 and 7. According to this, five different fragments (named N-R2, R3-6, R7-8, N-R6 and R3-8) can be produced with changed properties for receptor-binding and signalling (**Figure 3**) [47]. Since the smallest biologically active fragment from repeat 3 to 6 is crucial for reelin-receptor-binding and cellular signalling *in vivo*, cleavage is not impairing protein activity [49].

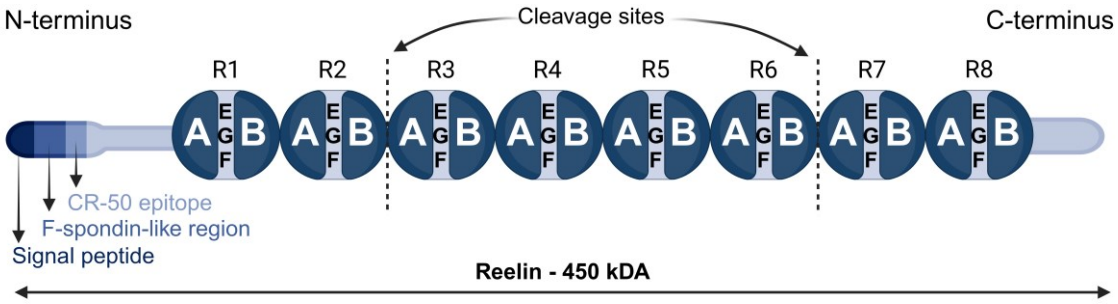

Figure 3. Schematic illustration of the reelin protein structure. The glycosylated form of the extracellular matrix protein reelin has a molecular weight of around 450 kDA. It consists of eight repeats composed of two sub-repeats (A and B) with an EGF-like motif between them. At the N-terminal end are a signal peptide, an F-spondin-like region, and a CR-50 epitope. Between the R2/R3 and R6/R7 repeats, the protein can be cleaved, resulting in five possible reelin fragments. EGF = epidermal growth factor; kDA = kilodalton. Created with BioRender.com.

1.2.3 Signalling pathway of reelin in neuronal cells

By binding of reelin to various receptors, different signalling pathways are triggered. Binding of oligomerised reelin to the apolipoprotein E receptor 2 (ApoER2), very low-density lipoprotein receptor (VLDLR) and amyloid precursor protein (APP) triggers a shared intracellular signalling cascade [50, 51]. Thereby, the oligomerisation of the reelin protein leads to clustering of the receptors, which is crucial for following signal transduction [46]. The intracellular signalling cascade starts with the phosphorylation of intracellular adaptor-protein Disabled-1 (Dab-1) [50]. Phosphorylated Dab-1 in turn activates src family tyrosine kinase (SFK) [52] and phosphatidylinositol 3 (PI3) kinases to manage positioning of neurons during brain development, synaptic plasticity, and memory formation (**Figure 4**) [53-55]. To maintain a balance, reelin simultaneously promotes Dab-1 degradation by ubiquitin-proteasomes and its own degradation as well [54, 55]. Thereby, reelin is internalised and degraded by the lysosomes of the target cells [46, 56]. Other reelin receptors are the integrin $\alpha_3\beta_1$ receptor and cadherin-related neuronal receptors to activate possible signal transduction pathways [57, 58].

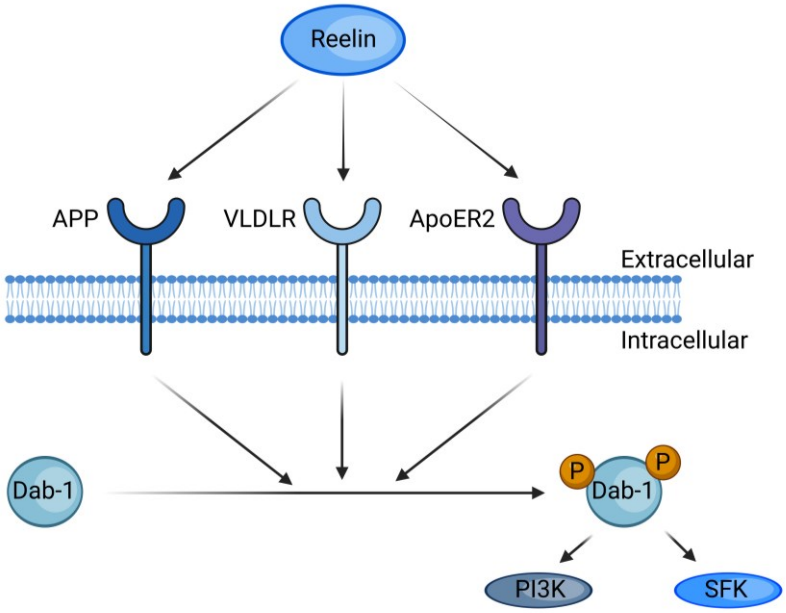

Figure 4. Reelin receptors on neuronal cell surface. Binding of reelin to APP, VLDLR and ApoER2 on neuronal cells triggers phosphorylation of adaptor protein DAB-1. This activates the following SFKs and PI3 kinases, which contribute as a result to intact brain development. ApoER2 = apolipoprotein E receptor 2; APP = amyloid precursor protein; Dab-1 = disabled-1; PI3 = phosphatidylinositol 3; SFK = src family kinase; VLDLR = very low-density lipoprotein receptor. Created with BioRender.com.

1.2.4 Reelin and platelets

Reelin was also found to be present in megakaryocytes, which are the precursor cells of platelets, and in mature platelets, where it is stored in the α-granules [59]. Upon platelet activation, reelin can be released into the bloodstream, which in turn enables reelin binding to the GPIbα, ApoER2 and APP receptors on the platelet surface [53, 60]. It was recently shown that reelin also interacts with the GPVI receptor (**Figure 5**). Binding of reelin to the different receptors on the platelet surface induces various signalling pathways, including spleen tyrosine kinase (SYK), phospholipase C (PLC)γ2 and Rho GTPases (ras-related C3 botulinum toxin substrate 1 (Rac1) & ras homolog family member A (RhoA)). Activation of these signalling pathways leads to platelet adhesion to fibrinogen and collagen, as well as initiation of the integrin $\alpha_{IIb}\beta_3$-mediated outside-in signalling pathway. In addition, a signal amplification loop was found that is induced after reelin binding to the GPVI receptor. Upon GPVI-dependent platelet activation, reelin is released into the circulation and subsequently increases platelet activation, adhesion and degranulation via GPVI binding [53].

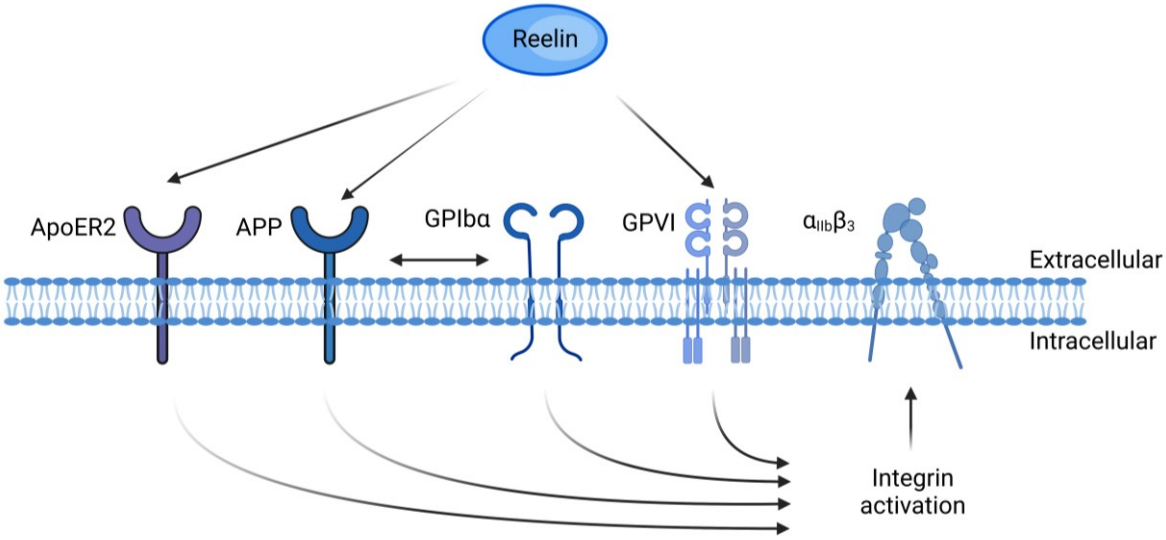

Figure 5. Reelin receptors on platelet cell surface. Reelin is able to bind to various receptors on platelet surface including the APP, ApoER2, GPIbα and GPVI receptor. This is followed by the stimulation of signalling cascades that contribute to the activation of integrin $\alpha_{IIb}\beta_3$, which leads to increased platelet function. ApoER2 = apolipoprotein E receptor 2; APP = amyloid precursor protein; GP = glycoprotein. Created with BioRender.com.

1.2.5 Reelin in neuronal and cardiovascular diseases

As already mentioned, reelin is crucial for brain development and therefore associated with human neurodevelopmental and neuropsychiatric disorders like autism, schizophrenia, and bipolar disorder [38]. It was shown to be 50% downregulated in brain under pathological conditions. But also changes in the reelin gene structure (regarding DNA methylation, single nucleotide polymorphism) or in signalling pathways are associated with these human neurological disorders. Altered reelin expression or lack of reelin receptors can influence following reelin signalling pathways resulting in impaired brain development. Changes in the organisation of brain layers through improper neuronal migration, synaptic formation, plasticity and connectivity can lead to motor and cognitive deficits that finally results in neurological disorders [46]. However, reelin is also present in the circulation, liver and other tissues and thus promoting CVDs [39, 61]. In the cardiovascular system, reelin can enhance the adhesion of leukocytes to endothelial cells through an increase in the most important adhesion molecules ICAM-1 (intercellular adhesion molecule 1), VCAM-1 (vascular cell adhesion molecule 1) and E-Selectin, thereby supporting vascular inflammation and contributing to atherosclerosis [61]. In addition, reelin also promotes arterial thrombosis through platelet adhesion, activation and thrombus formation via binding to APP, GPIb and GPVI. Reelin binding to these receptors triggers intracellular signalling pathways, including activation of protein kinase B (AKT), extracellular signal-regulated kinase (ERK), SYK and PLCγ2 [53, 60]. Through

the upregulation of thrombin formation and the formation of fibrin clots, reelin is also able to promote coagulation [62].

1.3 Abdominal aortic aneurysm

An abdominal aortic aneurysm (AAA) is a CVD characterised by a pathophysiological and progressive dilatation of the infrarenal part of the aorta with a size of more than 150% or a maximum diameter of 3 cm [63]. Risk factors for AAA development including e.g. age, smoking, family history, hypertension and male gender [64]. It was shown that the prevalence of AAA in men is 6 fold higher than in woman [65]. Furthermore, in over 75% of AAA patients an intraluminal thrombus is present [66]. Since the AAA is usually asymptomatic until rupture, it is often diagnosed incidentally by ultrasound (USG), abdominal computed tomography (CT) or magnetic resonance imaging (MRI) performed for other purposes [63, 67]. Actually, there are two possible intervention options in case of diagnosis: the open surgical repair (OR) and the endovascular aneurysm repair (EVAR). The choice of treatment option depends on several factors such as the morphology of the aneurysm and the condition of the patient. If the aneurysm remains undetected, the risk of rupture increases with size, growth rate and persistent hypertension [68]. In case of rupture, less than 50% of patients reach the hospital alive. Even 30 – 70% of them do not survive the surgical intervention, resulting in a very high mortality rate for AAA [69, 70]. In 2021, AAA was in fact the 10th most common cause of death in terms of CVDs worldwide [71]. Depending on their shape, aneurysms can be divided into saccular and fusiform aneurysms. The fusiform aneurysm has a circumferential bulge around the aorta, whereas in saccular aneurysms only one side of the aorta is affected by the dilatation [72]. In addition, aneurysms can also be clinically differentiated according to their location in relation to the renal arteries. Infrarenal aneurysms are located under the renal arteries, while pararenal aneurysms include the renal arteries. Whereas juxtarenal aneurysms only affect the aorta below the renal arteries, suprarenal aneurysms can even extend to the celiac trunk (**Figure 6**) [73].

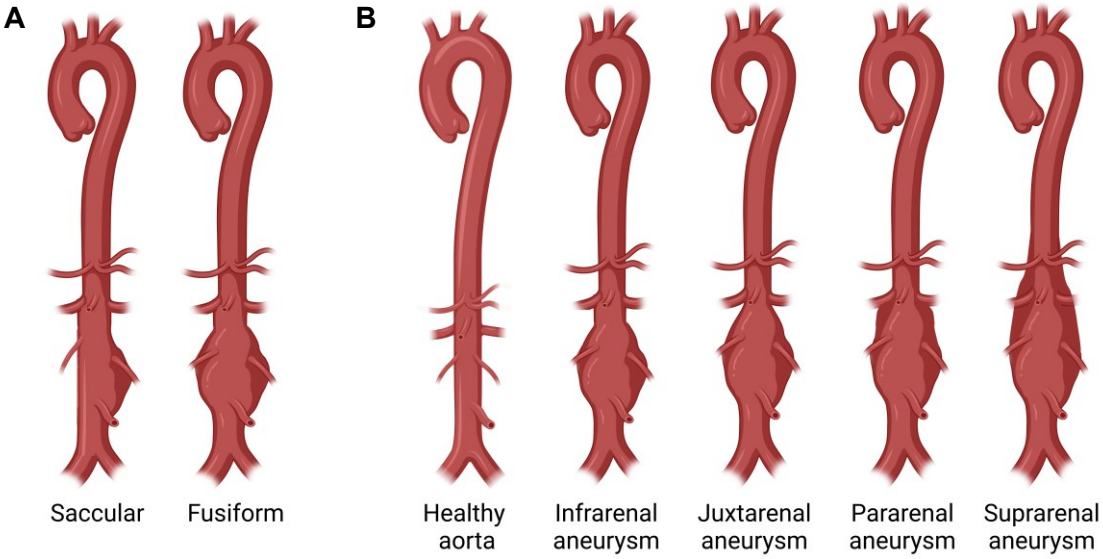

Figure 6. Variations and locations of abdominal aortic aneurysm. (**A**) Depending on their shape, aneurysms can be divided into saccular and fusiform aneurysms. (**B**) Depending on their particular location, aneurysms are classified as infrarenal, juxtarenal, pararenal and suprarenal. Created with BioRender.com.

1.3.1 Structure of the aorta

The aorta is the largest artery in the body, transporting oxygen-rich blood from the left ventricle of the heart to all organs in the body [74]. Only recently, the aorta was officially defined as an independent organ [75]. Physiologically, the vascular wall of the aorta is divided into three distinct layers. The inner layer is the tunica intima, followed by the tunica media and the abluminal tunica adventitia. Between these layers, thin elastic lamellae (internal and external) are separating the layers from each other. The tunica intima consists of a single layer of endothelial cells that functions as barrier to the bloodstream [76]. The tunica media consists of elastic fibres and circumferentially oriented vascular smooth muscle cells (VSMC), which are the predominant cells within this layer. Thereby, VSMCs are the main cell type producing elastin, but also other ECM proteins such as collagen, glycoproteins and proteoglycans [77-79]. The outer layer, the tunica adventitia, supports vessel structure and consists of small blood vessels (vasa vasorum), nerves, fibroblasts and different extracellular matrix proteins including collagen and elastin [76]. The ECM is crucial for the structural and functional integrity of the aortic wall [77]. While elastic fibres are important for the recoil properties and flexibility of the aortic wall, its resistance to tensile loads to manage high blood pressure is provided by collagen fibres [78]. Thereby, VSMCs are able to react on haemodynamic changes by remodelling of the vessel wall [78]. Physiological remodelling of aortic wall is characterised by a balanced degradation of ECM proteins by proteases such as matrix

metalloproteinases (MMPs) and the synthesis of new ECM proteins. In this context, the proteolytic activity of MMPs is highly regulated by tissue inhibitors of proteases (TIMPs) (**Figure 7**) [77].

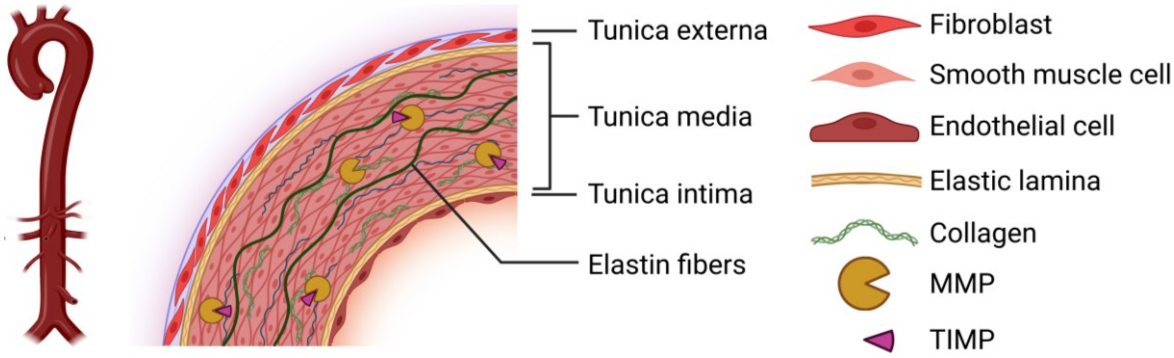

Figure 7. Vessel wall structure of a healthy aorta. The aorta is composed of three layers containing the tunica intima, tunica media and tunica adventitia. The luminal tunica intima consists of a single layer of endothelial cells. The predominant cell type of the tunica media are the VSMCs producing elastin and other ECM proteins. Thus, VSMCs are able to react on haemodynamic changes with ECM remodelling. In healthy tissue, physiological remodelling is highly regulated by MMPs and their respective TIMPs. The abluminal tunica adventitia contains mainly fibroblasts and ECM molecules. ECM = extracellular matrix; MMP = matrix metalloproteinase; TIMP = tissue inhibitor of metalloproteinases; VSMC = vascular smooth muscle cell. Created with BioRender.com.

1.3.2 Pathophysiological changes of the aorta in AAA disease

In AAA patients, the physiological processes in the aortic wall are disturbed. Pathophysiologic characteristics of AAA leading to the destruction of the vascular integrity including the apoptosis of VSMCs, oxidative stress and development of an intraluminal thrombus (ILT) [80-82]. The major events of the AAA pathology are the degeneration of the ECM leading to vascular wall remodelling, accompanied by chronic inflammation. During the remodelling process, apoptosis of VSMCs and degradation of ECM proteins such as elastin and collagen by proteases result into a thinning and weakening of the aortic wall. This degradation is a result of an imbalance between MMPs and their TIMPs activity (**Figure 8**). Thereby, it was already shown that MMP-1, -3, and -9 are highly upregulated in large sized aneurysms, whereas MMP-2, primarily produced by VSMCs, is the main MMP in patients with small sized aneurysms [83-86]. Furthermore, a type III collagen turnover was detected in aortic tissue of AAA patients contributing to vascular wall remodelling [87]. During inflammation, platelets, neutrophils, macrophages, lymphocytes and plasma cells invade the aortic tissue. These inflammatory cells are the main source for inflammatory cytokines but can also secrete

ECM-degrading MMPs and serine proteases [88-90]. Additionally, inflammatory leukocytes contribute to oxidative stress by producing reactive oxygen species (ROS). Oxidative stress is characterised by the accumulation of ROS, including free superoxide radicals O^{2-} or hydrogen peroxide H_2O_2, within the aneurysm wall resulting in tissue damage and cell apoptosis [81, 91]. All these processes contribute to a disturbed vessel wall integrity preventing the vascular wall from withstanding haemodynamic forces. As a result, this can cause aortic rupture if the vessel wall cannot resist blood pressure. [84] .

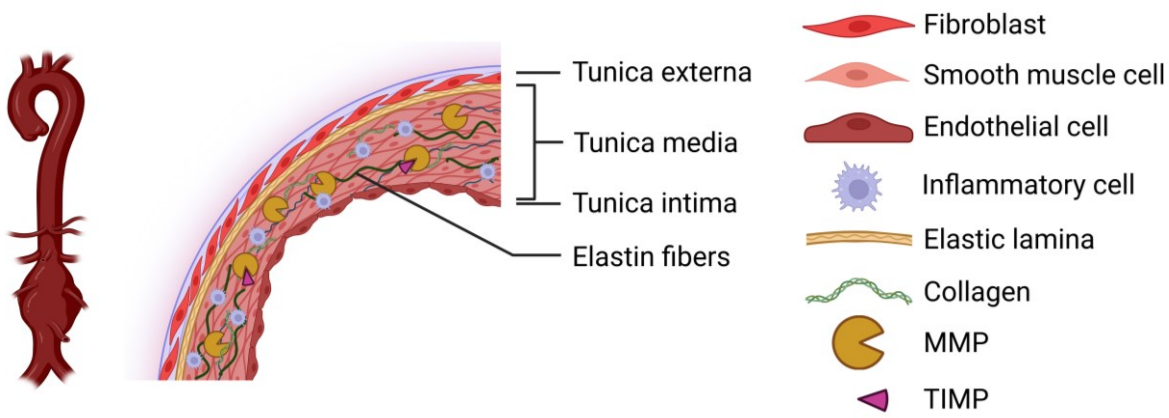

Figure 8. Structure of the vessel wall in AAA pathology. In the pathology of AAA the vascular wall integrity is destroyed by different events including VSMC apoptosis, degeneration of the ECM and infiltration of inflammatory cells such as macrophages. During the remodelling of the ECM, structural proteins like collagen and elastin are degraded resulting from an imbalance of matrix metalloproteinases and their TIMPs. AAA = abdominal aortic aneurysm; ECM = extracellular matrix; MMP = matrix metalloproteinase; TIMP = tissue inhibitor of metalloproteinases; VSMC = vascular smooth muscle cell. Created with BioRender.com.

1.3.3 The intraluminal thrombus

As already mentioned, the formation of an ILT is one of the pathological events in AAA, occurring in about 75% of all AAA patients [66]. This ILT is a mostly multi-layered biologically active entity built up by cells such as platelets, erythrocytes and neutrophils [82, 92, 93]. Thereby, this multi-layer can be observed in 80% of all ILT, reflecting the periodic growth of the thrombus [94]. These ILTs are composed of three different layers: the luminal, medial and abluminal layer (**Figure 9**).

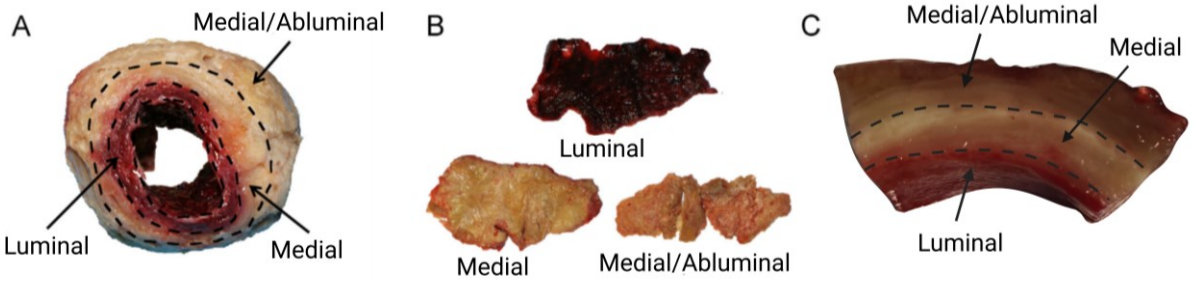

Figure 9. Structure of a multi-layered ILT. Macroscopic pictures of an ILT with a three-layered structure including the luminal, medial and abluminal layer. The different layers are shown (**A**) in the intact thrombus, (**B**) as separated single layers and (**C**) in a cross-section of the prepared thrombus. ILT = intraluminal thrombus. Images in (**A**) and (**B**) were taken by O' Leary *et al*. [95].

The blood-facing luminal layer has a dense fibrin network of cross-linked fibres and contains an enhanced cellular content consisting of platelets, red blood cells and leukocytes. In the medial layer, the dense fibrin network loses its secondary cross-links, indicating matrix degradation. Finally, the acellular wall-facing abluminal layer shows only barely organised fibrin structures (**Figure 10**) [96]. The aforementioned periodic growth of the ILT is caused by platelets in the luminal layer. Thereby, platelets located within the luminal layer release platelet activation marker, contributing to platelet recruitment as well as aggregation and thus developing of the thrombus [97]. Furthermore, all three layers are transversed by a continuous network of interconnected canaliculi containing an infiltrate including neutrophils, lymphocytes, macrophages and platelets. This enables macromolecules to penetrate from the lumen through the thrombus into the aortic wall contributing to aneurysm enlargement [94]. Another way the thrombus supports aneurysm formation and development is the conversion of fibrin-bound plasminogen to plasmin at the abluminal ILT layer. Since plasmin leads to MMP activation, this process promotes aneurysm enlargement by the degradation of ECM proteins [97]. In addition, the permanent contact of the luminal layer with the bloodstream allows not only platelets but also neutrophils, to be recruited into the thrombus tissue.

These cells are able to produce MMPs and elastase, also promoting the development of an aneurysm [97]. Nevertheless, it is known that the ILT, in addition to all these aneurysm-promoting characteristics, reduces the mechanical stress on the aortic wall and thus protects against rupture of the aneurysm. [98]. However, the underlying mechanisms of ILT formation are poorly understood. Therefore, it is still not clear whether the thrombus has a more protective or damaging function.

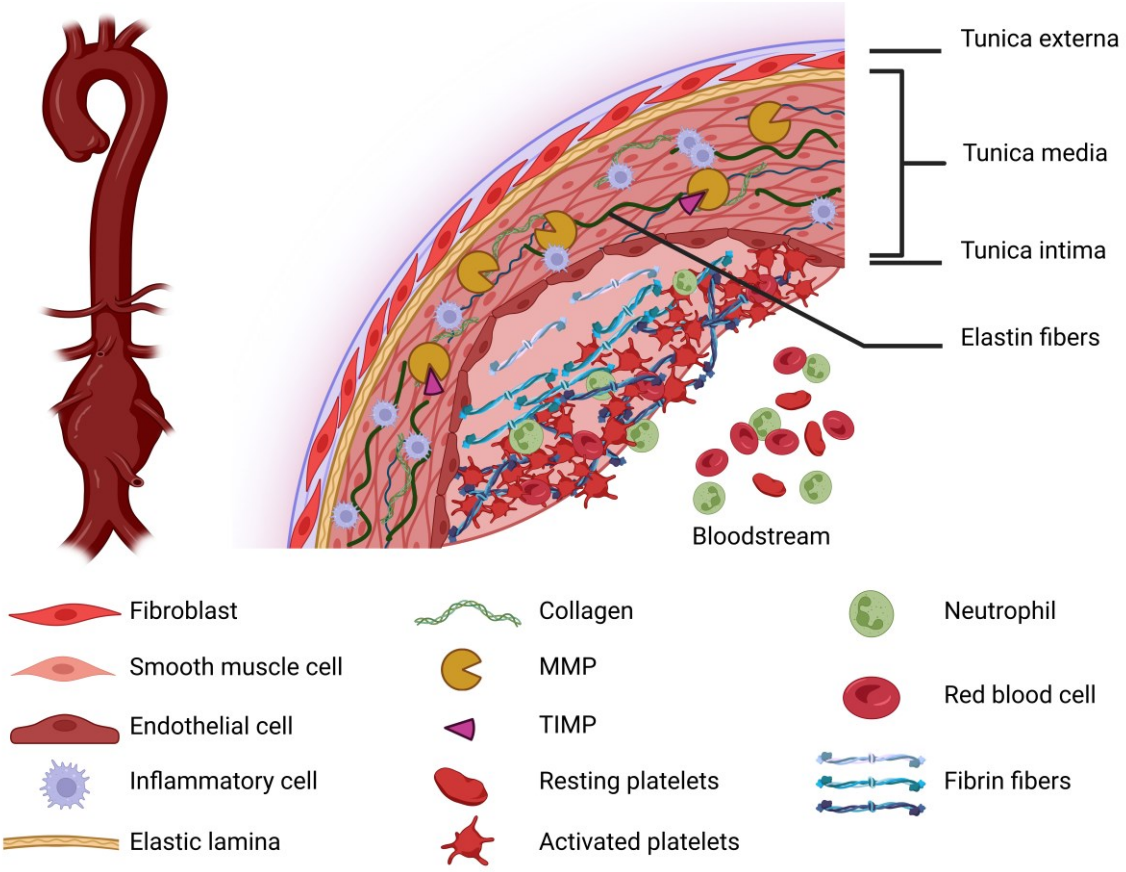

Figure 10. Molecular composition of an ILT. The distinct layers of the ILT consist of different cells and molecules. As the luminal layer is in constant contact with circulating blood, it contains a dense fibrin network that includes platelets, red blood cells and neutrophils. The dense fibrin network is degraded in the medial layer of the thrombus due to the loss of cross-links between the fibrin fibres. Finally, the acellular abluminal layer contains poorly organised fibrin fibres. ILT = intraluminal thrombus; MMP = matrix metalloproteinase; TIMP = tissue inhibitor of metalloproteinases. Created with BioRender.com.

1.3.4 Experimental animal models of AAA

Experimental AAA models are important for a better understanding of the underlying pathophysiological mechanisms of AAA development, to identify new potential therapeutic targets. The first animal model for AAA was described in the early 1950s

[99]. In this rats were fed with sweet peas containing β-aminopropionitrile (BAPN), an active agent. This BAPN inhibits the lysyl oxidase (LOX), which prevents the cross-linking of collagen and elastin, leading to the formation of an aneurysm and spontaneous rupture of the aorta [100, 101]. In addition to such chemical-induced AAA models, surgical models have been developed and performed to induce the aneurysm formation. Currently there are four common mouse models for the induction of AAA: the porcine pancreatic elastase (PPE) model, the external porcine pancreatic elastase application (ePPE) model, the angiotensin II (Ang II) infusion model and the calcium chloride ($CaCl_2$) model [102]. The classic PPE model was first described in rats by Anidjar *et al*. in 1990 and later adapted to mice by Pyo *et al*. in 2000. In this model, the aorta is infused with porcine pancreatic elastase under a certain pressure of 120 mm Hg, which leads to the development of an aneurysm in this area. The aneurysmal dilatation is accompanied by the degradation of elastin fibres and the infiltration of inflammatory cells into the aortic wall [103, 104]. For the ePPE model, puncturing the aorta is not necessary as a topical elastase application is conducted. This model was introduced in 2012 by Bhamidipati *et al*. and is usually combined with the oral administration of BAPN. The additional treatment with BAPN prevents the cross-linking of elastin and collagen fibres, which weakens the stability of the matrix and promotes aneurysm formation [105, 106]. A major advantage compared to the PPE model is that the endothelial layer of the aorta is not mechanically destroyed by an infusion catheter, enabling a better comparability with the human pathology [107]. Furthermore, the formation of an ILT, which is characteristic for the human AAA pathology, can be observed [106, 108]. In 2000, Daugherty *et al*. implanted osmotic minipumps with Ang II into mice to identify a way to increase blood pressure in atherosclerotic mice. Unexpectedly, they found systemic infiltration of Ang II led to the development of abdominal aortic aneurysms in *ApoE*$^{-/-}$ mice with this atherosclerotic background [109]. The Ang II mouse model is also often combined with the administration of BAPN via the drinking water or infusion in wild-type (WT) mice [110, 111]. The last most common model mentioned above is the $CaCl_2$ model. In 2001, Chiou *et al*. first described a reproducible $CaCl_2$ model. Therefore, a cotton sheet pre-soaked with $CaCl_2$ is placed on the aorta to induce aneurysm formation with elastin degradation, inflammation and calcification [112].

1.3.5 Role of platelets in the pathology of AAA

Platelets have been shown to play a crucial role in CVDs such as atherosclerosis, thrombosis and AAA [113]. Clinical studies have demonstrated that AAA patients have a significantly higher MPV and a significantly lower platelet count compared to healthy controls. The reduced platelet count is associated with coagulation disorders and may

be the result of increased platelet activation in the aneurysm, leading to an enhanced platelet turnover. The increased platelet activation can be detected in AAA patients by an increased level of soluble P-selectin, which serves as marker for platelet activity [114]. As part of therapeutic treatment, patients diagnosed with CVD are given low-dose aspirin (ASA) or clopidogrel as secondary prophylaxis to reduce platelet activation and aggregation and thereby prevent ischemic events [115-118]. Thus, by using anti-platelet therapies, the mortality rate of AAA patients could be significantly reduced [119]. Depending on size of the aneurysm (4.0 – 4.9 cm), it has been shown that the administration of ASA can reduce the rate of aneurysm expansion as well [120]. All these conditions support the evidence of platelets being important in human AAA pathology. However, the role of platelets has not only been shown to be important in AAA patients. In the experimental PPE mouse model it was demonstrated that platelets contribute to aneurysm formation as well. Through the interaction of platelets with macrophages, the production of the inflammatory protein osteopontin and various cytokines is increased. Thus, they are contributing to inflammation and remodelling of the matrix, but also to platelet adhesion and migration into the aortic wall. Consequently, it has been shown that a general depletion of platelets reduces inflammation and remodelling of the ECM [89]. Furthermore, the partial inhibition of platelet activation and aggregation by the administration of platelet receptor antagonists showed a reduction in the development of AAA in various experimental animal models. For example, administration of the $P2Y_{12}$ receptor inhibitor AZD6140 in the rat xenograft model or clopidogrel in the Ang II mouse model was able to reduce aortic diameter and rupture of the aneurysm [121, 122]. However, depletion or inhibition of platelets can lead to bleeding disorders, so treatment of AAA with such drugs may cause other complications [123]. Therefore, it is important to further investigate the role of platelets in AAA and the underlying molecular mechanisms in order to find a possible basis for the development of future drug-based therapies against AAA.

1.4 Aim of the study

AAA is a severe CVD. The high mortality rate in AAA results from the mostly asymptomatic course of the disease, leading to an increased risk of rupture. It was already shown that platelet counts and other platelet-specific parameters such as elevated activation are altered in AAA patients. In addition, it was confirmed in various experimental animal models of AAA that platelets play a crucial role in the formation and progression of AAA. However, the underlying mechanism are still unclear and further investigations are necessary for a better understanding of the AAA pathology.

1.4.1 Characterisation of platelets after PPE surgery

In the first part of this thesis, different platelet-specific parameters were characterised in the experimental PPE mouse model. For this purpose, wild-type mice (C57Bl/6J mice) were analysed at days 3, 10 and 28 after elastase infusion and compared to sham-operated control mice. Using ultrasound measurements, aneurysm formation was observed, and blood cell counts were analysed. Various platelet-specific parameters were analysed via flow cytometry, including platelet activation upon stimulation with different agonists and changes in glycoproteins on platelet surface. In this context, ELISA were performed to investigate plasma concentration of possibly shed platelet receptors, namely GPVI and GPIb. In addition, formation of circulating platelet-leukocyte aggregates and platelet PS exposure were determined. Further, the deposition of the inflammatory and remodelling-related protein osteopontin within the aortic wall and plasma was analysed.

1.4.2 The role of platelet-derived reelin in AAA formation

After general characterisation of platelet-specific changes in the PPE model, the next goal was to investigate the role of platelet-derived reelin in AAA pathology. The protein reelin has been shown to promote CVDs by binding to various platelet receptors thereby increasing platelet activation. Furthermore, reelin can be released upon platelet activation, resulting in an amplification loop. Using *Rln$^{fl/fl}$; PF4-cre^{-}* and *Rln$^{fl/fl}$; PF4-cre^{+}* mice in the experimental PPE mouse model, the influence of platelet-derived reelin on the development and progression of AAA was analysed at days 7 and 28 after surgery. In this context, aortic diameter was determined, different platelet-specific parameters were measured using flow cytometry (see chapter **1.4.1**) and blood cell counts were analysed. Additionally, the influence of reelin deficiency in platelets was analysed by histological and immunofluorescence stainings of the aortic wall to investigate the effects on inflammation and remodelling of the aorta. Thereby, the aortic wall thickness, elastin degradation and VSMC apoptosis, but also the content of platelets and macrophages in the aortic wall were determined.

1.4.3 Establishment of the external porcine pancreatic elastase application (ePPE) model as a novel experimental AAA mouse model

To investigate the pathological mechanisms associated with AAA, several experimental AAA mouse models have been developed within the last years. Thereby, our group could clearly show that the PPE model reflects almost all relevant features of human AAA pathology. Nevertheless, the PPE model does not lead to ILT formation. Therefore,

Lu *et al*. described in 2017 the ePPE model as an efficient and powerful method to study ILT formation in AAA pathology. Busch *et al*. claimed that thrombus formation occurs even 28 days after ePPE surgery [106]. For the establishment of this mouse model, wild-type mice (C57Bl/6J mice) were used and investigated for AAA formation within 28 days after surgery. The mice treated with elastase were compared to a control group of sham-operated mice. In this context, different concentrations of BAPN were tested to achieve sufficient aneurysm formation with a minimum diameter dilatation of 150%. AAA formation was analysed by determination of the aortic diameter, the incidence and the survival rate of AAA formation.

1.4.4 Characterisation of aortic aneurysm formation and progression in ePPE-operated mice

After the establishment of the ePPE model, platelet-specific parameters such as activation and aggregation were characterised. For this purpose, wild-type mice (C57Bl/6J mice) were used. The elastase treated mice were compared with sham-operated control mice 28 days after ePPE surgery. To characterise the platelets, various parameters were analysed using flow cytometry as in the PPE model (see chapter **1.4.1**). In addition, histological and various immunofluorescence stainings were performed to investigate the effects on inflammation and remodelling of the aorta as well as thrombus formation. Moreover, plasma concentration of possibly shed platelet receptors, sGPVI and glycocalicin, were examined.

The overall aim of this study was to characterise platelets in the PPE model, to increase the understanding of the role of platelets and in specific platelet-derived reelin on AAA formation and to further establish another experimental mouse model (ePPE) important to analyse thrombus formation in AAA mice. Both, the role of reelin and the establishment of the ePPE mouse model are important to find new therapeutic approaches in future to treat AAA patients.

2 Material

2.1 Experimental animals

Mice used for the animal experiments were either purchased from external animal breeders or were generated and bred in the animal facility "Zentrale Einrichtung für Tierforschung und wissenschaftliche Tierschutzaufgaben" (ZETT) of the Heinrich-Heine-University of Duesseldorf. According to the guidelines of Federation of European Laboratory Animal Science Association (FELASA) all mice were maintained under standard laboratory specific-pathogen free conditions (SPF). They were housed in groups in Makrolon cages type III for genetically modified organisms (GMOs) and followed a standardised 12-hour day-night rhythm in a temperature- and humidity-controlled room. The mice were fed with a standard laboratory diet and water *ad libitum*. Pathogen-free C57BL/6J mice were purchased from Janvier Labs. Rln^{flox}-mice were obtained from Prof. Hans Bock (Clinic for Gastroenterology, Hepatology and Infectiology, UKD), originally from Prof. Joachim Herz (Dept. of Molecular Genetics, UTSW) and crossed to PF4-cre mice, which were purchased from the Jackson Laboratory (C57BL/6-Tg [PF4-cre] Q3Rsko/J). These newly generated *$Rln^{fl/fl}$; PF4-cre^{-}* and *$Rln^{fl/fl}$; PF4-cre^{+}* mice were used for the experiments in this thesis. The *$Rln^{fl/fl}$; PF4-cre* mice were raised in inbreeding strains in the animal facility of the Heinrich-Heine-University of Duesseldorf (ZETT). For all experiments in this study, male mice between the age of 10 – 12 weeks were used. All animal experiments were performed in accordance with the Declaration of Helsinki and the guidelines of Directive 2010/63/EU of the European Parliament on the protection of animals. The protocols were authorised by the Animal Welfare Commission of the Heinrich-Heine-University and the North Rhine-Westphalia State Office for Nature, Environment and Consumer Protection (LANUV, NRW; Permit Numbers 81-02.04.2021.A429; 81-02-04.2018.A409; 81-02.05.40.21.041; O86/12).

Table 2. Experimental mouse strains.

Summary of experimental mouse strains used in this study together with corresponding experimental approaches. ePPE = external porcine pancreatic elastase application; PPE = porcine pancreatic elastase; Rln = reelin.

Mouse strains	Term	Experimental model
C57BL/6J	C57BL/6J	PPE, ePPE
$Rln^{fl/fl}$; PF4-cre	*$Rln^{fl/fl}$; PF4-cre^{-}* *$Rln^{fl/fl}$; PF4-cre^{+}*	PPE

Agnes Bosbach has attended a laboratory animal science course in accordance with the FELASA guidelines (category B). According to § 16 Abs. 1 Satz 5 TierSchVersV, Mrs. Agnes Bosbach has an exceptional authorisation. This allows her to perform the surgical animal experiments described in the above-mentioned permission for the external porcine pancreatic elastase application (ePPE) mouse model (permit number 81-02.04.2021.A429). The other surgical animal model (permit number 81-02-04.2018.A409) was conducted by surgeons of the Clinic of Vascular and Endovascular Surgery and the S1-project of the Transregio (TRR)259.

2.2 Standard devices and equipment

Table 3. Standard devices.

Device	Model	Company
Automatic microtome	Microm HM355	Thermo Fisher Scientific
Bench scales	AE166 Quintix® 1102 EMB 100-3	Mettler Sartorius Kern & Sohn
Blot module	XCell II™	Invitrogen™
Centrifuges	5804 R 5424 R S8030-5000	Eppendorf Eppendorf Starlab
Chemiluminescence imager	Vilber Fusion-FX6	Vilber Lourmat
Electrophoresis cell	XCell SureLock™	Invitrogen™
Filter paper		Whatman
Flow cytometer	FACSCalibur™ FACSSymphony™ A1	BD Biosciences BD Biosciences
Haematology analyser	KX-21N XP-300	Sysmex Sysmex

Incubators	BE 300 UM 500	Memmert Memmert
Magnetic stirrer	RET basic	IKA Labortechnik
Micropipettes	Research® plus ErgoOne®	Eppendorf Starlab
Microscope camera	Axiocam 503 color	Zeiss
Microscope lighting equipment	HXP 120C	Zeiss
Microscopes	Axio Observer.D1 Axioskop 20	Zeiss Zeiss
Microtiter plate reader	GloMax® Multi+	Promega
Microwave	NN-E201W	Panasonic
Multipipette	Multipette® plus peqPETTE 200M	Eppendorf PEQLAB
Paraffin dispenser	47311 43900	Medax Medax
Paraffin bath	MH8517	Electrothermal
pH-Meter	pH526	WTW
Pipettor	ErgoOne®Fast	Starlab
Power supply	PowerPac™ Universal	Bio-Rad
Roll mixer	RM5	CAT
Thermo shaker	TS-100C incl. SC-24NC	BioSan

Table 4. Standard equipment.

Equipment	Company
Coverslides	24x60 mm; Engelbrecht 24x70 mm; O. Kindler 18x18 mm; A. Hartenstein
Cryogenic vials	2 mL, 10018-754; VWR®
FACS-tubes	5 mL, 75x12 mm, PS; Sarstedt
Glass capillaries	Minicaps®, Na-heparin; Hirschmann
Needles	27G x ¾, 21G x 1 ½; Sterican®; Braun
Nitrocellulose membrane	Amersham™ Protran® Premium 0.2 µm; Cytivia Life Sciences™
Safe-lock tubes (0.2; 0.5; 1.5; 2 mL)	Sarstedt
Slides	76x26 mm; Marienfeld Superior™
Pipette tips (10-20; 200; 1000 µL)	TipOne®
Syringes (1; 5; 10; 20 mL)	Injekt®; Braun
Tissue cassettes	M490-2; Simport™ Scientific CXN3.1; Roth
Transfer pipettes (1; 5; 10; 25 mL)	Stripette™; Corning® Costar®
Conical tube (15; 50 mL)	Polypropylen conical tube; Falcon®

2.3 Special devices and equipment for surgical procedures and mouse experiments

Table 5. Surgical devices for surgical procedures and mouse experiments.

Device	Model	Company
Controller for Axio Zoom	EMS3	Zeiss
Face mask	For mouse	UNO
Flowmeter	Type CM2	UNO
Hot bead sterilizer	Type 250	Fine Science Tools
Infrared lamp	IL 35	Beurer
Isoflurane induction box	For mouse	UNO
Stereomicroscope for surgery	Discovery.V20	Zeiss
Stereomicroscope for harvesting	MSZ5000-IL-TL	Krüss
Stereomicroscope lights	LED High Power Spotlight	Brunel
Razor	Isis GT420	Aesculap
Temperature controller	Piccolo P116 PID	Eurotherm
Ultrasound imaging system	Vevo 3100®	VisualSonics
Ultrasound transducer	MX550D	VisualSonics
Vaporizer	Sigma Delta Isoflurane Vaporizer	Penlon

Table 6. Surgical equipment for surgical procedures and mouse experiments.

Equipment	Model	Company
Blunt retractors	#18200-11	Fine Science Tools

Catheter tube	#MRE-010 #427401	Braintree Scientific BD Biosciences
Coated vicryl suture 8-0	#V548G	Ethicon
Cotton swab	#71010	MaiMed®
Csatroviejo micro needle holders	#12060-01	Fine Science Tools
Disinfection spray	Kodan® tincture forte colourless	Schülke & Mayr GmbH
Dumont #5 forceps	#11251-20	Fine Science Tools
Dumont #5/45 forceps	#11251-35	Fine Science Tools
Extra narrow scissor	#14088-10	Fine Science Tools
Eye lotion		Bepanthen®
Fixing tape	#1527	Transpore™, 3M™
Hair removal cream		Veet
Infusion system	#4186109	Braun
Needle for puncturing	#4656300, 30G x ½”	Sterican®; Braun
Nylon black suture 10-0	#03171	S&T
Precision wipes	#7551	Kimtech™ Science
Pressure bag	#MX4805	ICU Medical
Prolene suture 7-0	#8701H	Ethicon
Ring forcep	#11103-09	Fine Science Tools
Sealing foil	#PM-996	Parafilm®
Standard pattern forcep	#11000-12	Fine Science Tools
Vascular clamp	#00396-01, B-1V	Fine Science Tools

2.4 Chemicals and buffers

Table 7. Chemicals.

Chemicals	Company
Adenosine diphosphate (ADP)	A2754; Sigma-Aldrich
Agarose	A9539; Sigma-Aldrich
Apyrase	A7646; Sigma-Aldrich
β-aminopropionitrile (BAPN)	A3134; Sigma-Aldrich
Bovine serum albumin (BSA)	A7906; Sigma-Aldrich
Buprenorphine – “Buprenovet Multidose”	PZN - 18760711; VetViva Richter GmbH
Calcium chloride ($CaCl_2$)	C5080; Sigma-Aldrich
Citric acid ($C_6H_8O_7$)	6490; Sigma-Aldrich
Collagen-related peptide (CRP)	XL1; University of Cambridge, UK CRP-A; Pplus Products, UK
DL-Dithiothreitol (DTT)	D0632; Sigma-Aldrich
Eosin G-solution	3139; Carl ROTH GmbH
Ethanol 100% (EtOH)	100983; Merck Millipore
Ethylenediaminetetraacetate (EDTA) solution (0.5 M)	03690; Sigma-Aldrich
Fluoromount^{TM} aqueous mounting medium	F4680; Sigma-Aldrich
Glucose	HN06; Carl ROTH GmbH
Goat serum	ZIE.SE.0100; Bio & Sell
Heparin-sodium-25000	2047217; B Braun
HEPES	H4034; Sigma-Aldrich

Hydrochloric acid 25%	1.00316; Sigma-Aldrich
IGEPAL® CA-630	I8896; Sigma-Aldrich
Isoflurane	PZN - 09714675; Piramal Critical Care
Ketaset	PZN – 12467832; Zoetis
Magnesium chloride ($MgCl_2$)	KK36; Carl ROTH GmbH
Mayer's hemalum solution	1.09249; Sigma-Aldrich
Microvette® 500 EDTA K3E	20.1341.100; Sarstedt
Midori green	MG04; NIPPON Genetics JAPAN
Milk powder	T145; Carl ROTH GmbH
NuPAGE™ 7% Tris-acetate gel	EA03555BOX; Invitrogen™
NuPAGE™ LDS sample buffer	NP0007; Invitrogen™
NuPAGE™ transferbuffer (20x)	NP0006; Invitrogen™
PAR4 peptide	3494; Tocris Bioscience
Paraffin	P3558; Sigma-Aldrich
Phosphate buffered saline (PBS)	D8537; Sigma-Aldrich
Potassium chloride (KCl)	9023717; Merck Millipore
Precision Plus Protein™ dual colour standards	1610374; Bio-Rad
Prostaglandin I_2 (PGI_2)	538925; Merck Millipore
Proteinase-inhibitor	04693124001; Roche
Protein block	X0909; DAKO

Recombinant reelin	AG Korth; Institute for Neuropathology, University Hospital Duesseldorf
Roti®Histofix (Paraformaldehyde 4%)	P087; Carl ROTH GmbH
Roti®Histokitt	6638; Carl ROTH GmbH
Roti®Histol	6640; Carl ROTH GmbH
Sodium acid (NaN_3)	S2002; Sigma-Aldrich
Sodium chloride (NaCl; 0.9%; fluid)	PZN – 00412205; Fresenius PZN – 00809061; Fresenius
Sodium chloride (NaCl; powder)	S3014; Sigma-Aldrich
Sodium dihydrogen phosphate (NaH_2PO_4)	6345; Merck Millipore
Sodium hydrogen carbonate ($NaHCO_3$)	6885; Carl ROTH GmbH
Sodium orthovanadate (Na_3VO_4)	S6508; Sigma-Aldrich
Sodium phosphate, dibasic (Na_2HPO_4)	4984; Carl ROTH GmbH
Tri-sodium citrate dehydrate (Tri-Na-Citrat)	3580; Carl ROTH GmbH
Triton™ X-100	T8787; Sigma-Aldrich
Trizma® hydrochlorid (Tris-HCl)	T5941; Sigma-Aldrich
Tween® 20	822184; Merck Millipore
Type I porcine pancreatic elastase	E1250; Sigma-Aldrich
U46619 (U46)	1932; Tocris Bioscience
Ultrasound gel	GELLO® GmbH
Western HRP substrate	WBKLS0500; Millipore
Xylazine 20 mg/mL	PZN – 14022086; Serumwerk Bernburg AG

Table 8. Buffers and solutions.

Buffer/Solution	Components
ADP solution (20 mM)	0.1 g ADP 11.7 mL PBS pH 7.4
Binding buffer	10 mM HEPES 140 mM NaCl 2.5 mM $CaCl_2$ pH 7.4
$CaCl_2$ solution (100 mM)	1.47 g $CaCl_2$ 100 mL dH_2O
Citrate buffer	41 mL 0.1 M Tri-Na-Citrat 9 mL 0.1 M citric acid 450 mL dH_2O pH 6.0
Heparin solution (20 U/mL)	40 µL Heparin-Sodium-25000 10 mL PBS
Hydrochloric acid-alcohol solution	10 mL Hydrochloric acid 25% 990 mL EtOH 70%
Western HRP substrate solution	50% Luminol 50% Peroxide solution
IP-buffer (stock solution 5x)	15 mM Tris-HCl 155 mM NaCl 1 mM EDTA 0,005% NaN3 1 L dH_2O
Murine lysis buffer	5 x IP-Puffer (2 mL) 5% IGEPAL 5 mM Na_3VO4 1x Proteinase-inhibitor

Murine Tyrode's buffer	134 mM NaCl 12 mM $NaHCO_3$ 2.9 mM KCl 0.34 mM Na_2HPO_4 20 mM HEPES 10 mM $MgCl_2$ 5 mM glucose 0.2 mM $CaCl_2$ 1 L dH_2O pH 7.35
PBS-T	500 mL PBS 500 µL Tween
Tris buffered saline (TBS) buffer (stock solution 5x)	15,8 g Tris-HCl 45 g NaCl 1 L dH_2O pH 7.6
TBS-T	100 mL 5x TBS buffer 400 mL dH_2O 500 µL Tween

2.5 Antibodies

Table 9. Primary antibodies.

Antibody	Isotype	Clonality	Company
Rabbit anti-mouse (EPR25A); Isotype control	IgG	monoclonal	ab172730; abcam
Rabbit anti-mouse β-Actin (13E5)	IgG	monoclonal	4970; Cell Signaling
Rabbit anti-mouse alpha smooth muscle actin (α-SMA)	IgG	polyclonal	ab5694; abcam

Rabbit anti-mouse cleaved caspase-3 (Asp175) (Casp3)	IgG	polyclonal	9661; Cell Signaling
Rabbit anti-mouse Osteopontin (OPN, N-terminal)	IgG	polyclonal	ab181440; abcam
Rat anti-mouse CD107b (Mac3)	IgG1	monoclonal	550292; BD Pharmingen™
Rat anti-mouse CD42b (GPIbα)	IgG1	monoclonal	M042-0; Emfret Analytics
Rat anti-mouse IgG; Isotype control	IgG1	monoclonal	C301; Emfret Analytics
Mouse anti-mouse reelin	IgG	monoclonal	AG Korth; Institute for Neuropathology, University Hospital Duesseldorf

Table 10. Secondary antibodies.

Antibody	Isotype	Conjugate	Dilution	Company
Donkey anti-rabbit IgG (H+L) highly cross-adsorbed secondary antibody	IgG	Alexa Fluor™ Plus 555	1:100	A32794; Invitrogen™ Thermo Fisher Scientific
Goat anti-rat IgG (H+L) antibody, biotinylated	IgG	-	1:200	BA-9400; Vector Laboratories
Donkey anti-rabbit IgG	IgG	HRP	1:2500	NA934; Cytivia Life Sciences™
Sheep anti-mouse IgG	IgG	HRP	1:2500	NA931; Cytivia Life Sciences™

Table 11. Antibodies for flow cytometry.

Antibody	Clone	Conjugate	Company
Rat anti-mouse CD11b	M1/70	APC	553312; BD Biosciences
Rat anti-mouse CD14	Sa14-2	APC	123311; BioLegend
Rat anti-mouse CD3	17A2	APC	100235; BioLegend
Rat anti-mouse CD41/61 (active form)	JON/A	PE	D200; Emfret Analytics
Rat anti-mouse CD42b	Xia.G5	PE	M040-2; Emfret Analytics
Rat anti-mouse CD45	30-F11	APC	559864; BD Biosciences
Rat anti-mouse CD49e	Tap.A12	FITC	M080-1; Emfret Analytics
Rat anti-mouse CD61	Luc.H11	FITC	M031-1; Emfret Analytics
Rat anti-mouse CD62P	Wug.E9	FITC	D200; Emfret Analytics
Rat anti-mouse GPVI	JAQ1	FITC	M011-1;Emfret Analytics
Rat anti-mouse Ly6G	1A8	APC	127614; BioLegend

2.6 Dyes

Table 12. Dyes.

Dye	Dilution	Company
4′,6-diamidino-2-phenylindole (DAPI)	1:3000	10236276001; Roche
Cy™5 Annexin V	1:10	559934; BD Bioscience
eBioscience™ streptavidin eFluor™ 660 conjugate	1:20	50-4317-82; Invitrogen™ Thermo Fisher Scientific

2.7 Kits

Table 13. Kits.

Kit	Catalog No.	Company
AccuStart™ II PCR Genotyping Kit	733-2236	Quantabio
Mouse Neutrophil Elastase/ELA2 Quantikine ELISA Kit	MELA20	R&D
Mouse Soluble Glycoprotein VI (SGPVI) ELISA Kit	MBS109240	MyBioSource
Mouse Glycocalicin ELISA Kit	MBS042712	MyBioSource
Mouse DuoSet ELISA	DY441	R&D
Elastic stain Kit	HT25A-1KT	Sigma-Aldrich

2.8 Software

Table 14: Software.

Software	Company
BioRender	Biorender.com
CellQuest	BD Biosciences
Endnote X8	Clarivate
FACSDiva™	BD Biosciences
Graph Pad Prism 8.4.3	GraphPad Software, LLC
Microsoft Office 365	Microsoft Corporation
VEVO Lab 5.5.0 Software	VisualSonics
ZEN 3.5 (blue edition)	Zeiss

3 Methods

3.1 Experimental mouse models of AAA

3.1.1 Preparation, analgesia and anaesthesia

Before surgery, the mice received a subcutaneous injection of buprenorphine diluted in $NaCl_2$ (0.1 mg/kg) to avoid pain. After 30 min, the mice were first sedated in an anaesthesia chamber with isoflurane [2 – 3%] and oxygen [0.75 L/min] until reaching the surgical tolerance phase. The mice were weighed and placed with their noses into an isoflurane mask under a stereomicroscope. A heated mat under the cork plate allowed maintaining body temperature to prevent mice from cooling down during surgery. The isoflurane nose mask ensured a constant flow of isoflurane [2 – 3%] and oxygen [0.75 L/min] during the entire surgical procedure. To protect the cornea from dehydration, the eyes were covered with an eye lotion. Testing the interdigital reflex ensured complete pain elimination, the mice were placed backwards and then fixed in position using elastic bands and pins. Then the abdominal area was depilated, cleaned and sterilised. The entire surgical procedure was performed under a stereomicroscope in combination with two flexible neck lamps for better exposure of the surgical area. For pain relief after surgery, the mice received buprenorphine subcutaneously every four hours for three days during the daylight phase. In addition, buprenorphine was administered via drinking water [9 µg/ml] to maintain pain relief also in the dark phase.

3.1.2 Porcine pancreatic elastase (PPE) model

To induce experimental AAA via the porcine pancreatic elastase (PPE) model (**Figure 11**), a median laparotomy was performed to expose the blood vessels in the abdomen including the aorta. For this purpose, the abdominal organs, especially the colon, needed to be carefully pushed aside and fixed with blunt retractors. The aorta is not directly visible as it is still covered by tissue. Therefore, the fine tissue above the aorta had to be removed. After exposure, the abdominal aorta was temporarily ligated to ensure subsequent puncturing without severe bleeding. For this purpose, a vascular clamp was used infrarenally. Distally, a piece of the catheter tube was placed under the aorta. The subsequent pulling up of the catheter provides a better angle for puncturing of the aorta. Finally, using a catheter inserted into the aorta, fresh sterile isotonic saline ($NaCl_2$, 0.9%) containing porcine pancreatic elastase [2.5 U/mL] was infused into the aorta at 120 mm Hg for 5 min. In control (sham) mice sterile isotonic

saline was applied instead of elastase. After time expired, the catheter was removed, and the aortic hole was closed using a 10-0 nylon black suture without constricting the aorta. Afterwards, the abdomen was closed. An 8-0 coated vicryl suture was used to close the peritoneum, while the uppermost layer of skin was sutured with a 7-0 prolene suture. This operation model was conducted by surgeons of the Clinic of Vascular and Endovascular Surgery and S1-project of the TRR259.

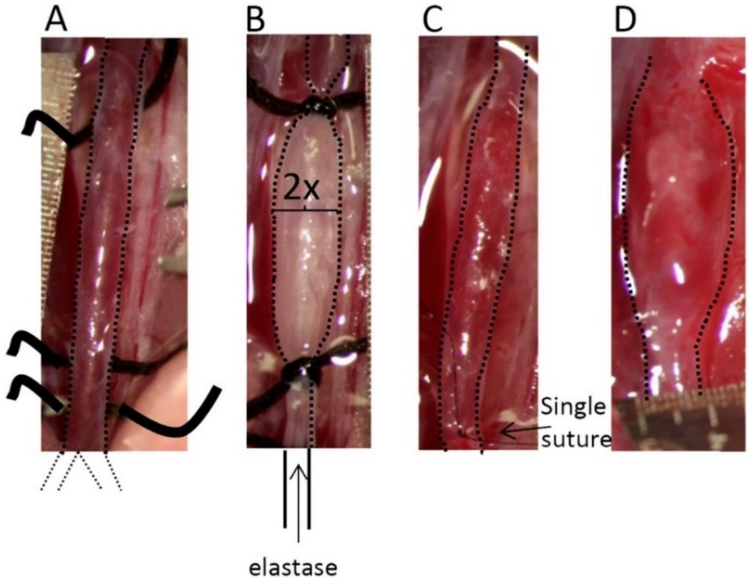

Figure 11. The PPE model. (**A**) Important for the surgical procedure is the exposure of the abdominal aorta. (**B**) After infrarenal and distal ligation, the aorta is punctured and then porcine pancreatic elastase is infused via a catheter for 5 min at 120 mmHg. (**C**) After catheter removal the aortic hole is closed without constriction. (**D**) Aneurysm formation after 14 days post surgery. PPE = porcine pancreatic elastase. Image taken from Lysgaard Poulsen *et al*., 2016 [124].

3.1.3 External porcine pancreatic elastase application (ePPE) model

To induce experimental AAA using a different mouse model, the external porcine pancreatic elastase application (ePPE) model was performed (**Figure 12**). Initially, this surgery model was developed and verified by Dr. Guanyi Lu at the University of Michigan [105]. Based on his protocol, the model was established and modified at the University Hospital of Duesseldorf. Thereby, as in the PPE model (see chapter **3.1.2**), a median laparotomy was performed to expose the blood vessels including the aorta. After exposition, the aorta was isolated from the *vena cava* with the utmost care in order to avoid damaging the tissue and in particular the blood vessels. Once the aorta had been separated from the *vena cava* by carefully removing the tissue between the two sensitive blood vessels, parafilm was placed under the aorta. Therefore, a piece of fine paper tissue was placed on the *vena cava* and the parafilm cut to size was

placed over it. The aorta was then carefully lifted to pull the piece of parafilm under the aorta to the other side using an angled pair of forceps. Then the parafilm was used to form a shell for the elastase. In this step, it was important to ensure that the shell was sufficiently closed to avoid the elastase from leaking and damaging surrounding tissue. Finally, the shell was filled with 10 µl elastase [25.5 U/mL] for 5 min. For sham-operated control mice, heat-deactivated elastase was used. Heat-deactivation was performed for 30 min at 100 °C. After removing the elastase with a cotton swab a washing step with $NaCl_2$ followed. The parafilm shell was carefully opened and removed before the abdomen was closed. Afterwards, the peritoneum was sutured with an 8-0 coated vicryl suture, while the skin layer was closed with a 7-0 prolene suture. In addition to surgical intervention, the mice received β-aminopropionitrile (BAPN) in their drinking water. BAPN weakens the stability of the matrix and promotes the formation of aneurysms by preventing the cross-linking of elastin and collagen fibres. For establishing the ePPE procedure, different BAPN concentrations [0.1% and 1%] were tested and additionally compared with results obtained without BAPN administration. Supplementation of BAPN began 3 days prior to surgery and was maintained throughout the experiment. Thereby, the drinking water with BAPN had to be changed every 2 – 3 days. The establishment of the surgical procedure and following surgeries were performed by myself.

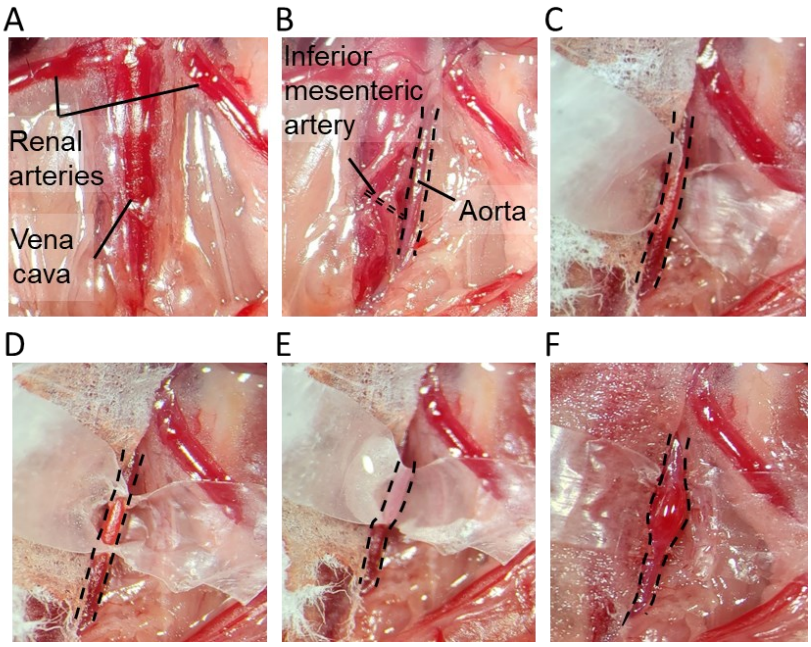

Figure 12. The ePPE model. To establish the ePPE model, (**A**) the blood vessels in the abdomen have to be exposed. (**B**) The aorta is often not visible and has to be isolated from the *vena cava*. (**C**) After separating the aorta from the *vena cava*, parafilm is placed under the aorta, (**D**) forming a shell. (**E**) This shell is filled with 10 µl elastase for 5 min. (**F**) After removing the elastase, a washing step with $NaCl_2$ follows before the abdomen is closed. ePPE = external porcine pancreatic elastase application.

3.2 Monitoring and harvesting of animals

3.2.1 Ultrasound measurements

To monitor the formation and progression of abdominal aortic aneurysms, ultrasound imaging was performed using a Vevo 3100® High-Resolution In Vivo Micro-Imaging System. Thereby, the maximum aortic diameters were measured at the aneurysm site before (baseline), on day 3, 7, 14, 21 and 28 after surgery. For this procedure, the mice were initially anaesthetised with isoflurane [2 – 3%] and oxygen [0.75 L/min] in an isolated anaesthetic chamber. After initial anaesthesia, the mice were placed back down on a hot plate at 37 °C with their nose in an isoflurane mask to prevent movement while ultrasound measurements. For sufficient ultrasound imaging the abdomen was depilated. Ultrasound gel was applied to the abdomen and the ultrasound probe was placed vertically on top of the mouse. A standardised imaging algorithm with longitudinal B-mode images of the systolic phase was used to monitor the progressive inner aortic diameter dilatation. Once the aneurysm had been located and imaged, the ultrasound gel was removed, and the mouse was taken out of the anaesthetic mask. Finally, the mouse was weighed and placed back in the cage to awake.

3.2.2 Blood and tissue collection

At the end of the experiments, blood was collected from mice. Therefore, the mice were anaesthetised with isoflurane [2 – 3%] and oxygen [0.75 L/min] in an anaesthetic chamber. The sufficient depth of anaesthesia was determined based on the toe pain reflex. Using microcapillaries, the blood was taken retrobulbar by puncturing the venous complex located behind the eye. Blood samples were collected in 1.5 mL tubes containing 300 µl of anti-coagulant heparin buffer for flow cytometric analyses (see chapter **3.4.1**) or for preparation of platelet lysates (see chapter **3.4.2**). Blood collection in EDTA tubes was performed to determine the blood cell count (see chapter **3.4.3**) and prepare plasma samples (see chapter **3.6.1**). These plasma samples were stored at - 70 °C until use. To collect and preserve the mouse tissue for histological analysis, the mice were euthanised by cervical dislocation. Subsequently, the abdomen and thorax were opened to expose the heart for flushing the circulatory system. A syringe filled with ice-cold $NaCl_2$ was placed in the *apex cordis*. Systemic flushing was ensured by incising the right atrium before. Once the circulating blood has been removed, the thoracic and abdominal aorta were collected using a stereomicroscope to remove the surrounding tissue. Finally, the aortic tissue

was stored in 4% PFA at 4 °C overnight as preparation for embedding in paraffin (see chapter **3.3.1**).

3.3 Preparation of murine tissue and blood

3.3.1 Paraffin fixation

For histological and immunofluorescence analysis, the aortic tissue of mice was embedded in paraffin. Therefore, the tissue was fixed for at least 24h at 4 °C in 4% PFA after collection. The next day, the aortic tissue was incubated for 1 – 2h in ascending order in each ethanol solution [70%, 80%, 90%, 96%, 100%] and transferred to Roti®Histol (Carl Roth) overnight at RT. Finally, the tissue was equilibrated in liquid paraffin for at least 4h before embedding. For histological and immunofluorescence staining, 5 µm tissue sections were prepared using a microtome (see chapter **3.5.1**).

3.3.2 Washing of murine whole blood

For flow cytometric analyses, murine whole blood was washed to remove the heparin. Therefore, the heparinised blood was centrifuged at 650 x g for 5 min. The supernatant was discarded, and remaining blood was diluted with 500 µl murine Tyrode's buffer before a further centrifugation step at 650 x g for 5 min. Again, the supernatant was discarded, and the blood was diluted with 700 µl murine Tyrode's buffer. The blood was divided into fresh tubes: 150 µl for the measurement of AnnexinV-binding, 250 µl for the measurement of aggregates and the remaining blood was used for the measurement of platelet activation, degranulation, and glycoprotein externalisation. After separating the blood, the last centrifugation step was performed at 650 x g for 5 min. Again, the supernatant was discarded. For the AnnexinV measurements, the blood was taken within binding buffer and for all other measurements in Tyrode's buffer supplemented with 1 mM $CaCl_2$.

3.4 Cell biological methods

3.4.1 Flow cytometry of murine samples

Flow cytometry is a method that enables the single-cell analysis of cells from a suspension. For this purpose, the cells are transported into the system under negative pressure and guided past a laser. This laser differentiates the cells according to their size (forward scattering, FSC) and granularity (side scattering, SSC). For a more

detailed analysis of the cells, fluorescence-labelled antibodies can be used, which bind to specific cell receptors. In this thesis, flow cytometric analysis was performed with washed whole blood from mice. The specific SSC and FSC profile and the fluorescence obtained by using platelet-specific antibodies were used to gate the cells. The experiments with blood from PPE mice were performed using the FACSCalibur™ flow cytometer, while the experiments with blood from ePPE mice were performed using the FACSymphony™ flow cytometer. The stimulation of surface receptors by different agonists was performed in both flow cytometers with agonists in a ratio of 1:10 in a total reaction volume of 30 µl. In this context, it is important to mention that the CRP concentration can differ between experiments, depending on the used FACS device, but also on the manufacturer and the activity of the CRP. Each new vial was tested and titrated previously to receive mild, moderate and high stimulation. Thereby the same experimental groups (PPE vs. sham; Rln WT vs. Rln KO; ePPE vs. sham) were measured with the same CRP on the same device for comparability. In addition to CRP, ADP, U46 and PAR4 were used as agonists. For analysis and processing of the flow cytometry data measured with the FACSCalibur™ the CellQuest software was used, while the data obtained with the FACSymphony™ were analysed with the FACSDiva™ software.

3.4.1.1 Murine platelet activation

Platelet activation and degranulation in murine whole blood was measured by two-colour analysis. Therefore, fluorescence-labelled antibodies were used to determine the expression of P-selectin (Wug.E9-FITC) and the active form of integrin $\alpha_{IIb}\beta_3$ (JON/A-PE). For the analyses with the FACSCalibur™, these antibodies were mixed in a ratio of 1:10 in a total reaction volume of 30 µl with the washed and calcium-enriched mouse blood. When using the FACSymphony™, the antibodies were mixed with the blood at a ratio of 1:100, as well in a total reaction volume of 30 µl. After 15 min of stimulation at RT including respective agonists, antibody binding was stopped with 300 µl PBS and measured immediately.

3.4.1.2 Glycoprotein externalisation

Glycoprotein surface expression of GPVI and GPIb on murine platelets was measured by two-colour analysis. Therefore, fluorescence-linked antibodies against the GPVI (JAQ1) and GPIb (Xia.G5) receptor were used. The surface expression of the other glycoproteins was measured separately. Here, antibodies against the integrin α_5 (Tap.A12) and against the integrin β_3 (Luc.H11) receptor were used. The integrin β_3 antibody binds the β_3 subunit of integrin $\alpha_{IIb}\beta_3$. All antibodies against the various

surface glycoproteins were used in a ratio of 1:10 for the measurements on the FACSCalibur™. While the dilution of the antibody directed against the integrin α_5 receptor remained the same for both flow cytometers, all other antibodies were used on the FACSymphony™ at a final dilution of 1:100 in the total reaction volume of 30 µl. After incubation of the blood samples with the respective antibodies for 15 min at RT, antibody binding was stopped with 300 µl PBS and measured directly.

3.4.1.3 AnnexinV-binding of platelets

AnnexinV-binding was used to detect PS exposure on platelets. Therefore, washed murine whole blood was diluted in binding buffer. In both flow cytometers, the AnnexinV antibody was mixed at a ratio of 1:10 in a total reaction volume of 30 µl with whole blood. 300 µl binding buffer was used to stop the reaction after incubation for 20 min at RT.

3.4.1.4 Platelet-aggregates with inflammatory cells

To measure aggregates of platelets with other blood cells, different antibody mixtures were used for two-colour analysis. The GPIb antibody was used for labelling platelets. Furthermore, a Ly6G (1A8) antibody for labelling neutrophils, a CD45 (30-F11) antibody for detecting leukocytes, a CD3 (17A2) antibody for identifying CD3 T-cells, a CD14 (Sa14-2) antibody for labelling monocytes and macrophages and a CD11b (M1/70) antibody for detecting monocytes, macrophages and granulocytes were used. For the FACSCalibur™, the antibodies for the platelet-leukocyte and platelet-neutrophil aggregates were diluted 1:12 (GPIb) and 1:30 (Ly6G and CD45) in a total reaction volume of 30 µl. The final dilution for the platelet antibody was 1:10 and for all other antibodies 1:100 for the FACSymphonie™. Antibody binding was stopped after incubation for 15 min at RT with 300 µl PBS and measured immediately.

3.4.2 Murine platelet preparation

For the preparation of murine platelets, blood collection was performed as described above (see chapter **3.2.2**). In a first centrifugation step, the heparinised blood was centrifuged for 5 min at 250 x g. After transferring the supernatant and interphase to a new reaction tube, a further centrifugation step was performed at 50 x g for 5 min. The whole blood pellet was discarded. After centrifugation, the platelet-rich plasma (PRP) was transferred to a new reaction tube, while the remaining pellet was resuspended in 200 µL of murine Tyrode's buffer. Apyrase [0.02 U/mL] and PGI_2 [0.5 µM] were added in this and all following steps to prevent pre-activation of

platelets. The suspension was centrifuged again at 50 x g for 5 min. The resulting PRP was transferred to the previously collected PRP and centrifuged again at 650 x g for 5 min. Next, the occurring platelet pellet was washed once with 1 ml of Tyrode's buffer supplemented with PGI_2 and apyrase. After discarding the supernatant, the pellet is finally resuspended in 200 µL Tyrode's buffer supplemented with calcium [0.2 mM] to provide proper platelet activation. At the end, the platelet count was determined as described in chapter **3.4.3**.

3.4.3 Blood cell count analysis

Blood cell counts were determined using an automated haematology analyser (Sysmex KX-21N, Sysmex XP-300). For this purpose, blood from PPE mice was collected in heparin, while blood from ePPE mice was collected in EDTA tubes. In this analysis, platelet count, mean platelet volume (MPV), white blood cell (WBC) count and red blood cell (RBC) count were determined. The measurement of platelet count after preparation of mouse platelets was conducted at a dilution of 1:10 in PBS and was necessary to adjust the count for the preparation of platelet releasates (see chapter **3.4.4**).

3.4.4 Murine platelet releasates

For the preparation of platelet releasates, prior isolation of murine platelets (see chapter **3.4.2**) with following determination of the platelet count (see chapter **3.4.3**) is required. A total of 80 x 10^6 platelets/sample were transferred into fresh tubes to analyse the reelin content in platelets. Next, the isolated platelet suspension was centrifuged at 650 x g for 5 min with the addition of apyrase [0.02 U/mL] and PGI_2 [0.5 µM]. The resulting platelet pellet was resuspended in 11 µl murine lysis buffer [1 x] and lysis was performed for 10 min at 4 °C. After vortexing, the samples were centrifuged at 10,000 x g at 4 °C for 5 min. The supernatant was transferred to a new tube, mixed with 3 µl NuPAGE® LDS Sample Buffer and 1 µL dithiothreitol (DTT) and stored at - 70 °C until use.

3.5 Histological and immunofluorescence analysis

3.5.1 Preparation of aortic tissue slides for staining

Following embedding of aortas in paraffin blocks, 5 µm sections were made using a microtome. The sliced 5 µm sections were placed in a pre-heated water bath [37 °C] to smoothen the paraffin including the tissue. The sections were taken with a

microscope slide and heat-fixed overnight at 37 °C on the slide. For staining, the tissue sections were deparaffinised by a descending ethanol series after incubation for 10 min in Roti®Histol. Afterwards, the slides were incubated for 2 min in each ethanol concentration [100%, 96%, 70%].

3.5.2 Hematoxylin and eosin staining of murine aortic tissue

The histological haematoxylin and eosin (H/E) staining is a common technique for differentiating tissue components. Haematoxylin stains ribosomes and nucleic acids blue, while proteins such as collagen and elastin are stained pink by eosin. After deparaffinisation, the tissue was incubated for 10 min in a pure hematoxylin (Mayer's hemalum) solution. The slides were washed briefly in tap water. To remove unspecific background and excess haematoxylin staining from tissue, a differentiation step was performed with a hydrochloric acid-alcohol solution for 30 – 60 sec until only the nuclei remained stained. The slides were then washed again briefly with tap water. To achieve a colour change, bluing was performed under running tap water for 10 min. Finally, the aortic tissue was incubated in eosin solution for 20 sec to stain the surrounding tissue. To finish, the tissue was dehydrated with an ascending ethanol series [70%, 96%, 100%] before incubation in Roti®Histol for further 10 min followed by covering using Roti®Histokit and coverslides. The H/E staining was used to determine aortic wall thickness.

3.5.3 EvG-staining

The Elastica-van-Gieson staining is a trichrome staining method and enables the differentiation between connective tissue and elastic fibres. The Elastica staining solution stains elastin fibres and cell nuclei, while the van Gieson solution differentiates between cytoplasm (yellow) and connective tissue (red). After deparaffinisation of the tissue, the slides were incubated in the Elastica staining solution for 30 min. After a washing step in distilled water for 1 min, the tissue was incubated in a ferric-III-chloride solution for 4 – 5 min to remove unspecific background and excess staining from the tissue. As in H/E staining, a 10 min bluing was performed under running tap water to achieve a colour change. To remove the iodine, the slides were briefly washed in 96% EtOH solution and then in distilled water. This was followed by staining with van Gieson solution for 5 min, before dehydration with 96% EtOH for 1 min and briefly with 100% EtOH. Finally, the tissue was incubated in Roti®Histol for 10 min before being mounted using Roti®Histokit and coverslips. Elastin degradation was assessed using the following classification (**Figure 13**).

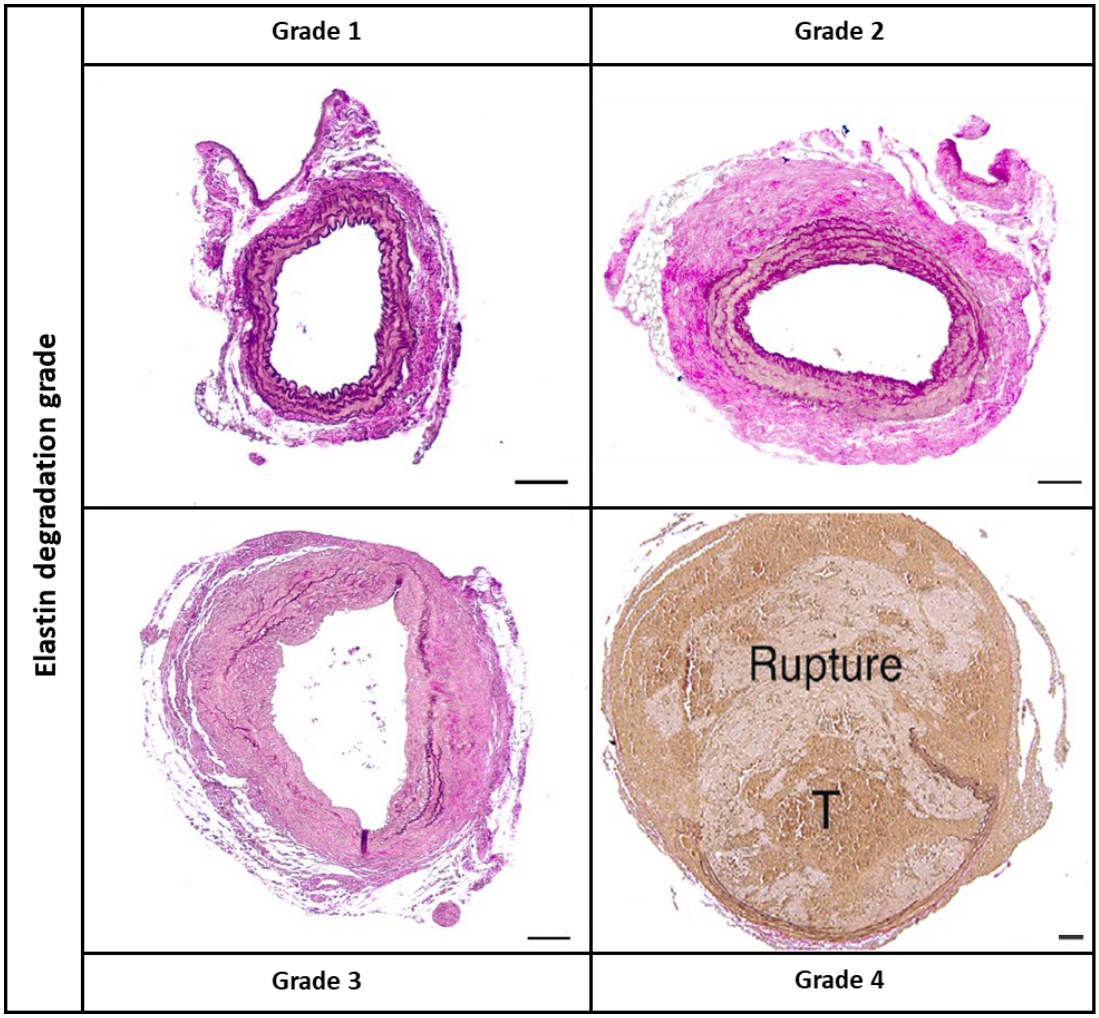

Figure 13. Elastin degradation grade. Exemplary images for the evaluation of elastin degradation grades using EvG staining. Grade 1 = intact elastin fibres without visible breaks. Grade 2 = up to 50% of the elastic fibres are markedly degraded. Grade 3 = elastic fibres partially visible but degraded in more than 50% of the tunica media. Grade 4 = ruptured vessel wall without intact elastic fibres. Scale bar: 50 µm. Image for grade 4 was taken and adapted from Ho *et al*. [125].

3.5.4 Immunofluorescence staining

Immunofluorescence stainings can be used to detect the presence and distribution of specific antigens and proteins by labelling with antibodies. This technique was used to visualise platelets (anti-GPIb), macrophages (anti-Mac3), VSMCs (anti-α-SMA) and apoptotic vascular cells including VSMCs (anti-caspase3). Before starting, the aortic tissue was deparaffinised by a descending ethanol series (see chapter **3.5.1**). The slides were then transferred to citrate buffer and boiled in the microwave for 10 min at 360 W in order to unmask the antigens on the tissue from surrounding paraffin. After cooling in citrate buffer for 30 min, the tissue was washed in PBS for 5 min. All subsequent washing steps were performed three times for 5 min with PBS. To prevent dehydration the slides were transferred into a humid chamber. To block

non-specific binding sites in casp3 and α-SMA staining, a blocking solution (5% goat serum in PBS) with 0.3% Triton for simultaneous permeabilisation of the cell membranes was incubated on the tissue for 1 h at RT. For staining of platelets and macrophages, a specific protein blocking solution (DAKO) was used instead. The respective primary antibodies were diluted (anti-caspase3, anti-α-SMA and, anti-GPIb 1:50; anti-Mac3 1:10) in PBS with 1% goat serum to bind to the target cells/molecules in the tissue. Respective rat IgG and rabbit IgG antibodies were used as IgG controls. The tissue was incubated overnight at 4 °C with the primary antibodies. The next day, the unbound antibodies were washed off with PBS. For staining of the VSMCs (α-SMA) and apoptotic VSMCs (casp3), a donkey anti-rabbit 555 secondary antibody was used. After 1 h of incubation, all unbound antibodies were again washed away with PBS. DAPI [1.67 µg/mL] was used to stain the cell nuclei and incubated on the tissue for 5 min. After a final washing step with PBS, the tissue was covered with coverslips and mounting medium. For platelet and macrophage staining, a streptavidin-biotin complex was used to amplify the signal of the target antigen. The tetrameric streptavidin is able to bind four biotinylated molecules, which enables enhanced signal detection. For this purpose, a biotin-labelled secondary antibody rat anti-mouse was used and incubated for 1 h at RT. Washing with PBS was followed by 30 min incubation with a 660 fluorophore-labelled streptavidin. After washing, the nuclei staining and covering of the tissue was performed as described above. Visualisation of stained tissue was conducted using a Zeiss Observer.D1 miscroscope and the ZEN software (blue edition, version 3.3). This ZEN software was also used for the analysis. For quantification of α-SMA, casp3, GPIb and Mac3 content, the mean fluorescence intensity (MFI) was determined. Thereby, the MFI of each section was normalised to the total area of the aortic tissue.

3.6 Protein biochemical methods

3.6.1 ELISA

In this study, plasma samples were used for the ELISA analyses. Therefore, collected blood in EDTA tubes was centrifuged at 2,500 x g for 5 min at RT. Afterwards, the plasma was transferred to fresh tubes and stored at - 70 °C until use. For the detection of the quantitative concentration of distinct proteins in mouse plasma, respective ELISA kits were used. The concentration of soluble (s)GPVI and glycocalicin were determined using the Mouse Soluble Glycoprotein VI (sGPVI) and the Mouse Glycocalicin ELISA kits from MyBioSource. The Mouse Neutrophil Elastase/ELA2 Quantikine ELISA kit from R&D Systems was used to detect the amount of neutrophil

elastase and the Mouse Osteopontin DuoSet ELISA kit from R&D Systems to detect the plasma concentration of osteopontin (OPN). All ELISA were performed according to the manufacturer's protocol and are based on the principle of the ‘sandwich ELISA technique’. In this technique, a monoclonal primary antibody is pre-fixed on a 96-well microtiter plate. After adding the sample to the plate, this primary antibody binds specifically to the target antigen of the protein contained in the sample. The following polyclonal secondary antibody also binds specifically to the antigen in the sample and is conjugated with a horseradish peroxidase (HRP). This HRP enzyme converts the substrate solution added in the following step. Thereby, an enzymatic colour reaction can be observed in which a blue product is formed. When the stop solution is added to stop the enzymatic reaction, a colour change from blue to yellow occurs. The colour reaction is proportional to the amount of specific antigen in the sample. Finally, the colour intensity was measured photometrically at 450 nm, with a wavelength correction at 540 nm if necessary, using the GloMax microplate reader. Depending on the manufacturer and type of kit, some steps may be performed together.

3.6.2 Gel electrophoresis and wet Western blot transfer

The method of electrophoresis with subsequent Western blot analysis can be used to analyse proteins. In electrophoresis, proteins are separated in an electric field based on their molecular weight and charge. For the separation of proteins in platelet lysates for the analysis of the protein reelin, the NuPage® electrophoresis system with an XCell SureLock™ electrophoresis cell was used. Recombinant Reelin [5 nM] and platelet lysates (see chapter **3.4.4**) from Rln WT, Rln KO, C57BL/6J (WT) and reeler mice were applied to a ready-to-use NuPage® 7% tris-acetate gel. Thereby, 11 µl of the recombinant reelin were also mixed with 3 µl NuPAGE® LDS sample buffer and 1 µl dithiothreitol (DTT). The Precision Plus Protein™ Dual Colour Standards was used as marker to determine the size of the reelin protein. Electrophoresis was performed for about 1.5 h at 40 mA. After electrophoresis, the gel was transferred to a wet-tank transfer system to transfer the size-separated proteins to a suitable membrane. The wet-tank transfer system used for this thesis was the XCell II™ Blot Module in the already before used XCell SureLock™ System. Before stacking the different layers, the nitrocellulose membrane and the blotting pads were soaked in 1 x transfer buffer. The Whatman filter paper was soaked briefly just before use. The blotting system was assembled according to the following scheme, starting from the cathode: two blotting pads, Whatman filter paper, the tris-acetate gel, activated nitrocellulose membrane, Whatman filter paper, two blotting pads. Afterwards, the blotting chamber was assembled by placing the anode core on the cathode core

including layering and placed into the XCell SureLock™ System. In order to ensure this construction was firmly attached, a gel tension wedge was additionally installed and tightened. Finally, the XCell II™ Blot Module is filled with 1 x transfer buffer until the layering including the gel is completely covered. The XCell SureLock™ system is filled with around 650 ml dH_2O. Blotting was carried out overnight for about 16 h at 30 mA and 4 °C. After protein transfer, the membrane was blocked with 5% skimmed milk powder in PBS-T for 1 h at RT. The membrane was then washed three times for 5 min with PBS-T and incubated overnight at 4 °C with the primary antibody. The primary mouse anti-mouse reelin antibody was provided by the AG Korth and was diluted 1:500 in PBS-T with milk powder [5%]. The next day, the membrane was washed three times with TBS-T and incubated with an HRP-conjugated secondary anti-mouse IgG antibody in 5% skimmed milk powder in TBS-T for 1 h at RT. Finally, the membrane was washed again three times with TBS-T and incubated for 1 – 2 min with Immobilon™ Western Chemiluminescent HRP substrate solution (BioRad) to visualise the protein bands. The resulting chemiluminescence signal was detected using a Vilber Fusion-FX6-EDGE V.070 imaging system. As a control, the membrane was then incubated overnight with a rabbit anti-mouse β-actin antibody at 4 °C after the membrane had been washed three times with TBS-T. The next day, the same procedure as the day before was performed with the respective secondary anti-rabbit antibody to visualise the β-actin protein bands.

3.7 Statistical analysis

The number of analysed individuals is indicated as n. As inbred mouse strains were used and the number of independent biological replicates for *in vivo* experiments was low, the statistical analysis was performed based on the normality assumption. In all graphs, the mean value (MW) is shown with the standard error of the mean (± SEM). The statistical analysis for systemic differences in two or more matrices within separate groups was calculated using Graph Pad Prism 8 software (version 8.4.3). In this thesis, two-way ANOVA, followed by the recommended post-hoc test, unpaired student's t-test and unpaired multiple t-test were considered as appropriate and used as described in the respective figure legends. In addition, survival rates were analysed using a log-rank model (Mantel-Cox) and the incidence of AAA in mice using a Fisher's exact test. The non-parametric Spearman correlation was used to determine the correlation between two parameters. All significant differences were labelled with an asterisk in the graphs and categorised as follows: $p \leq 0.05$ = *, $p \leq 0.01$ = **, $p \leq 0.001$ = ***.

4 Results

4.1 Platelet activation and pro-coagulant activity play a central role for the progression of experimental AAA

The classic porcine pancreatic elastase (PPE) mouse model is used to study experimental AAA development and progression. Thereby, the aorta of male wild-type mice (C57Bl/6J) is infused with elastase to induce AAA formation. The resulting degeneration of elastin fibres in the aortic wall induces aneurysmal dilatation, accompanied by inflammation and remodelling of the aortic wall. In this study, the PPE model was used to investigate the impact of platelets on the formation and progression of experimental AAA. Therefore, platelet activation, platelet surface expression of glycoproteins and phosphatidylserine (PS) as well as platelet-aggregate formation with inflammatory cells were analysed in PPE- and sham-operated mice. Furthermore, also blood cell counts and the deposition of the inflammatory and stiffness-related cytokine osteopontin (OPN) into the murine aneurysmal wall were investigated. Overall, these analyses were performed 3, 10 and 28 days after PPE surgery.

4.1.1 Aortic diameter in PPE-operated mice was significantly increased, while platelet count was not altered

In order to verify the efficiency of the recently established PPE mouse model, basic analyses of aortic diameter progression and AAA incidence were performed over a time period of 28 days (**Figure 14 A**). The AAA incidence describes the rate of mice developing an aneurysm. Therefore, in our analyses the threshold was set at 150% of the initial aortic diameter, because an AAA in humans is defined as an enlargement of the aorta by at least 150%. In this context, a significant increased incidence of aneurysm formation was detected in PPE-operated compared to sham-operated mice (sham: 0%; PPE: 66.7%; $p = 0.0053$) (**Figure 14 B**). Ultrasound measurements of the inner aortic diameter during a time course of 28 days after PPE surgery, revealed a mild aortic dilatation (~110%) in sham-operated mice within the first seven days. After this initial growth, the aortic diameter reached a plateau with no further increase. In contrast, the aortic diameter in PPE-operated mice showed persistent growth, reaching the threshold of 150% on day 14. Beginning at day 14, the PPE-operated mice indicated a significantly increased aortic diameter compared to sham-operated mice ($p < 0.001$) (**Figure 14 C** and **D**). On day 28 after surgery, the aorta reached an average inner diameter of 175% ± 6.5% (**Figure 14 D** and **E**).

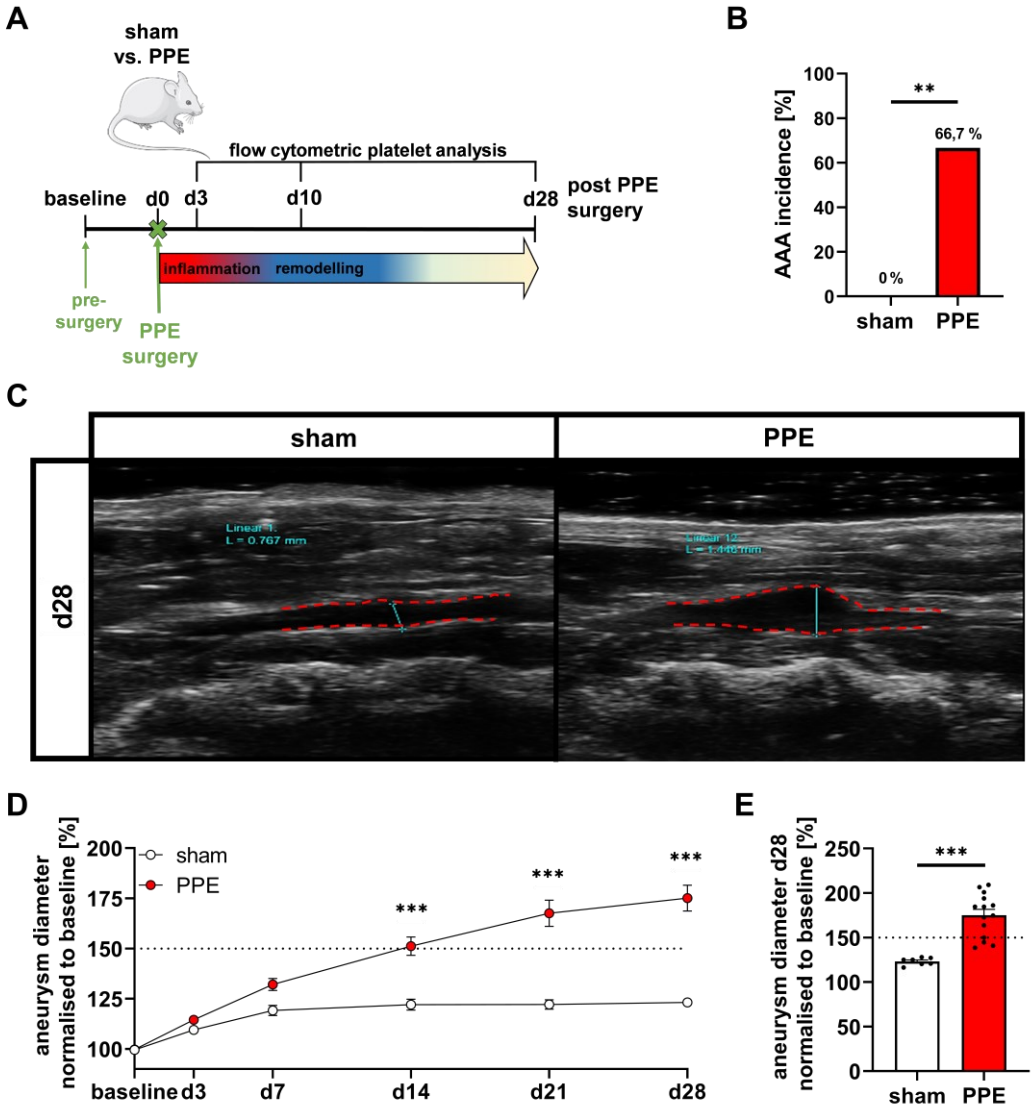

Figure 14. Aortic diameter in PPE-operated mice was significantly increased compared to sham-operated mice. (**A**) Scheme of experimental procedure: C57BL/6J mice underwent elastase treatment upon PPE surgery. As controls, sham-operated mice were treated with sterile $NaCl_2$. The mice were sacrificed at the indicated time points on day 3, 10 and 28. (**B**) AAA incidence of sham- and PPE-operated mice (n = 10 – 15) with an average aortic diameter of > 150% in PPE-operated mice at day 28 after surgery. (**C**) Representative ultrasound images of aneurysm formation 28 days after surgery in sham- and PPE-operated mice. (**D** and **E**) Ultrasound measurements were performed before surgery (baseline) and on day 3, 7, 14, 21 and 28 after surgery (n = 7 – 14). Data were normalised to baseline. All data are represented as mean values ± SEM. Statistical significance was determined by (**B**) Fisher's exact test, (**D**) two-way ANOVA with a Sidak's multiple comparisons post-hoc test and (**E**) an unpaired student's t-test. $^{**}p < 0.01$, $^{***}p < 0.001$. AAA = abdominal aortic aneurysm; PPE = porcine pancreatic elastase (infusion). Data published in Wagenhäuser *et al.*, 2024 [89].

After verifying the efficiency of the PPE surgery, blood cell counts were measured, and a following detailed analysis of platelets was performed. Therefore, blood cell

counts were determined including platelet count (**Figure 15 A**), mean platelet volume (MPV) (**Figure 15 B**) and white blood cell (WBC) count (**Figure 15 C**) on day 3, 10 and 28 after elastase treatment. No differences were found with the exception that increased numbers of WBCs were detected on day 3 in the PPE-operated mice (sham = 5.51 ± 0.61 in 10^3/µL; PPE = 7.34 ± 0.59 in 10^3/µL; p = 0.044).

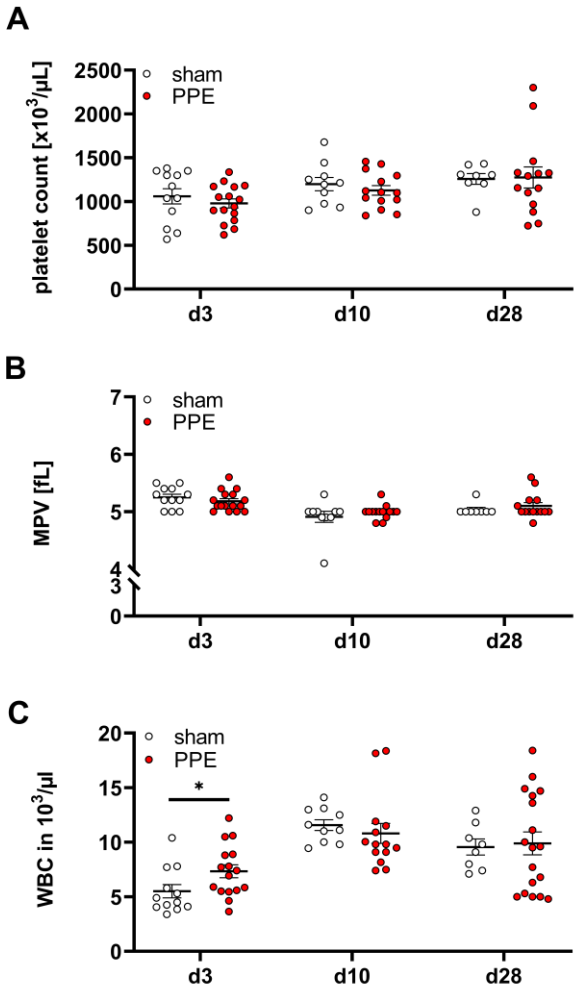

Figure 15. White blood cell (WBC) counts were increased 3 days after PPE surgery. (**A**) Platelet counts, (**B**) MPV and (**C**) the number of WBCs were measured on day 3, 10 and 28 post surgery in whole blood samples of sham- and PPE-operated mice using a haematology analyser (n = 8 – 16). Data are represented as mean values ± SEM. Statistical significance was determined by an unpaired multiple t-test. *p < 0.05. MPV = mean platelet volume; PPE = porcine pancreatic elastase (infusion); WBC = white blood cell. Data partially published in Wagenhäuser *et al.*, 2024 [89].

For the analysis of basal platelet function, the expression of surface receptors was examined. In this context, detection of integrin α_5 (**Figure 16 A**) and integrin β_3 expression on the platelet surface on day 3 (**Figure 16 B**), 10 (**Figure 16 C**), and 28 (**Figure 16 D**) showed no differences between sham- and PPE-operated mice under

resting conditions. Only under mild stimulation with CRP [0.1 µg/mL] PPE-operated mice displayed a significant decrease in integrin β_3 externalisation on day 3 after surgery (sham: 114.88 ± 3.33 MFI; PPE: 100.08 ± 3.89 MFI; p = 0.017) (**Figure 16 B**).

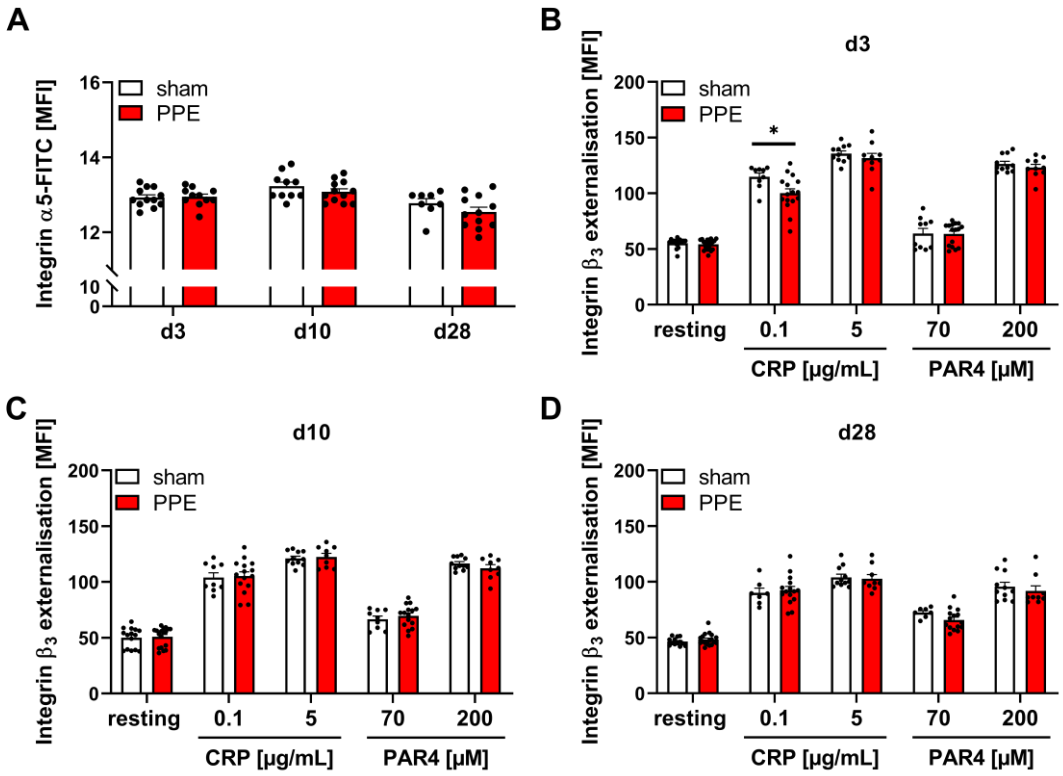

Figure 16. Integrin β_3 externalisation on the platelet surface in PPE-operated mice was altered upon mild CRP stimulation 3 days after surgery. Surface exposure of (**A**) integrin α_5 and (**B** – **D**) integrin β_3 on the platelet surface under resting conditions and upon stimulation with indicated agonists (n = 8 – 12) were measured in whole blood samples of sham- and PPE-operated mice at day 3, 10 and 28 after surgery. Data were obtained by flow cytometric analyses and were represented as mean ± SEM. Statistical significance was determined by an unpaired multiple t-tests. *p < 0.05. CRP = collagen-related peptide; MFI = mean fluorescence intensity; PAR4 = protease-activated receptor 4 activating peptide; PPE = porcine pancreatic elastase (infusion). Data published in Wagenhäuser *et al.*, 2024 [89].

In addition, the expression of the two glycoproteins (GP) GPIb and GPVI, which are crucial for haemostasis, was measured. Thereby, no differences in GPVI surface exposure but an enhanced GPIb exposition on the platelet surface in whole blood samples of PPE-operated mice were observed 3 days post surgery (sham: 61.4 ± 3.91 MFI; PPE: 72.68 ± 3.39 MFI; p = 0.039) (**Figure 17 A** and **C**). In addition, the plasma concentration of soluble (s)GPVI and GPIb was determined. Thereby, no difference in the sGPVI concentration was detected between sham- and ePPE-operated mice on day 28 after surgery (**Figure 17 B)**. In contrast, glycocalicin,

the soluble form of GPIb, was found to be increased in PPE-operated mice (sham: 0.8918 ± 0.09 µg/mL; PPE: 1.340 ± 0.14 µg/mL; p = 0.027) on day 28 after surgery (**Figure 17 D**).

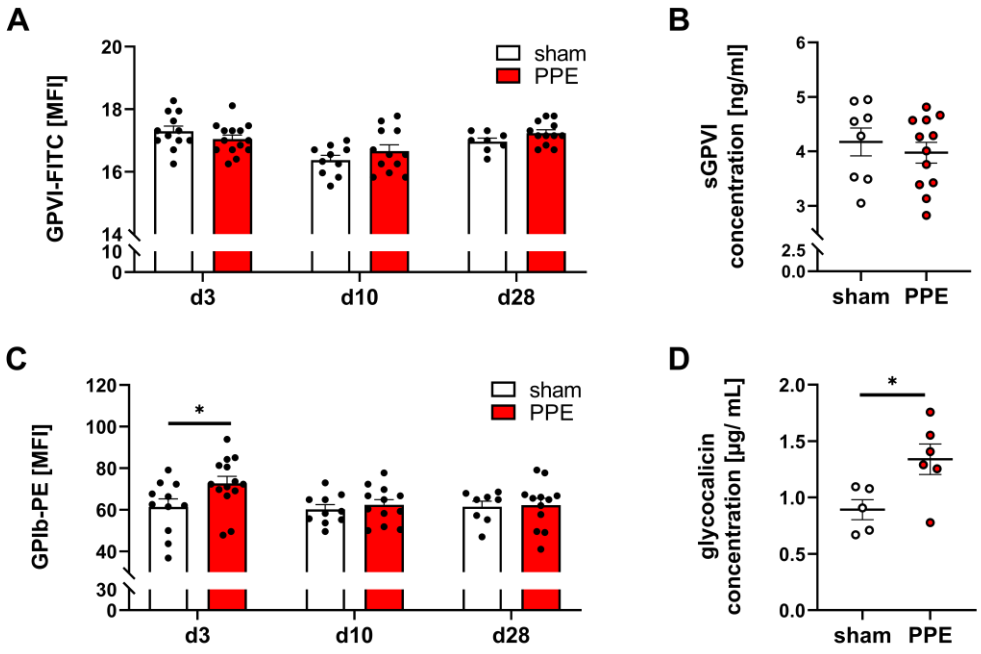

Figure 17. Soluble GPIb, glycocalicin, showed elevated plasma level. (**A**) GPVI and (**C**) GPIb exposure on platelet surface were determined on day 3, 10 and 28 after PPE surgery in PPE- and sham-operated mice using whole blood samples in flow cytometry (n = 8 – 14). Plasma levels of (**B**) sGPVI (n = 8 – 12) and (**D**) glycocalicin (n = 5 – 6) were measured via ELISA 28 days after PPE surgery. Data are represented as mean ± SEM. Statistical significance was determined by (**A** and **C**) unpaired multiple t-tests and (**B** and **D**) unpaired student's t-test. *p < 0.05. GP = glycoprotein; MFI = mean fluorescence intensity; PPE = porcine pancreatic elastase (infusion); sGPVI = soluble GPVI.

4.1.2 Platelet activation and pro-coagulant activity were enhanced in late stages of aneurysm formation

Another important aspect of analysing platelets is the investigation of platelet activation and degranulation. Thereby, decreased platelet degranulation (P-selectin-FITC) after stimulation of the PAR4 receptor 3 days after surgery was observed in PPE-operated mice (PAR4 [70 µM]: p = 0.015). The integrin $\alpha_{IIb}\beta_3$ activation (JON/A-PE) was reduced as well (PAR4 [70 µM]: p = 0.0008; PAR4 [100 µM]: p = 0.0072) (**Figure 18 A**). On day 10 after surgery no differences were detected (**Figure 18 B**). In contrast, on day 28 after surgery platelet degranulation (P-selectin-FITC) and integrin $\alpha_{IIb}\beta_3$ activation (JON/A-PE) upon stimulation of the GPVI receptor were increased in PPE-operated mice

(*P-selectin*: CRP [0.1 µg/mL]: p = 0.028; CRP [5 µg/mL]: p = 0.0059; *JON/A*: CRP [0.1 µg/mL]: p = 0.042) (**Figure 18 C**).

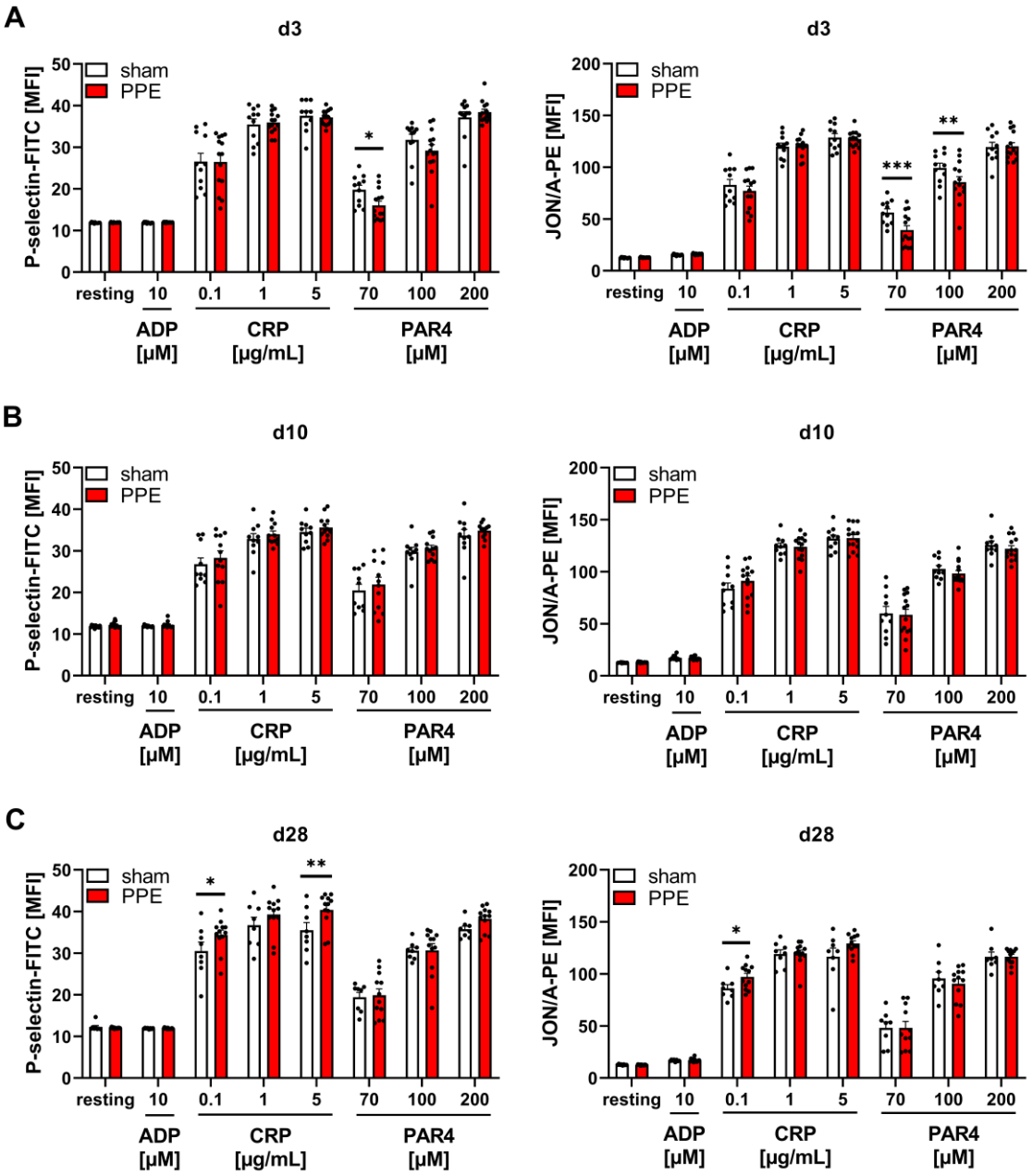

Figure 18. Platelet activation was increased in late stages of aneurysm progression. Platelet degranulation (P-selectin-FITC) and integrin $\alpha_{IIb}\beta_3$ activation (JON/A-PE) were measured in whole blood of sham- and PPE-operated mice (**A**) 3, (**B**) 10 and (**C**) 28 days after surgery via flow cytometry. Platelets were stimulated with indicated agonists (n = 8 – 14). Data are represented as mean ± SEM. Statistical significance was determined by unpaired multiple t-tests. *p < 0.05, **p < 0.01, ***p < 0.001. ADP = adenosine diphosphate; CRP = collagen-related peptide; MFI = mean fluorescence intensity; PAR4 = protease-activated receptor 4 activating peptide; PPE = porcine pancreatic elastase (infusion). Data published in Wagenhäuser *et al.*, 2024 [89].

Measurements of phosphatidylserine (PS) exposure on the platelet surface through AnnexinV binding is used for the analysis of platelet pro-coagulant activity. Since PS exposure promotes the assembly of essential coagulation factor complexes required for the conversion of pro-thrombin into thrombin [126], the pro-coagulant activity is crucial for thrombus formation. In this context, an increased AnnexinV-binding to platelets was observed in whole blood of PPE-operated mice on day 28 after surgery (sham: 100 ± 16.8%; PPE: 177.02 ± 23.98%; $p = 0.039$) (**Figure 19 C**). On day 3 and 10 after surgery, no changes in AnnexinV-binding were detected (**Figure 19 A** and **B**). In addition, a weak but significant correlation between PS exposure on the platelet surface and the aneurysm diameter was found using Spearman's correlation, based on data measured on day 3 and 28 after surgery (R = 0.3229; $p = 0.045$) (**Figure 19 D**).

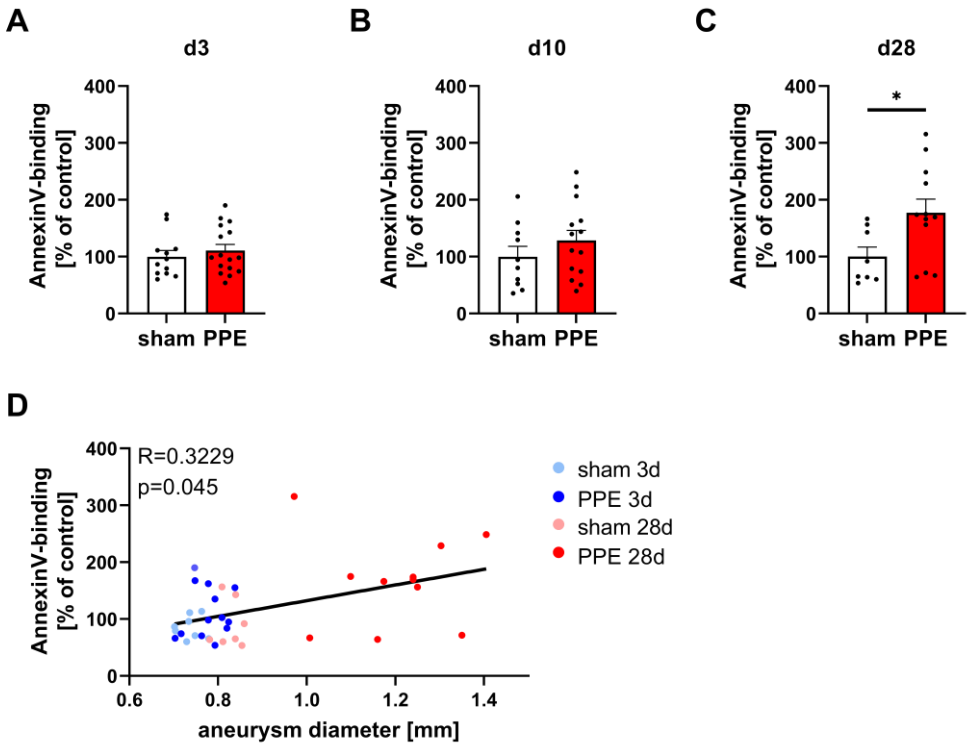

Figure 19. Pro-coagulant activity of platelets correlated with aortic diameter progression. AnnexinV-binding of platelets in whole blood samples of sham- and PPE-operated mice was measured on days (**A**) 3, (**B**) 10 and (**C**) 28 after surgery using flow cytometry ($n = 8 – 16$). Data are represented as percent of control. (**D**) A Spearman's correlation between AnnexinV-binding to platelets and aneurysm diameter was performed using data from day 3 and 28 after PPE surgery ($n = 8 – 16$). Statistical significance was determined by (**A** – **C**) unpaired student's t-test. *$p < 0.05$. PPE = porcine pancreatic elastase (infusion). Data published in Wagenhäuser *et al.*, 2024 [89].

4.1.3 Inflammation was enhanced in early stages of aneurysm formation

Furthermore, platelet-aggregate formation with circulating inflammatory cells were analysed. Thereby, increased formation of platelet ($CD42b^+$)- neutrophil ($Ly6G^+$)-aggregates could be detected at day 3 after PPE surgery in whole blood of PPE-operated mice compared to sham-operated control mice (sham: 39.84 ± 3.36%; PPE: 55.9 ± 1.47%; $p = 0.002$) (**Figure 20 B**). Analysis of platelet ($CD42b^+$)-leukocyte ($CD45^+$)-conjugates revealed no alteration between PPE- and sham-operated mice (**Figure 20 A**).

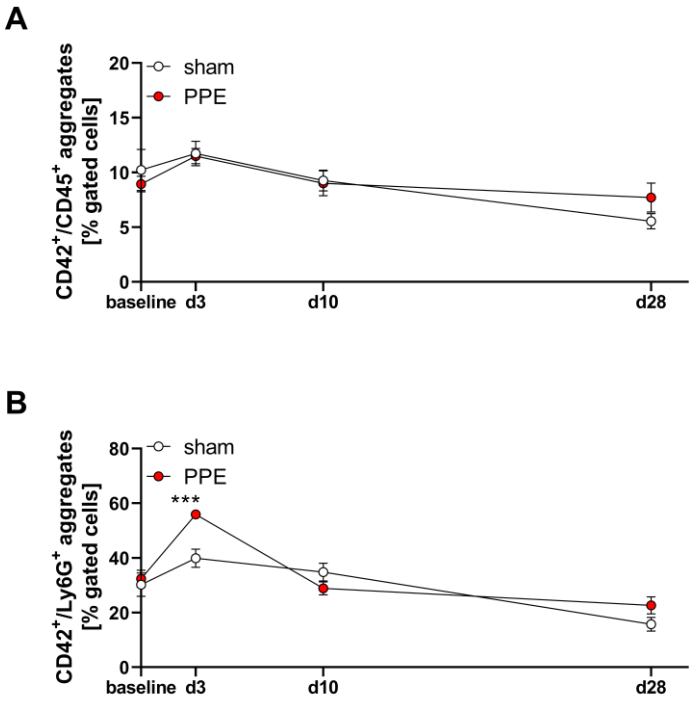

Figure 20. Formation of platelet-neutrophil aggregates was enhanced in early stages of aneurysm growth. (**A**) Platelet-leukocyte and (**B**) platelet-neutrophil aggregate formation were determined before (baseline), and on day 3, 10 and 28 after surgery using whole blood samples of sham- and PPE-operated mice ($n = 4 – 6$). Data are represented as percent of double-positive events for CD42b (platelet maker, GPIbα) and CD45 (leukocyte marker) or Ly6G (neutrophil marker). Statistical significance was determined by two-way ANOVA with Sidak's multiple comparison test. ***$p < 0.001$. PPE = porcine pancreatic elastase (infusion). Data published in Wagenhäuser *et al.*, 2024 [89].

In following experiments, the inflammatory and matricellular protein osteopontin (OPN) was analysed. Therefore, immunofluorescence staining and an ELISA were performed on day 28 after PPE surgery to detect OPN in aortic wall tissue and in the plasma of mice. Compared to aortic tissue of control mice, PPE-operated mice showed a strongly enhanced amount of OPN in the aortic wall (naive: 209.1 ± 41.72 MFI; PPE: 646.8 ± 137.4 MFI; $p = 0.0062$) (**Figure 21 A and B,**

Appendix Figure 54). In contrast, the plasma concentration of OPN revealed no differences between sham- and PPE-operated mice 28 days after surgery as detected by ELISA (**Figure 21 C**).

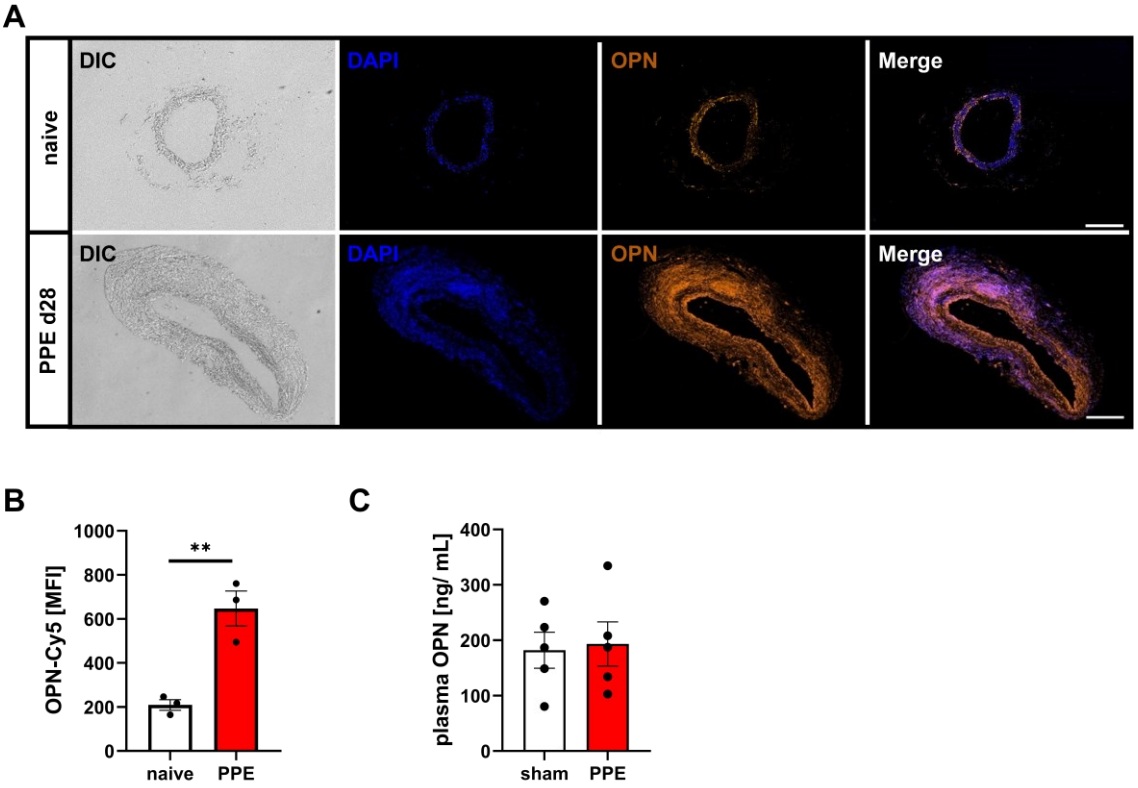

Figure 21. The inflammatory protein OPN was increased in aortic tissue of PPE-operated mice in late stages of aneurysm formation. (**A**) Representative immunofluorescent images and (**B**) quantification of OPN in aortic wall tissue from naive and PPE-operated mice 28 days after surgery. The aortic tissue was specifically stained for OPN (anti-OPN, orange), nuclei were stained with DAPI (blue) (*n* = 3). (**C**) Plasma concentrations of OPN in sham- and PPE-operated mice (*n* = 5) on day 28 after surgery, as detected by ELISA. Data are represented as mean ± SEM. Statistical significance was determined by unpaired student's t-tests. $^{**}p < 0.01$. Scale bar: 100 µm. DIC = differential interference contrast; DAPI = 4′,6-diamidino-2-phenylindole; MFI = mean fluorescence intensity; OPN = osteopontin; PPE = porcine pancreatic elastase (infusion). Data partially published in Wagenhäuser *et al.*, 2024 [89].

The previous conducted experiments revealed enhanced platelet activation, pro-coagulant activity and inflammation in mice that underwent PPE surgery. These processes are known to promote AAA formation. In addition, the soluble form of one of the most important platelet receptors, GPIb (glycocalicin), which is crucial for vWF binding upon vessel injury, showed increased plasma concentrations in mice after treatment with PPE.

4.2 Effect of platelet-specific loss of reelin on aneurysm formation

The extracellular matrix protein reelin, which was originally found to be produced by Cajal-Retzius cells in the brain during early brain development, also occurs in cells of adult organisms such as neurons, blood and liver cells. [33, 39]. Previous publications have shown that reelin is also present in blood in platelets, where it is stored in α-granules [59]. It is also known that reelin promotes CVDs such as atherosclerosis or arterial thrombosis by the modulation of platelet signalling pathways [53, 60, 61]. Therefore, the role of platelet-derived reelin on AAA formation should be investigated in this work by using mice with platelet-specific genetic reelin deletion. For this purpose, newly generated and genetically modified Rln WT (*Rln*$^{fl/fl}$*; PF4-cre*$^{-}$) and Rln KO (*Rln*$^{fl/fl}$*; PF4-cre*$^{+}$) mice were used for the experiments. These Rln WT and Rln KO mice underwent PPE surgery and were analysed for blood cell counts, platelet activation, surface expression of glycoproteins, aggregate formation and PS exposure 7 and 28 days after surgery. In addition, histological H/E and EvG stainings were performed to investigate the impact of reelin on aortic wall remodelling on day 28 post surgery. Moreover, alpha-smooth muscle actin (α-SMA) and caspase 3 (casp3) within the aneurysm segment were stained using specific immunofluorescence staining to analyse the content of vascular smooth muscle cells (VSCM) and cell apoptosis in the aortic wall 28 days post surgery.

4.2.1 Platelet- and aortic-specific characteristics were not affected by the genotype of the Rln KO mice

As the mouse strain was newly generated in our laboratory, initial measurements were performed with naive mice to obtain basic data on specific platelet and aortic parameters. Using ultrasound measurements, the aortic diameter of naive Rln WT and Rln KO was determined and no differences were observed (**Figure 22 A**). Similarly, when measuring blood cell counts including platelet count, MPV and WBC, no differences were detected between Rln WT and Rln KO mice (**Figure 22 B**).

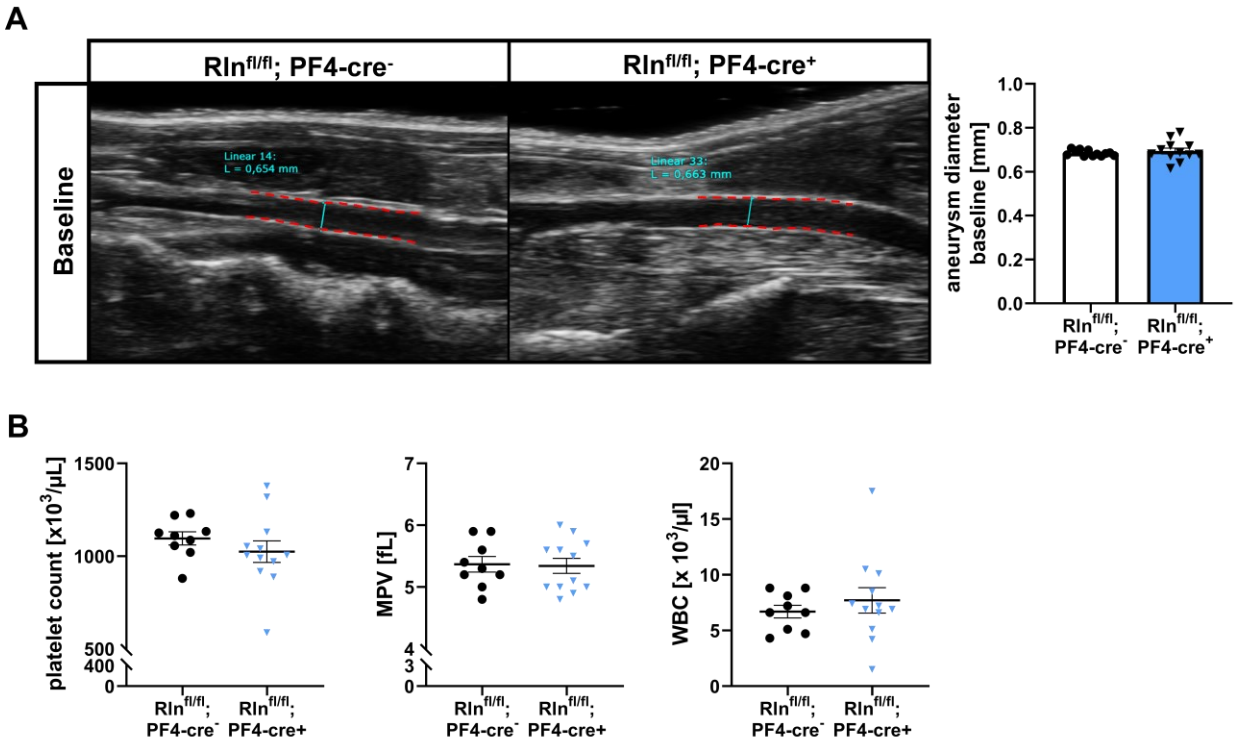

Figure 22. Aortic diameter and blood cell counts in naive Rln KO mice were not altered compared to WT controls. (**A**) Representative ultrasound images of the aortic diameter of naive Rln WT (*Rln$^{fl/fl}$; PF4-cre^{-}*) and Rln KO (*Rln$^{fl/fl}$; PF4-cre^{+}*) mice (*n* = 12). (**B**) Blood cell counts including platelet count, MPV and the number of WBCs were determined with a haematology analyser using whole blood samples from Rln WT and Rln KO mice (*n* = 9 – 12). Data are represented as mean values ± SEM. Statistical significance was determined by unpaired student's t-tests. KO = knockout; MPV = mean platelet volume; Rln = reelin; WBC = white blood cell; WT = wild-type.

A more detailed analysis of platelets, in which platelet degranulation (P-selectin-FITC) (**Figure 23 A**) and integrin $\alpha_{IIb}\beta_3$ activation (JON/A-PE) (**Figure 23 B**) were measured, revealed no differences in the activation profile of reelin-deficient platelets under resting conditions, as well as after stimulation with different agonists.

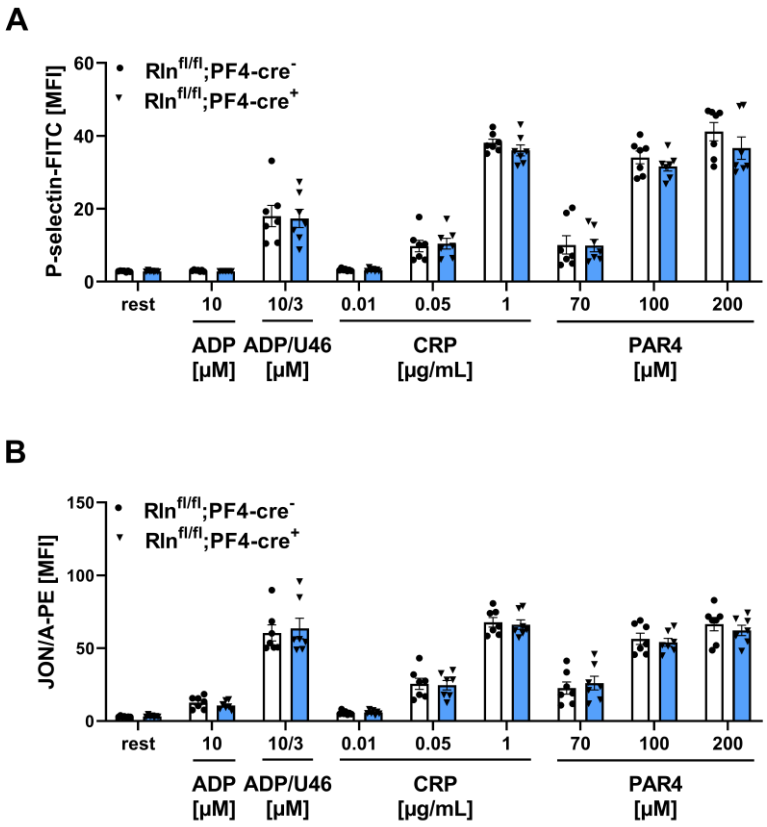

Figure 23. Platelet activation and degranulation was unaltered in naive Rln KO mice. (**A**) Platelet degranulation (P-selectin-FITC) and (**B**) integrin $\alpha_{IIb}\beta_3$ activation (JON/A-PE) were measured in whole blood samples of Rln WT (*Rln$^{fl/fl}$; PF4-cre$^-$*) and Rln KO (*Rln$^{fl/fl}$; PF4-cre$^+$*) mice using flow cytometry. Platelets were stimulated with indicated agonists (n = 5 – 7). Data are represented as mean values ± SEM. Statistical significance was determined by unpaired multiple t-tests. ADP = adenosine diphosphate; CRP = collagen-related peptide; KO = knockout; MFI = mean fluorescence intensity; PAR4 = protease-activated receptor 4 activating peptide; Rln = reelin; U46619 (U46) = thromboxane A_2 analogue; WT = wild-type.

Furthermore, the glycoprotein surface expressions showed no differences between naive Rln WT and Rln KO mice (**Figure 24 A**). Also in aggregate formation of platelets with inflammatory cells such as leukocytes and neutrophils (**Figure 24 B**) and pro-coagulant activity of platelets (**Figure 24 C**) no differences between naive Rln WT and Rln KO mice could be detected.

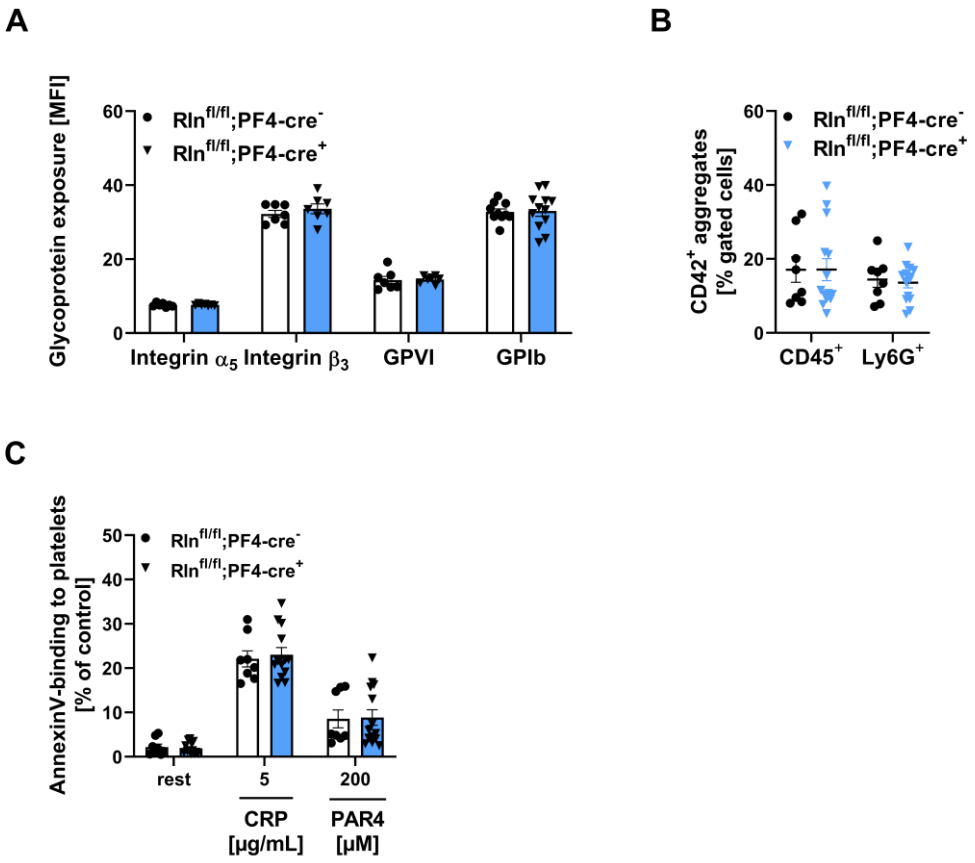

Figure 24. Glycoprotein expression, aggregate formation of platelets and leukocytes, and pro-coagulant activity in naive Rln KO were not altered. (**A**) Surface exposure of integrin α_5, integrin β_3, GPVI and GPIb on platelets (n = 7 – 12), (**B**) platelet-leukocyte and platelet-neutrophil aggregate formation (n = 8 – 14) and (**C**) AnnexinV-binding to platelets (n = 8 – 14) were measured in whole blood of Rln WT (*Rln$^{fl/fl}$; PF4-cre^{-}*) and Rln KO (*Rln$^{fl/fl}$; PF4-cre^{+}*) mice using flow cytometry. For aggregate formation (**B**), double-positive events for CD42b (platelet maker, GPIbα) and CD45 (leukocyte marker) or Ly6G (neutrophil marker) were detected. Data are represented as mean values ± SEM. Statistical significance was determined by unpaired multiple t-tests. CRP = Collagen-related peptide; GP = glycoprotein; MFI = mean fluorescence intensity; PAR4 = Protease-activated receptor 4 activating peptide; Rln = reelin.

To identify the impact of platelet-derived reelin on the aortic wall structure, aortic-specific parameters were analysed. Thereby, the intima/media thickness (**Figure 25 A**) as well as the degree of elastin degradation within the aortic media (**Figure 25 B**) were investigated showing no alterations between both groups**.**

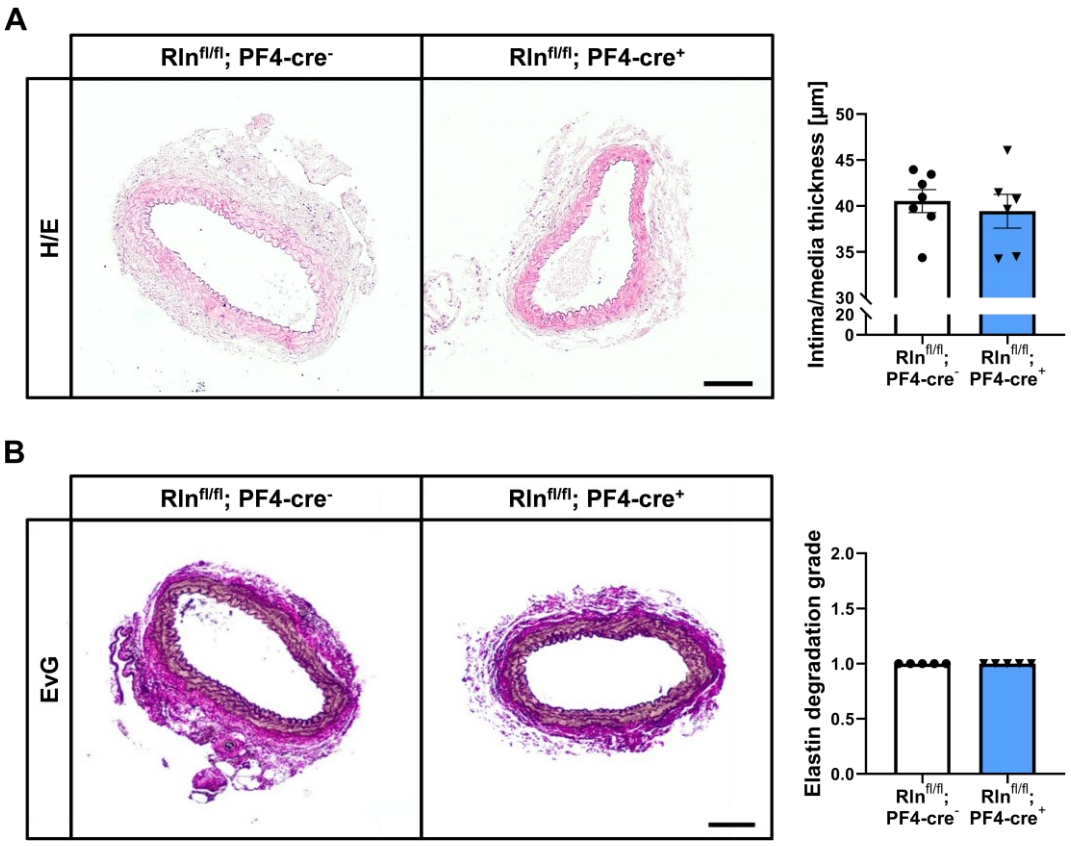

Figure 25. Aortic wall structure in naive Rln KO mice was unaltered compared to Rln WT mice. Representative images of histological (**A**) H/E staining (n = 6 – 7) including the evaluation of the intima/media thickness and (**B**) EvG staining (n = 5) with evaluated elastin degradation grade of aortic tissue of Rln WT (*Rln$^{fl/fl}$; PF4-cre^{-}*) and Rln KO (*Rln$^{fl/fl}$; PF4-cre^{+}*) mice. Data are represented as mean values ± SEM. Statistical significance was determined by an unpaired student's t-test. Scale bar: 100 µm. EvG = Elastica-van-Gieson; H/E = Haematoxylin-eosin; KO = knockout; Rln = reelin; WT = wild-type.

These results in naive mice indicate that differences in platelet- and aortic-specific parameters in Rln WT and Rln KO mice that might be detected after PPE surgery are not caused by their genetic modification.

4.2.2 Platelet-derived reelin did not alter experimental induced AAA formation during a time course of 28 days

To investigate the effect of reelin on aneurysm formation after PPE surgery, Rln WT and Rln KO mice were analysed 28 days after elastase treatment (**Figure 26 A**). Measurements of aortic diameter showed no differences at day 28 after surgery (**Figure 26 B** and **C**). In addition, the incidence of aneurysm formation (> 150%) was unaltered in both groups (Rln WT: 76.9%; Rln KO: 58.3%; $p = 0.41$) (**Figure 26 D**).

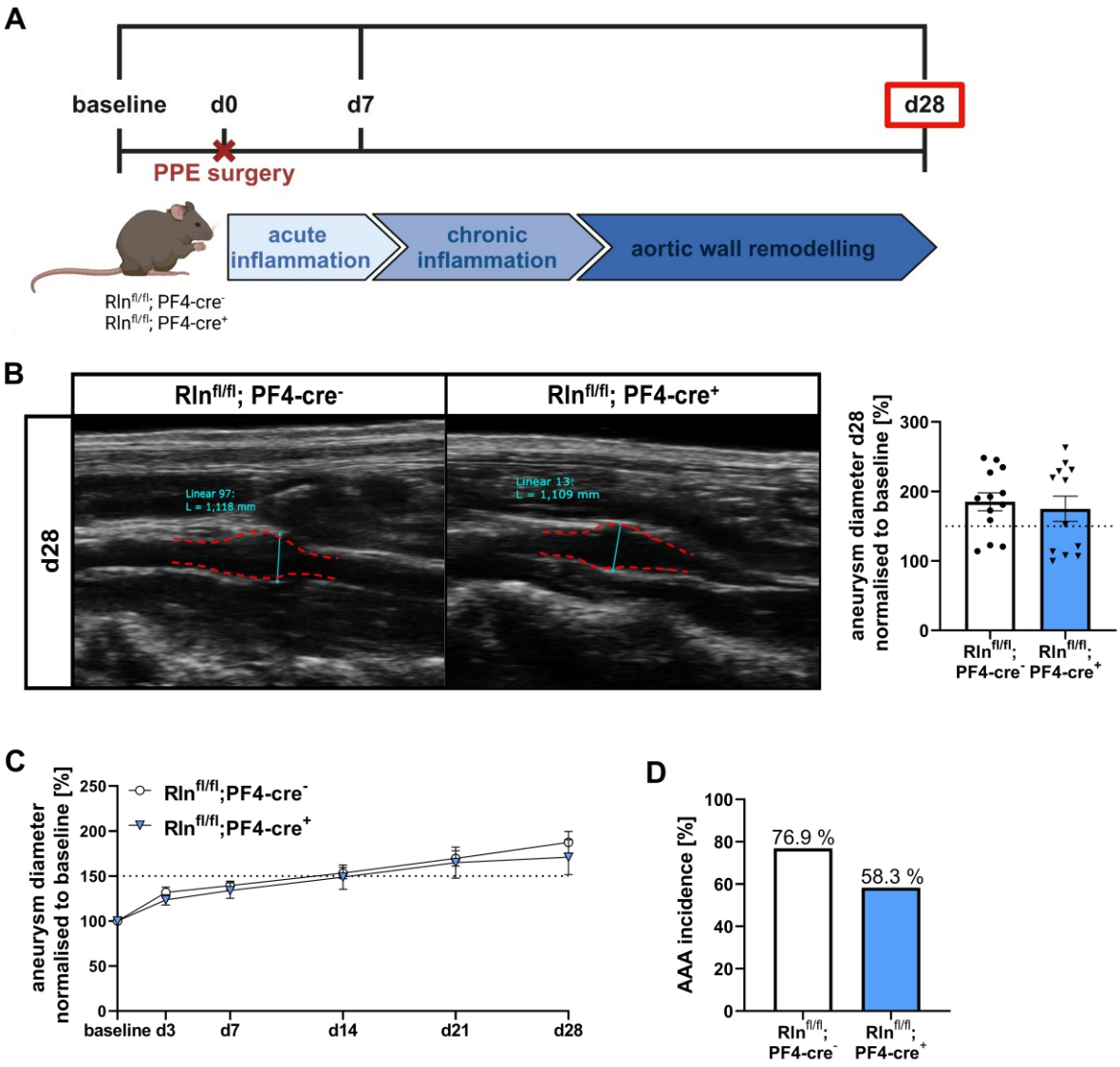

Figure 26. Platelet-specific reelin deficiency did not alter experimental induced aortic diameter progression. (**A**) Scheme of experimental procedure: Rln WT (*Rln$^{fl/fl}$; PF4-cre^{-}*) and Rln KO (*Rln$^{fl/fl}$; PF4-cre^{+}*) mice were analysed for 28 days after PPE surgery. (**B**) Representative ultrasound images and evaluation of aortic diameter of Rln WT and Rln KO (n = 12 – 13) mice 28 days after PPE surgery. (**C**) To investigate aneurysm diameter, ultrasound measurements were performed before surgery (baseline) and on day 3, 7, 14, 21 and 28 after surgery (n = 10 – 14). (**D**) AAA incidence of sham- and PPE-operated mice (n = 12 – 13) show percentage of mice with an aortic diameter of > 150% 28 days after surgery. Data are represented as mean values ± SEM. Statistical significance was

determined by (**B**) an unpaired student's t-test, (**C**) two-way ANOVA with a Sidak's multiple comparisons post-hoc test and (**D**) a Fisher's exact test. AAA = abdominal aortic aneurysm; KO = knockout; PPE = porcine pancreatic elastase (infusion); Rln = reelin; WT = wild-type.

The determination of blood cell counts including platelets, their MPV and WBCs (**Figure 27 A - C**) revealed no differences between Rln WT and Rln KO mice 28 days after PPE surgery.

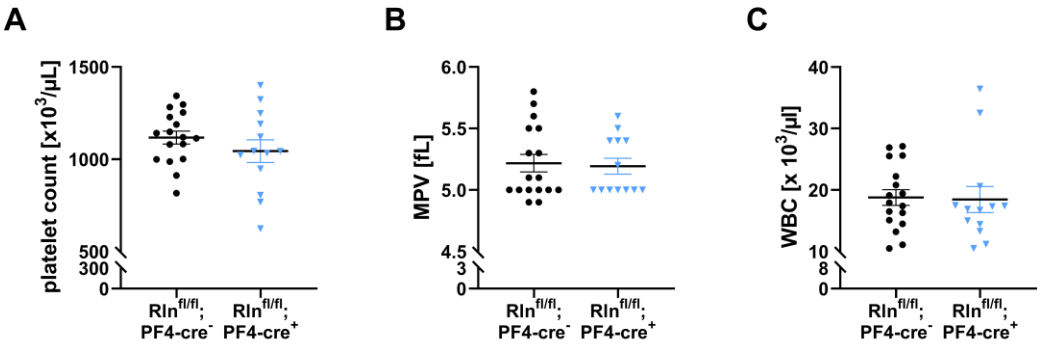

Figure 27. Platelet-specific reelin deficiency showed no effects on blood cell counts 28 days after PPE surgery. Blood cell counts including (**A**) platelet count, (**B**) MPV and (**C**) number of WBCs were determined with a haematology analyser using whole blood samples of Rln WT (*Rln$^{fl/fl}$; PF4-cre^{-})* and Rln KO (*Rln$^{fl/fl}$; PF4-cre^{+}*) mice (*n* = 13 – 17). Data are represented as mean values ± SEM. Statistical significance was determined by unpaired student's t-tests. KO = knockout; MPV = mean platelet volume; Rln = reelin; WBC = white blood cell; WT = wild-type.

For a detailed analysis, platelets were examined by flow cytometric analyses. Thereby, platelet degranulation (P-selectin-FITC) (**Figure 28 A**) and integrin $\alpha_{IIb}\beta_3$ activation (JON/A-PE) (**Figure 28 B**) showed no differences in Rln WT and Rln KO mice 28 days after PPE surgery.

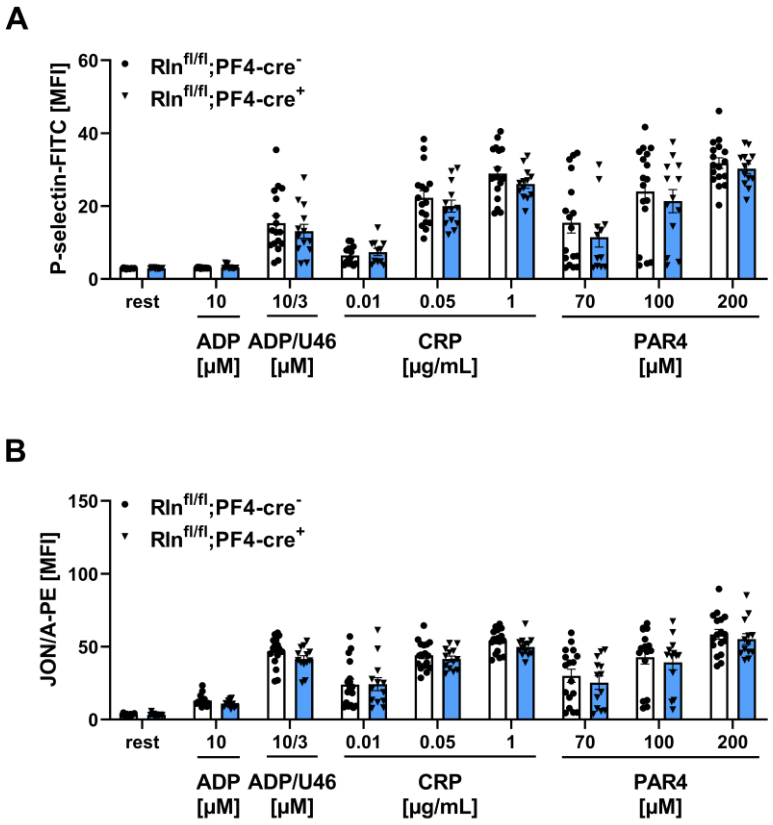

Figure 28. Platelet-specific reelin deficiency had no effect on platelet degranulation and activation at day 28 post PPE surgery. (**A**) Platelet degranulation (P-selectin-FITC) and (**B**) integrin $\alpha_{IIb}\beta_3$ activation (JON/A-PE) were measured in whole blood samples of Rln WT (*Rln$^{fl/fl}$; PF4-cre^{-}*) and Rln KO (*Rln$^{fl/fl}$; PF4-cre^{+}*) mice using flow cytometry. Platelets were stimulated with indicated agonists (*n* = 11 – 17). Data are represented as mean values ± SEM. Statistical significance was determined by unpaired multiple t-tests. ADP = adenosine diphosphate; CRP = collagen-related peptide; KO = knockout; MFI = mean fluorescence intensity; PAR4 = protease-activated receptor 4 activating peptide; Rln = reelin; U46619 (U46) = thromboxane A_2 analogue; WT = wild-type.

In addition, platelet glycoprotein exposure (**Figure 29 A**), the formation of aggregates of platelets with inflammatory cells such as leukocytes and neutrophils (**Figure 29 B**) and the pro-coagulant activity of platelets (**Figure 29 C**) showed no differences between Rln WT and Rln KO mice at day 28 day after PPE surgery.

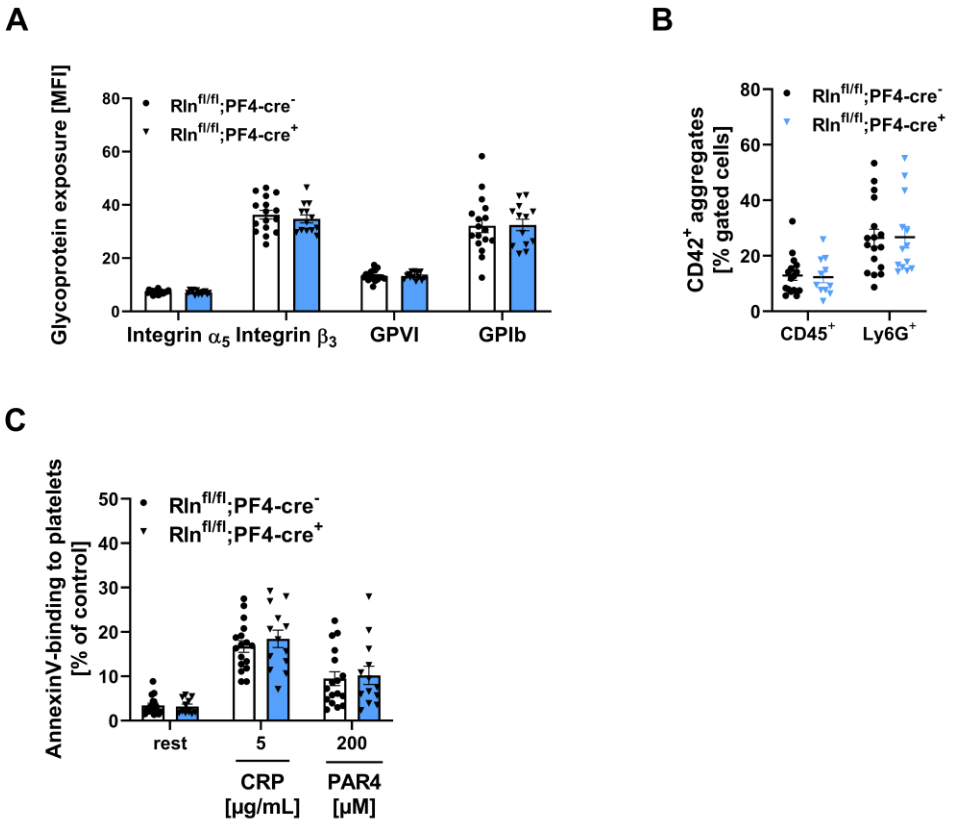

Figure 29. Platelet-specific reelin deficiency exerted no effect on glycoprotein exposure, aggregate formation and pro-coagulant activity 28 days after PPE surgery. (**A**) Surface exposure of integrin α_5, integrin β_3, GPVI and GPIb on platelets (n = 13 – 17), (**B**) platelet-leukocyte as well as platelet-neutrophil aggregate formation (n = 11 – 17) and (**C**) AnnexinV-binding to platelets (n = 11 – 17) were analysed in whole blood samples of Rln WT (*Rln$^{fl/fl}$; PF4-cre^{-}*) and Rln KO (*Rln$^{fl/fl}$; PF4-cre^{+}*) mice. (**B**) For the detection of aggregate formation, double-positive events for CD42b (platelet maker, GPIbα) and CD45 (leukocyte marker) or Ly6G (neutrophil marker) were measured. Data are represented as mean values ± SEM. Statistical significance was determined by unpaired multiple t-tests. CRP = collagen-related peptide; GP = glycoprotein; KO = knockout; MFI = mean fluorescence intensity; PAR4 = protease-activated receptor 4 activating peptide; Rln = reelin; WT = wild-type.

Apart from analysing the aortic diameter and different platelet-specific parameters, the aortic structure and remodelling of the extracellular matrix (ECM) were studied in Rln WT and Rln KO mice 28 days after PPE surgery. Therefore, H/E staining was performed (**Figure 30 A**) to determine the intima/media thickness, which is not different between both groups (**Figure 30 B**). There is also no correlation between aneurysm size and aortic wall thickness 28 days after elastase treatment (r = 0.09; *p* = 0.70) (**Figure 30 C)**.

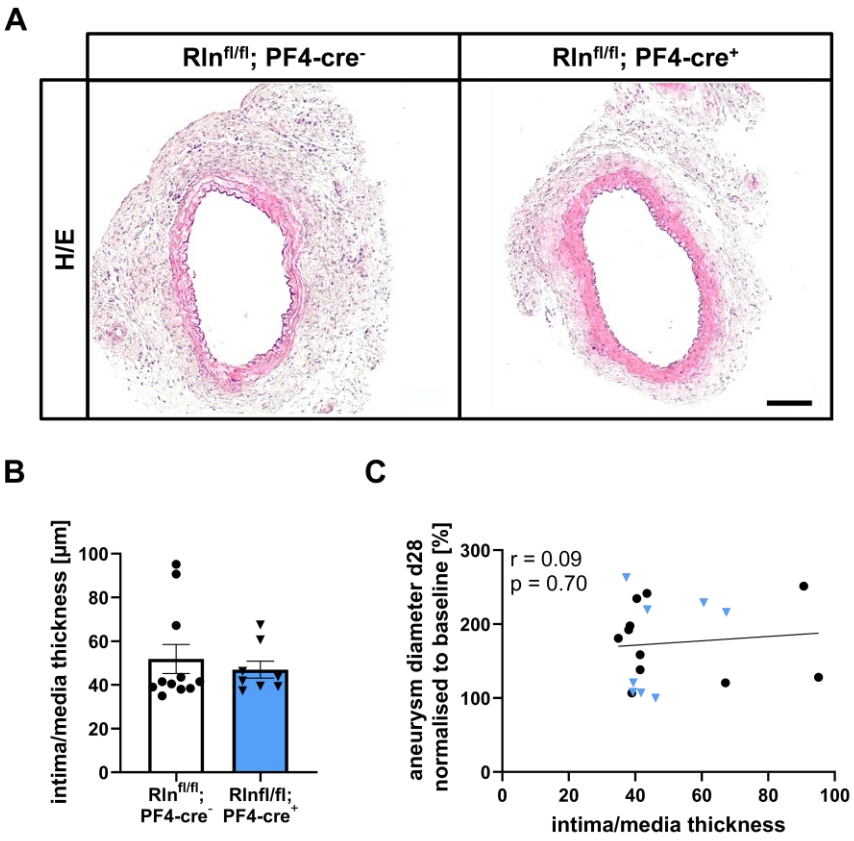

Figure 30. Platelet-specific reelin deficiency revealed no effect on aortic wall thickness at day 28 after PPE surgery. (**A**) Representative images of histological H/E stainings, (**B**) evaluation of the intima/media thickness (*n* = 8 – 11) and (**C**) Spearman's correlation between intima/media thickness and the aneurysm diameter (*n* = 8 – 11) at day 28 post PPE surgery of Rln WT (*Rln$^{fl/fl}$; PF4-cre^{-}*) and Rln KO (*Rln$^{fl/fl}$; PF4-cre^{+}*) mice. Data are represented as mean values ± SEM. Statistical significance was determined by an unpaired student's t-test. Scale bar: 100 µm. H/E = haematoxylin-eosin; KO = knockout; Rln = reelin; WT = wild-type.

The evaluation of the EvG staining (**Figure 31 A**) showed no differences in elastin degradation between Rln WT and Rln KO mice 28 days after PPE surgery (**Figure 31 B**). There is only a weak correlation between the aneurysm size and the degree of elastin degradation that does not reach statistical significance (r = 0.22; *p* = 0.30) (**Figure 31 C**).

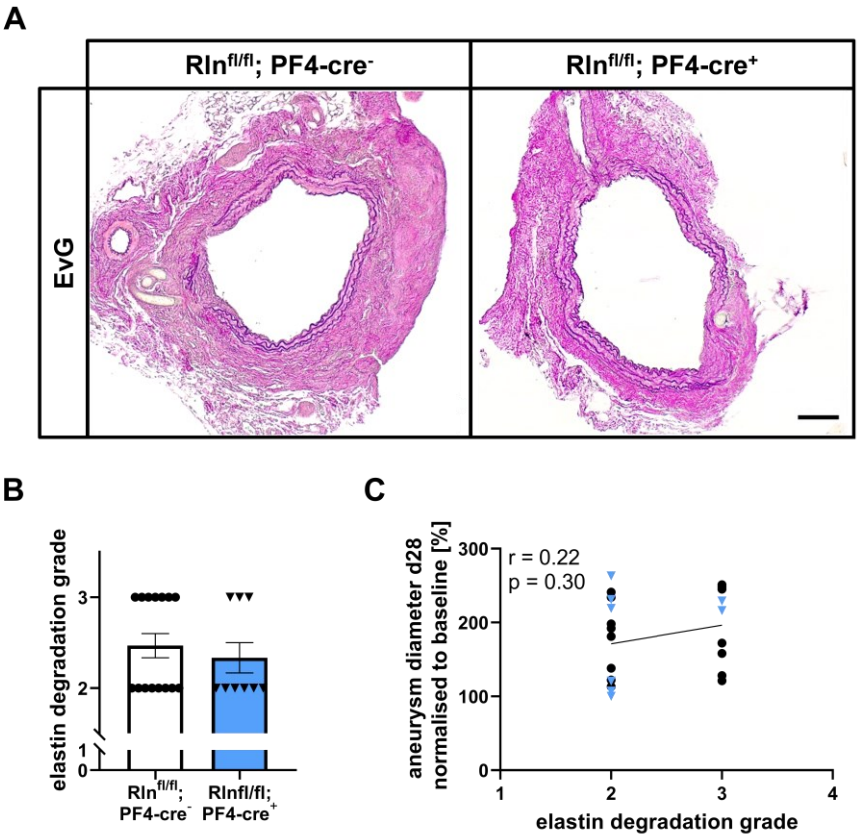

Figure 31. Platelet-specific reelin deficiency showed no effects on elastin degradation 28 days post PPE surgery. (**A**) Representative images of histological EvG staining and (**B**) evaluation of elastin degradation (*n* = 9 – 15). (**C**) Spearman's correlation between elastin degradation grade and the aneurysm diameter (*n* = 9 – 15) at day 28 post PPE surgery of Rln WT (*Rln$^{fl/fl}$; PF4-cre^{-}*) and Rln KO (*Rln$^{fl/fl}$; PF4-cre^{+}*) mice. Elastin degradation grade was categorised as described in **chapter 3.5.3**. Data are represented as mean values ± SEM. Statistical significance was determined by an unpaired student's t-test. Scale bar: 100 µm. EvG = Elastica-van-Gieson; KO = knockout; Rln = reelin; WT = wild-type.

To further analyse the progressive remodelling of the abdominal aortic wall, specific immunofluorescence staining of vascular smooth muscle cells (VSMC) was conducted, as apoptosis of VSMCs is described to be a characteristic feature of AAA. Therefore, immunofluorescence staining of α-SMA (**Figure 32 A,** *Appendix Figure 55*) was performed. Quantification of the α-SMA content within the aortic tissue of PPE-operated Rln WT and Rln KO mice revealed no alterations between both groups at day 28 post surgery (**Figure 32 B**). However, there is a weak correlation between aneurysm size and α-SMA content in the aortic wall without statistical significance (r = 0.38; *p* = 0.08) (**Figure 32 C**).

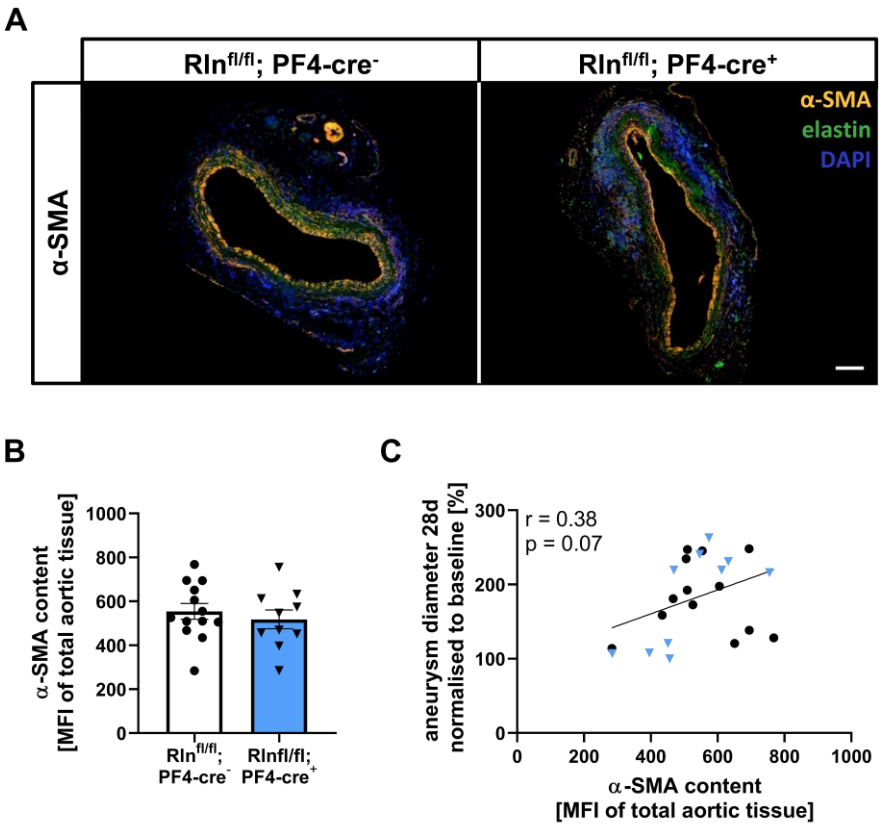

Figure 32. Platelet-specific reelin deficiency exhibited no effects on the aortic α-SMA content at day 28 post PPE surgery. (**A**) Representative images of immunofluorescence α-SMA staining with (**B**) quantification of the α-SMA content in the aortic wall of Rln WT (*Rln$^{fl/fl}$; PF4-cre^{-}*) and Rln KO (*Rln$^{fl/fl}$; PF4-cre^{+}*) mice (*n* = 10 – 13), specifically stained for α-SMA (anti-α-SMA, orange) and nuclei (DAPI, blue). Elastin fibres are shown by autofluorescence (green). (**C**) Spearman's correlation between α-SMA content and the aneurysm diameter (*n* = 10 – 13) at day 28 post PPE surgery of Rln WT and Rln KO mice. Data are represented as mean values ± SEM. Statistical significance was determined by an unpaired student's t-test. Scale bar: 100 µm. α-SMA = alpha smooth muscle cell actin; DAPI = 4′,6-diamidino-2-phenylindole; KO = knockout; MFI = mean fluorescence intensity; Rln = reelin; WT = wild-type.

In addition to the α-SMA content as a marker for VSMC abundance, caspase3 (casp3) can be used as an indicator for apoptosis of cells including VSMCs. Therefore, immunofluorescence staining for caspase3 was performed (**Figure 33 A,** *Appendix Figure 55*) indicating no differences between Rln WT and Rln KO mice with regard to caspase3 positive cells within the aortic tissue (**Figure 33 B**). Nevertheless, a weak correlation was found between the aneurysm diameter and the caspase3 content (r = 0.26; *p* = 0.46) (**Figure 33 C**).

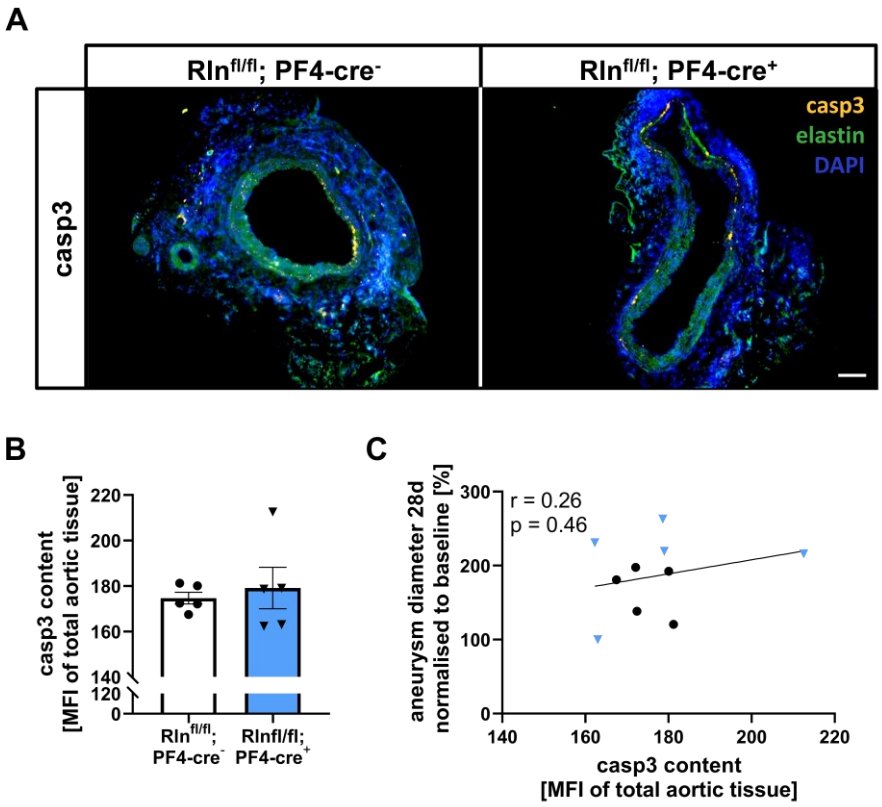

Figure 33. Platelet-specific reelin deficiency revealed no effects on the aortic caspase3 content 28 days post PPE surgery. (**A**) Representative images of immunofluorescence caspase3 staining with (**B**) quantification of caspase3 in the aortic wall (*n* = 5). Images were specifically stained for caspase 3 (anti-casp3, orange) and nuclei (DAPI, blue). Elastin fibres are shown by autofluorescence (green). (**C**) Spearman's correlation between the caspase3 content and the aneurysm diameter (*n* = 5) at day 28 post PPE surgery of Rln WT (*Rln$^{fl/fl}$; PF4-cre^{-}*) and Rln KO (*Rln$^{fl/fl}$; PF4-cre^{+}*) mice. Data are represented as mean values ± SEM. Statistical significance was determined by an unpaired student's t-test. Scale bar: 100 µm. Casp3 = caspase 3; DAPI = 4′,6-diamidino-2-phenylindole; KO = knockout; MFI = mean fluorescence intensity; Rln = reelin; WT = wild-type.

In conclusion, the results of Rln WT and Rln KO mice 28 days after PPE surgery indicated that platelet-specific reelin has no impact on aneurysm formation. Neither platelet-specific parameters nor ECM remodelling, including elastin degradation and VSMC apoptosis, were affected.

4.2.3 Platelet-specific reelin reduced aortic diameter progression in early stages of aneurysm formation

Although reelin showed no apparent effects on ECM remodelling and therefore on aneurysm formation after 28 days, Rln WT and Rln KO mice were also examined 7 days after PPE surgery to further investigate the impact of reelin on AAA related inflammation (**Figure 34 A**). Measurements of the aortic diameter revealed a significant decrease in Rln KO mice on day 7 after PPE surgery (Rln WT: 140.1 ± 20.16%; Rln KO: 112.9 ± 4.74%; p = 0.0062) (**Figure 34 B** – **D**).

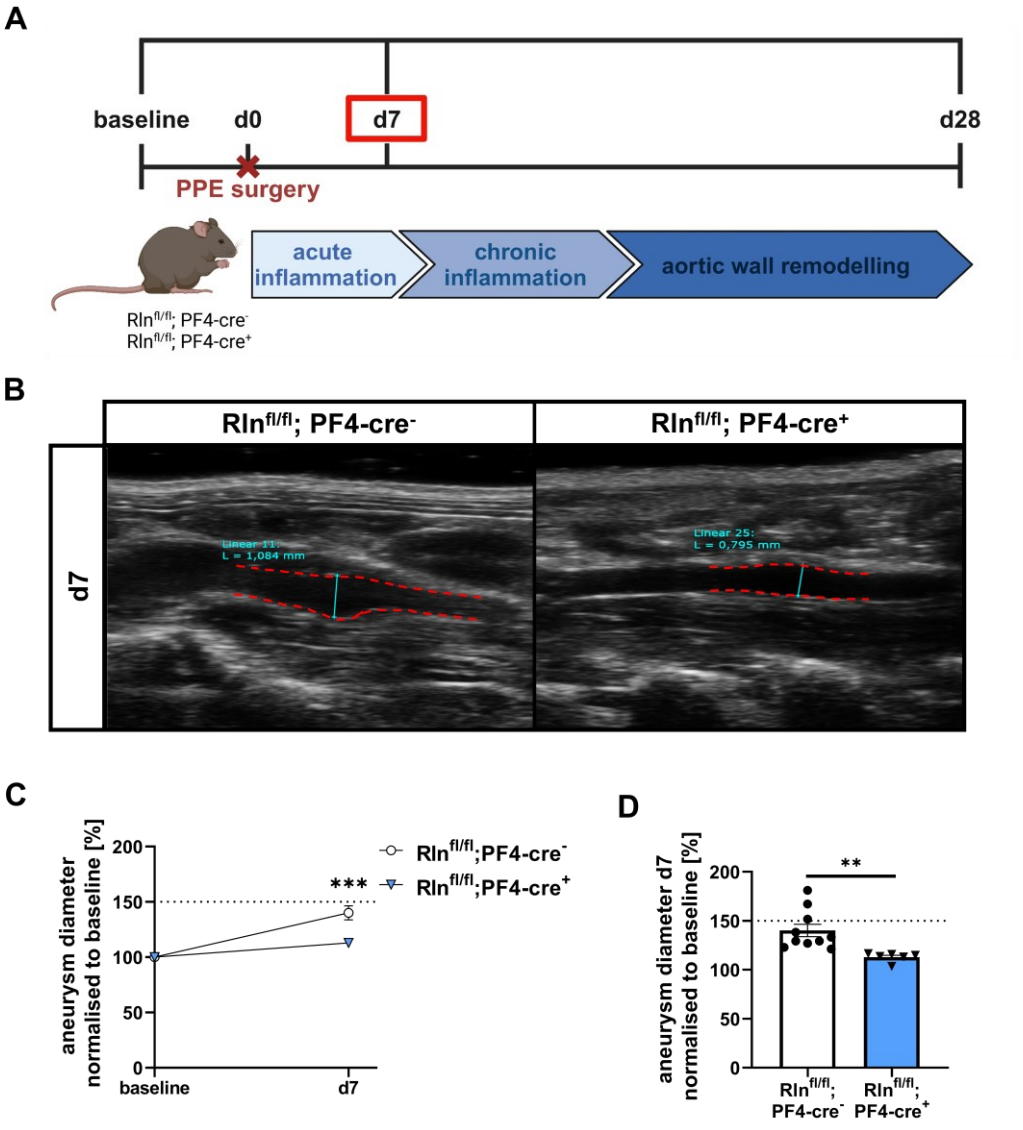

Figure 34. Platelet-specific reelin deficiency showed reduced aneurysm formation 7 days after PPE surgery. (**A**) Scheme of the experimental procedure: Rln WT (*Rln$^{fl/fl}$; PF4-cre^{-}*) and Rln KO (*Rln$^{fl/fl}$; PF4-cre^{+}*) mice were analysed at day 7 after PPE surgery. (**B**) Representative ultrasound images of the aortic diameter of Rln WT and Rln KO mice 7 days after PPE surgery. (**C**) For examination of aneurysm diameter, ultrasound measurements were performed before surgery (baseline) and on day 7 after surgery (n = 6 – 10). (**D**) Aneurysm diameter on day 7 after PPE surgery normalised to baseline

(*n* = 6 – 10). Data are represented as mean values ± SEM. Statistical significance was determined by (**C**) two-way ANOVA with a Sidak's multiple comparisons post-hoc test and (**D**) an unpaired student's t-test. $^{**}p < 0.01$, $^{***}p < 0.001$. KO = knockout; PPE = porcine pancreatic elastase (infusion); Rln = reelin; WT = wild-type.

Despite the reduced aortic diameter progression in an early stage of AAA formation, no differences in blood cell counts, including platelet count (**Figure 35 A**), MPV (**Figure 35 B**) and WBC count (**Figure 35 C**), were detected.

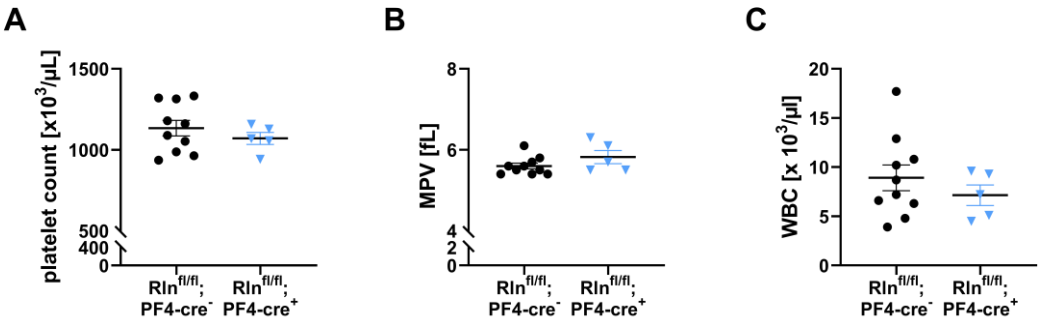

Figure 35. Platelet-specific reelin deficiency exhibited no effects on blood cell count 7 days after PPE surgery. Blood cell counts including (**A**) platelet count, (**B**) MPV and (**C**) WBC count were determined in whole blood of Rln WT (*Rln$^{fl/fl;}$ PF4-cre^{-}*) and Rln KO (*Rln$^{fl/fl;}$ PF4-cre^{+}*) mice (*n* = 5 – 10) using a haematology analyser. Data are represented as mean values ± SEM. Statistical significance was determined by unpaired student's t-tests. KO = knockout; MPV = mean platelet volume; Rln = reelin; WBC = white blood cell; WT = wild-type.

After the initial analysis of the aortic diameter progression and blood cell counts, flow cytometric analyses were performed to obtain more detailed insights into the platelet activation profile in early AAA formation. Thereby, measurements of platelet degranulation (P-selectin-FITC) 7 days after surgery revealed a reduced P-selectin exposure of reelin-deficient platelets under resting conditions (Rln WT: 3.04 ± 0.043 MFI; Rln KO: 2.80 ± 0.062 MFI; $p = 0.0066$). In contrast, Rln KO mice exhibit an increased degranulation after stimulation with ADP/U46 (Rln WT: 10.80 ± 0.76 MFI; Rln KO: 13.71 ± 1.06 MFI; $p = 0.040$) and a high concentration of CRP, stimulating the collagen receptor GPVI (Rln WT: 32.45 ± 2.15 MFI; Rln KO: 39.06 ± 2.41 MFI; $p = 0.081$) (**Figure 36 A**). In addition, integrin $\alpha_{IIb}\beta_3$ activation (JON/A-PE) is increased upon CRP stimulation in Rln KO mice on day 7 after elastase treatment (Rln WT: 54.76 ± 1.57 MFI; Rln KO: 62.78 ± 3.58 MFI; $p = 0.031$) (**Figure 36 B**).

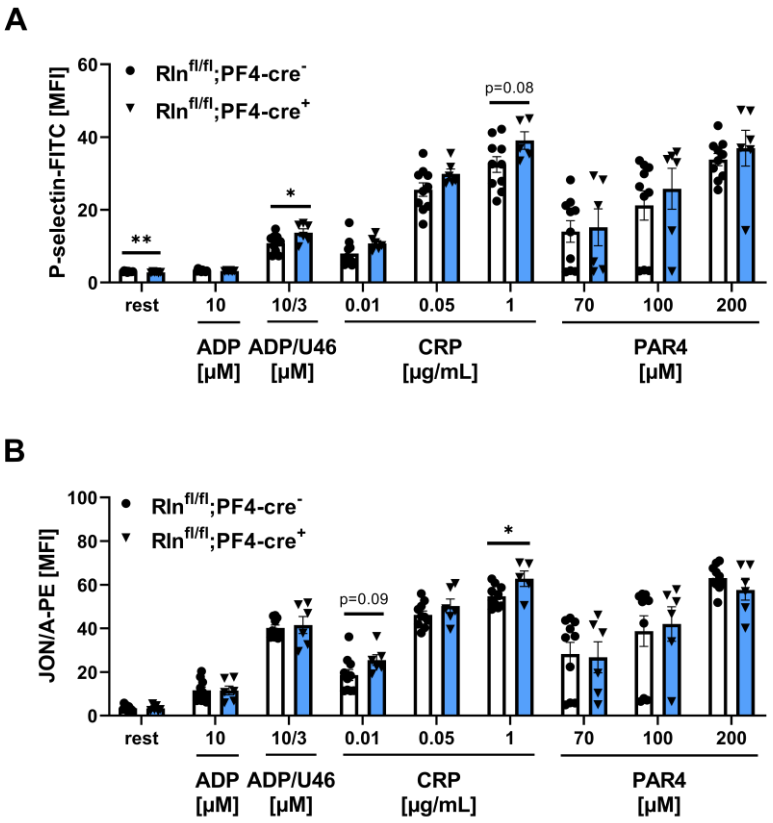

Figure 36. Reelin-deficient platelets showed reduced degranulation under resting conditions, but an increased integrin $\alpha_{IIb}\beta_3$ activation and degranulation upon stimulation in early AAA formation. (**A**) Platelet degranulation (P-selectin-FITC) and (**B**) activation of integrin $\alpha_{IIb}\beta_3$ (JON/A-PE) were measured in whole blood samples of Rln WT (*Rln$^{fl/fl}$; PF4-cre^{-}*) and Rln KO (*Rln$^{fl/fl}$; PF4-cre^{+}*) mice by flow cytometry. Platelets were stimulated with indicated agonists ($n = 5 – 10$). Data are represented as mean values ± SEM. Statistical significance was determined by unpaired multiple t-tests. *$p < 0.05$, **$p < 0.01$. ADP = adenosine diphosphate; CRP = collagen-related peptide; KO = knockout; MFI = mean fluorescence intensity; PAR4 = protease-activated receptor 4 activating peptide; Rln = reelin; U46619 (U46) = thromboxane A_2 analogue; WT = wild-type.

In addition, further platelet-specific parameters were examined using flow cytometry using whole blood of Rln WT and Rln KO mice. The analysis of the exposition of various glycoproteins at the cell surface revealed no differences in reelin-deficient platelets on day 7 after PPE surgery (**Figure 37 A**). In contrast, pro-coagulant activity in Rln KO mice is enhanced upon CRP stimulation (Rln WT: 8.57 ± 1.75%; Rln KO: 15.6 ± 2.54%; p = 0.034), while PAR4 stimulation (Rln WT: 9.85 ± 1.37%; Rln KO: 4.68 ± 0.29%; p = 0.021) causes a reduction in Rln KO mice (**Figure 37 B**). As a marker for platelet-mediated inflammation, the aggregate formation of platelets with circulating inflammatory cells was analysed. Thereby, less aggregate formation with neutrophils was observed on day 7 after PPE surgery with reelin-deficient platelets (Rln WT: 31.53 ± 2.14%; Rln KO: 21.06 ± 3.95%; p= 0.023) (**Figure 37 C**). Nevertheless, the concentration of neutrophil elastase in the plasma was not different in reelin-deficient compared to control WT mice (**Figure 37 D**).

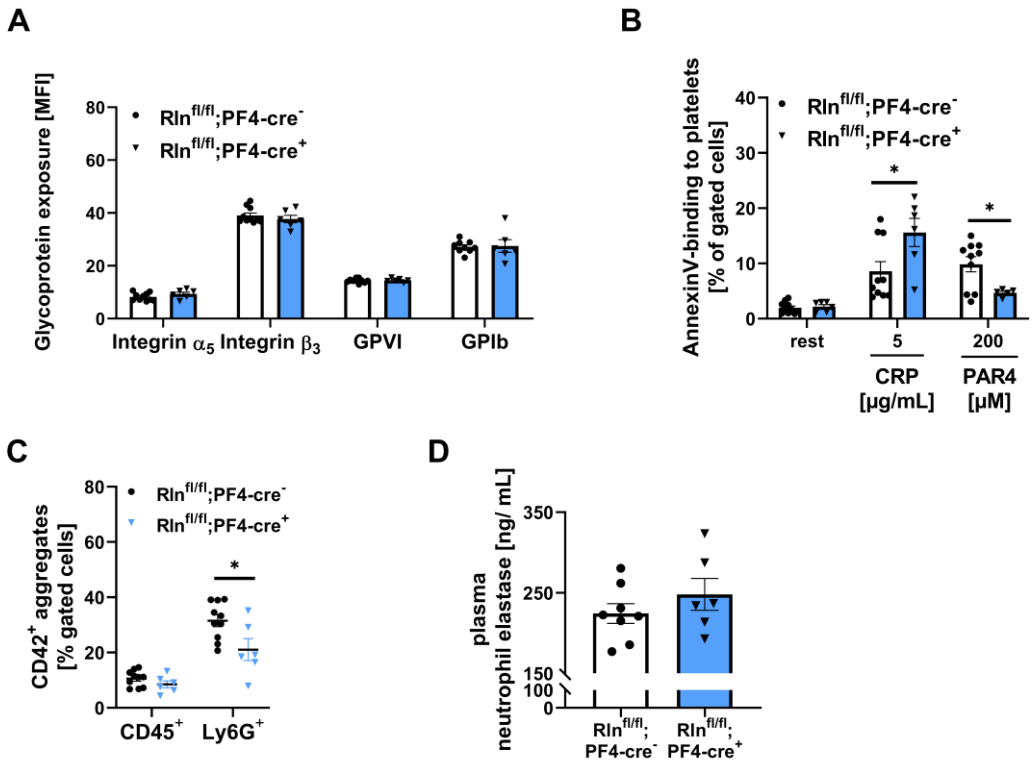

Figure 37. Platelet-specific reelin deficiency revealed altered pro-coagulant activity and decreased platelet-neutrophil aggregate formation 7 days after PPE surgery. (**A**) Surface exposure of integrin α_5, integrin β_3, GPVI and GPIb on platelets (n = 6 – 10). (**B**) AnnexinV-binding to platelets (n = 5 – 10) and (**C**) platelet-leukocyte and platelet-neutrophil aggregate formation (n = 6 – 10) were measured in whole blood samples of Rln WT (*Rln$^{fl/fl}$; PF4-cre^{-}*) and Rln KO (*Rln$^{fl/fl}$; PF4-cre^{+}*) mice using flow cytometry. (**B**) For aggregate formation, double-positive events for CD42b (platelet maker, GPIbα) and CD45 (leukocyte marker) or Ly6G (neutrophil marker) were analysed. (**D**) Measurement of plasma concentration of neutrophil elastase was performed via ELISA (n = 6 – 8). Data are represented as mean values ± SEM. Statistical significance was determined by (**A** – **C**) unpaired multiple t-tests and (**D**) an

unpaired student's t-test. *$p < 0.05$. CRP = collagen-related peptide; GP = glycoprotein; KO = knockout; MFI = mean fluorescence intensity; PAR4 = protease-activated receptor 4 activating peptide; Rln = reelin; WT = wild-type.

In contrast to previous studies in Rln WT and Rln KO mice on day 28, the analysis on day 7 after PPE surgery clearly showed an influence of platelet-derived reelin on early aneurysm formation. In summary, mice with reelin-deficient platelets revealed reduced aortic diameter, altered platelet degranulation and decreased aggregate formation of platelets with neutrophils on day 7 after surgery.

4.2.4 Platelets of Rln KO mice contained reelin despite platelet-specific gene deletion

The analysis of Rln WT and Rln KO mice revealed different results in aneurysm formation on day 7 and 28 following PPE surgery. A possible explanation for this discrepancy could be provided by the results of the Western blot analysis. The results of this Western Blot analysis in Rln WT and Rln KO mice showed that the Rln KO mice contain different amounts of reelin in their platelets despite the genetic deletion of reelin in megakaryocytes and platelets (**Figure 38 A**). Furthermore, the analysis of 28-day mice on day 7 as a direct comparison to the above shown results revealed two populations of mice that develop either reduced or elevated aneurysm diameter compared to control mice (**Figure 38 B**). Considering only the lower population in the red square and comparing this result to Rln WT mice showed similar results as observed in mice that were only analysed until day 7 (**Figure 38 C,** *already shown in* **34 D**). Western blot analysis of Rln WT and Rln KO mice was performed by Dr. Irena Krüger.

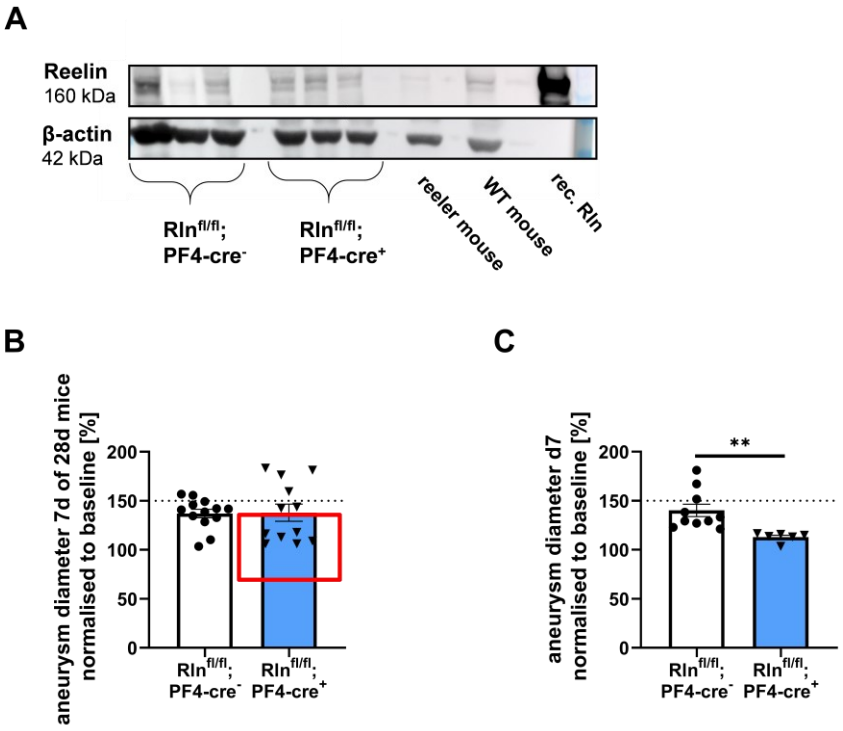

Figure 38. Platelets from Rln KO mice contained reelin. (**A**) Reelin content in platelet lysates from Rln WT and Rln KO mice using Western blot analysis (n = 4 – 5). Recombinant reelin and platelet lysates of reeler and WT mice were used as controls. (**B**) Aneurysm diameter normalised to baseline on day 7 of before analysed 28-day Rln WT and Rln KO mice (see chapter **4.2.2**) (n = 12 – 13). Red square indicates a specific population. (**C**) Aneurysm diameter normalised to baseline of analysed 7-day Rln WT and Rln KO mice (see chapter **4.2.3**). Data are represented as mean values ± SEM. Statistical significance was determined by (**B** and **C**) unpaired student's t-tests. KO = knockout; PPE = porcine pancreatic elastase (infusion); Rln = reelin; WT = wild-type. Data in (**A**) conducted by Dr. Irena Krüger.

These results demonstrated that both, platelets from Rln WT and from Rln KO mice contain reelin despite platelet-specific gene deletion.

4.3 Establishment of the ePPE model for experimental AAA induction in mice

An important characteristic of the human AAA pathology is the formation of an intraluminal thrombus (ILT), which is present in about 75% of all AAA patients [66]. Since the PPE model does not represent all aspects of human AAA pathology including ILT formation, another mouse model for AAA was established. In contrast to the PPE model, it is described that ILT formation takes place in the ePPE mouse model [106, 108]. The main difference of the ePPE model compared to the PPE model is the external peri-adventitial application of the elastase. In addition to the elastase treatment administration of β-aminopropionitrile (BAPN) in the drinking water is important for AAA development in the ePPE mouse model. BAPN, as an inhibitor of the lysyl oxidase (LOX), prevents cross-linking of newly formed elastin and collagen fibres and thus mimics the geriatric situation in humans. Sham-operated mice treated with heat-deactivated elastase served as controls. For the establishment of the ePPE model, two different BAPN concentrations of 0.1% and 1% in the drinking water were tested. As an additional control group ePPE mice received no BAPN. Survival probability, AAA incidence and aneurysm diameter progression were determined as markers for successful AAA induction during the 28 day time course after ePPE surgery. In addition, blood cell counts, including platelets, WBCs and RBCs, were analysed.

In the first group, where mice received no BAPN in the drinking water, the survival probability of all mice was 100% (**Figure 39 A**). In addition, the incidence of aneurysm formation in ePPE mice was 100% as well, while none of the sham-operated control mice developed an aneurysm (**Figure 39 B**). Already on day 7, the aortic diameter was significantly increased in the ePPE-operated mice compared to the sham controls (sham: 102.47 ± 1.24%; ePPE: 146.62 ± 3.85%; $p < 0.001$) and continued to increase until the end of the observation period. However, the increase in aneurysm diameter in ePPE-operated mice achieved almost a plateau at the end of the study period at day 28 (**Figure 39 D**). Nevertheless, the aortic diameter expansion of ePPE-operated mice reached a level of 200%, normalised to the initial size of the aorta, while the aneurysm diameter of the sham-operated mice showed no increase of the aortic size (sham: 105.8 ± 3.75%; ePPE: 208.4 ± 20.44%; $p < 0.001$) (**Figure 39 C** and **E**).

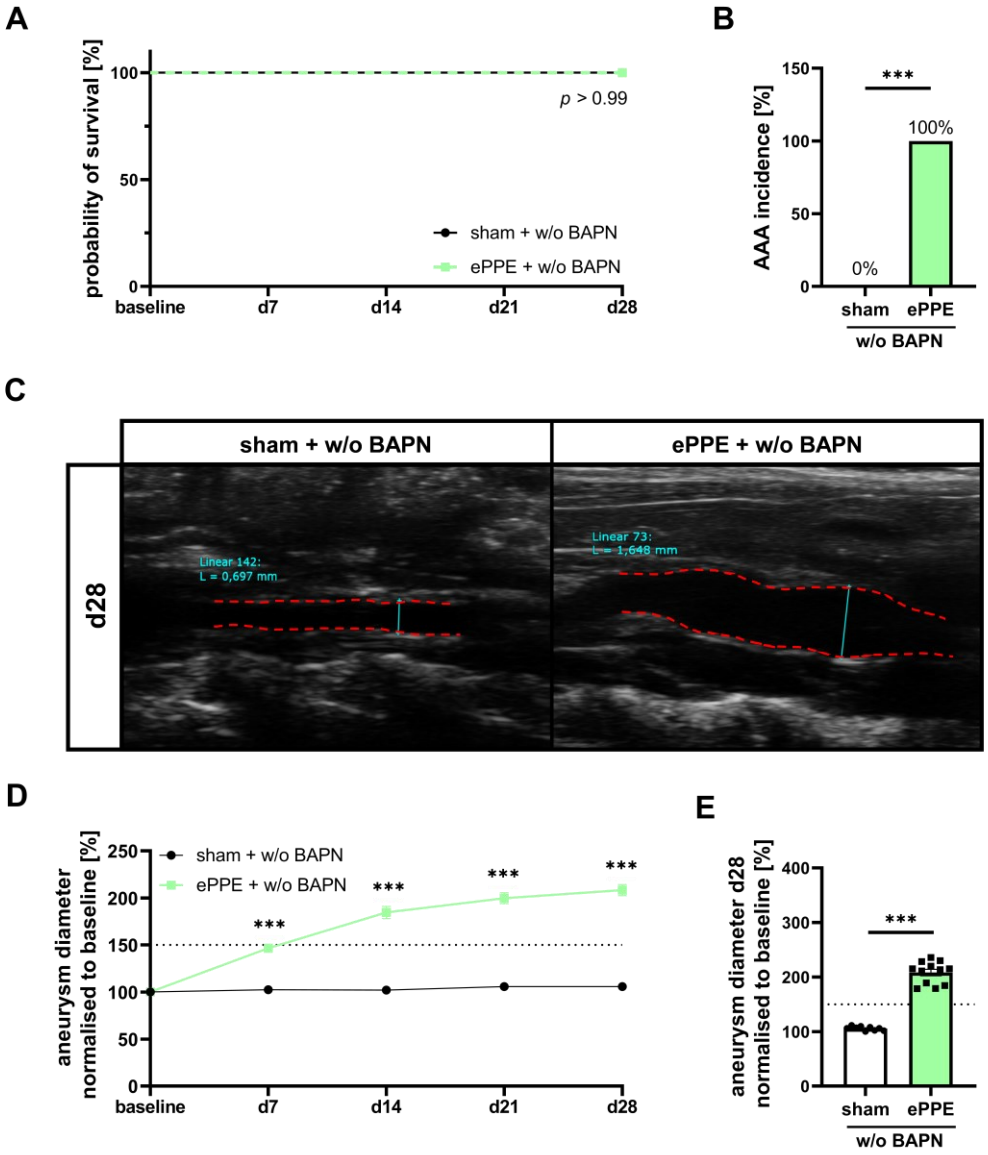

Figure 39. Effects of elastase treatment in mice undergoing ePPE surgery without BAPN administration. (**A**) Probability of survival of sham- and ePPE-operated mice without additional BAPN administration (n = 9 – 12). (**B**) The incidence for aneurysm formation (> 150%) was determined on day 28 after surgery (n = 9 – 12). (**C**) Representative images of ultrasound measurements of the aneurysm diameter. (**D** – **E**) To investigate aneurysm diameter, ultrasound measurements were performed before surgery (baseline) and on day 7, 14, 21 and 28 after surgery (n = 9 – 12). Data are represented as mean values ± SEM. Statistical significance was determined by a (**A**) Log-rank (Mantel-Cox) test, (**B**) Fisher's exact test, (**D**) two-way ANOVA with a Sidak's multiple comparisons post-hoc test and (**E**) an unpaired student's t-test. ***p < 0.001. AAA = abdominal aortic aneurysm; BAPN = β-aminopropionitrile; ePPE = external porcine pancreatic elastase (application); w/o = without.

In the second group, in which mice received 0.1% BAPN in drinking water, the overall survival probability for the sham-operated mice was 100% and for the ePPE-operated mice 85.7% (p = 0.22) (**Figure 40 A**). The incidence of aneurysm formation showed an identical outcome as the group without additional BAPN treatment. While the

ePPE-operated mice revealed an incidence of 100% for aneurysm formation, no dilatation of the aortic diameter was observed in sham-operated mice ($p < 0.001$) (**Figure 40 B**). Again, the aortic diameter in the ePPE-operated mice was already significantly increased at day 7 compared to the sham controls (sham: 102.89 ± 1.96%; ePPE: 146.2 ± 3.42%; $p < 0.001$) (**Figure 40 D**). On day 28 after elastase treatment, the aneurysm diameter, normalised to the initial measurements in naive mice, was almost 250% in the ePPE-operated mice. In comparison, the sham-operated mice revealed no increase in the aortic diameter (sham: 107.3 ± 6.84%; ePPE: 249.8 ± 51.82%; $p < 0.001$) (**Figure 40 C** and **E**).

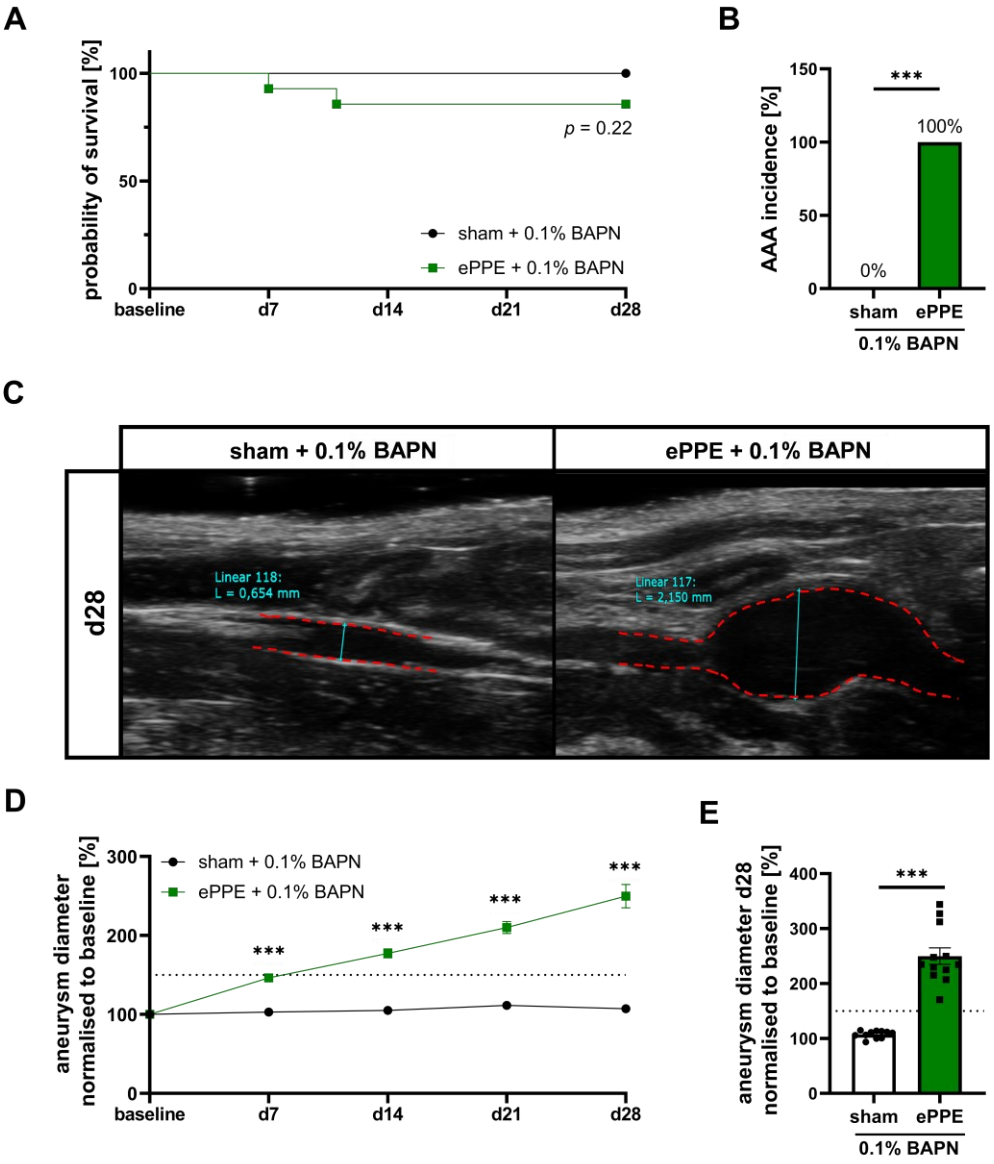

Figure 40. Effects of elastase treatment in mice undergoing ePPE surgery with administration of 0.1% BAPN. (**A**) Probability of survival of sham- and ePPE-operated mice with additional BAPN administration of 0.1% (n = 11 – 14). (**B**) The incidence for aneurysm formation (> 150%) was evaluated on day 28 after PPE surgery (n = 11 – 12). (**C**) Representative images of aortic diameter progression

determined by ultrasound measurements. (**D** – **E**) To investigate aneurysm diameter, ultrasound measurements were conducted before surgery (baseline) and on day 7, 14, 21 and 28 after surgery (n = 11 – 14). Data are represented as mean values ± SEM. Statistical significance was determined by (**A**) a Log-rank (Mantel-Cox) test, (**B**) Fisher's exact test, (**D**) two-way ANOVA with a Sidak's multiple comparisons post-hoc test and (**E**) an unpaired student's t-test. ***p < 0.001. AAA = abdominal aortic aneurysm; BAPN = β-aminopropionitrile; ePPE = external porcine pancreatic elastase (application).

In the last group for establishing the ePPE surgery, mice received 1% BAPN in their drinking water. The overall survival probability was 100% for the sham-operated and 75% for the ePPE-operated mice in this group (p = 0.30) (**Figure 41 A**). As in the other two groups, the incidence of aneurysm formation was 100% in the ePPE-operated mice and 0% in the sham controls (p < 0.001) (**Figure 41 B**). Similarly, the aneurysm diameter was significantly increased in the ePPE-operated mice compared to the sham-operated mice starting from day 7 after surgery (sham: 97.33 ± 3.6%; ePPE: 134.04 ± 2.64%; p = 0.0008) (**Figure 41 D**). Finally, on day 28, the aneurysm diameter of ePPE-operated mice reached a level of 260% compared to baseline measurements, while the aneurysm diameter of the sham-operated mice revealed no increase (sham: 98.31 ± 4.49%; ePPE: 261.7 ± 39.71%; p < 0.001) (**Figure 41 C** and **E**).

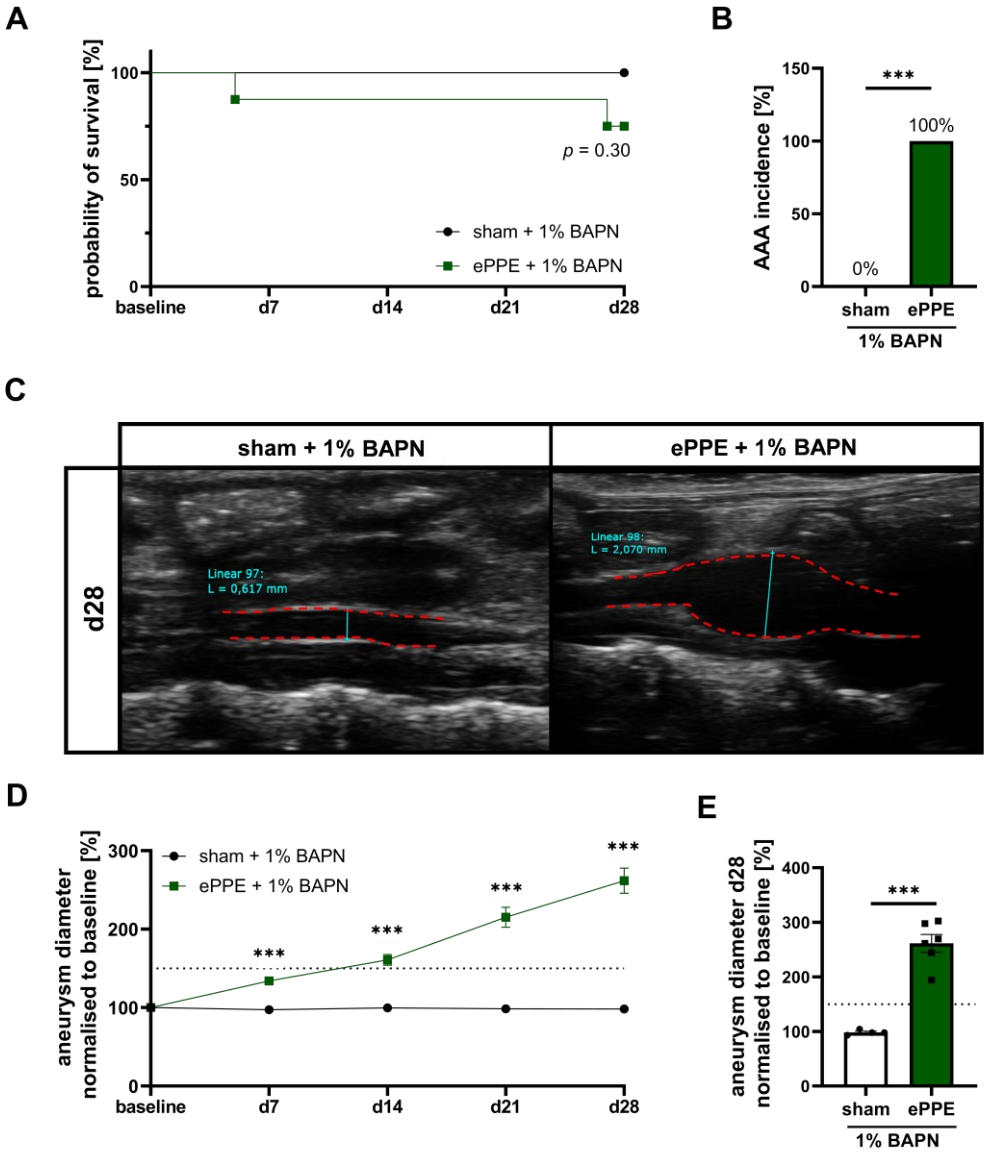

Figure 41. Effects of elastase treatment in mice undergoing ePPE surgery with 1% BAPN administration. (**A**) Probability of survival of sham- and ePPE-operated mice with additional BAPN administration of 1% (n = 4 – 8). (**B**) The incidence for aneurysm formation (> 150%) was determined on day 28 after surgery (n = 4 – 6). (**C**) Representative images of ultrasound measurements of the aneurysm diameter. (**D** – **E**) To investigate aneurysm diameter progression, ultrasound measurements were performed before surgery (baseline) and on day 7, 14, 21 and 28 after surgery (n = 4 – 8). Data are represented as mean values ± SEM. Statistical significance was determined by (**A**) a Log-rank (Mantel-Cox) test, (**B**) Fisher's exact test, (**D**) two-way ANOVA with a Sidak's multiple comparisons post-hoc test and (**E**) an unpaired student's t-test. ***p < 0.001. AAA = abdominal aortic aneurysm; BAPN = β-aminopropionitrile; ePPE = external porcine pancreatic elastase (application).

Comparing all three groups with different BAPN concentrations in the drinking water, a significant difference in aortic diameter expansion can be observed in the ePPE-operated mice between the group without (w/o) BAPN (208.43 ± 5.9%) and the other two groups with 0.1% (249.81 ± 14.96%; $p^{(w/o;0.1\%)}$ = 0.016) and 1%

(261.67 ± 16.21%; $p^{(w/o;1\%)}$ = 0.01) BAPN administration. In contrast, the aneurysm diameter in the two groups with BAPN administration of 0.1% and 1% was similar (p = 0.97) (**Figure 42 A**). In further investigations, the number of blood cells including platelet, WBC and RBC counts were determined. No differences in platelet counts were observed between all groups (**Figure 41 B**). The WBC counts were significantly reduced in sham-operated mice of the group treated with 1% BAPN (2.18 ± 0.26 in 10^3/µL) compared to the other two groups without BAPN treatment (8.07 ± 1.19 in 10^3/µL; $p^{(w/o;1\%)}$ = 0.003) and with administration of 0.1% BAPN (7.47 ± 0.93 in 10^3/µL; $p^{(0.1;1\%)}$ < 0.001) (**Figure 42 C**). The administration of 1% BAPN also resulted in a reduced RBC content in ePPE-operated mice (6.567 ± 0.34 in 10^6/µL) compared to ePPE-operated mice without BAPN administration (8.217 ± 0.15 in 10^6/µL; p < 0.001) (**Figure 42 D**).

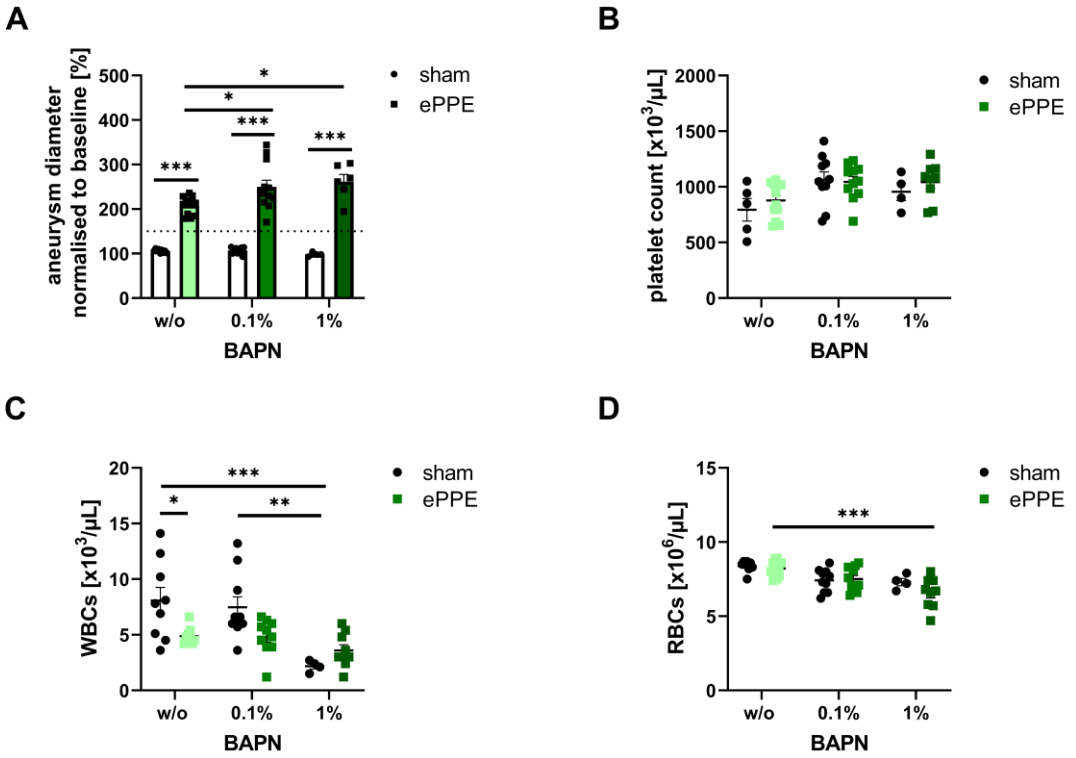

Figure 42. Administration of 0.1% BAPN revealed minimum secondary effects in the ePPE mouse model. (**A**) Aneurysm diameter of all three groups treated with different BAPN concentrations 28 days after ePPE surgery (n = 4 – 14). Blood cell counts including (**B**) platelet count, (**C**) WBC count and (**D**) RBC count were determined in whole blood samples of sham- and ePPE-operated mice treated with different concentration of BAPN using a haematology analyser. Data are represented as mean values ± SEM. Statistical significance was determined by (**A** – **D**) two-way ANOVA with a Tukey's multiple comparisons post-hoc test. *p < 0.05, **p < 0.01, ***p < 0.001. BAPN = β-aminopropionitrile; ePPE = external porcine pancreatic elastase (application); RBC = red blood cell; WBC = white blood cell.

Based on these results of aneurysm diameter expansion and blood cell counts during the establishment of the ePPE mouse model, the administration of 0.1% BAPN was used for further and more detailed analyses. This concentration was selected as it provides sufficient aneurysm diameter progression 28 days after surgery without secondary effects on WBC and RBC counts.

4.4 Platelet activation, inflammation and remodelling of the aortic wall support aneurysm formation in the ePPE mouse model

For further characterisation of the new established ePPE mouse model, different platelet- and aortic-specific parameters, as well as ILT formation were analysed. Flow cytometric analyses were performed to investigate platelet activation, the expression of glycoproteins on the platelet surface, aggregate formation of platelets with circulating immune cells and PS exposure as marker for pro-coagulant activity. In addition, plasma concentrations of soluble forms of the GPVI and GPIb receptor were determined. To analyse ECM remodelling of the aortic wall, histological H/E and EvG stainings, as well as specific immunofluorescence stainings for alpha smooth muscle cell actin (α-SMA) and caspase 3 (casp3) were performed. Further immunofluorescence stainings to analyse platelet (GPIb) and macrophage (Mac3) migration into aortic tissue were conducted.

4.4.1 Platelet degranulation and integrin $\alpha_{IIb}\beta_3$ activation were enhanced in ePPE-operated mice

Flow cytometric analyses of platelet degranulation (P-selectin-FITC) showed an increase in ePPE-operated mice upon low-dose stimulation with PAR4 (PAR4 [70 µM]: sham: 22.3 ± 2.7 MFI; ePPE: 44.78 ± 7.84 MFI; p = 0.012) (**Figure 43 A**). Furthermore, platelets of ePPE-operated mice are in a pre-activated state under resting conditions indicated by enhanced integrin $\alpha_{IIb}\beta_3$ activation without addition of any agonist (JON/A-PE) (sham: 11.5 ± 1.15 MFI; ePPE: 15.64 ± 1.3 MFI; p = 0.029). In addition, these mice revealed increased integrin $\alpha_{IIb}\beta_3$ activation upon stimulation with ADP/U46 (sham: 603.4 ± 17.3 MFI; ePPE: 691.18 ± 33 MFI; p = 0.034) as well as PAR4 (PAR4 [100 µM]: sham: 756. ± 62.95 MFI; ePPE: 952.18 ± 43.57 MFI; p = 0.018) compared to sham-operated mice (**Figure 43 B**).

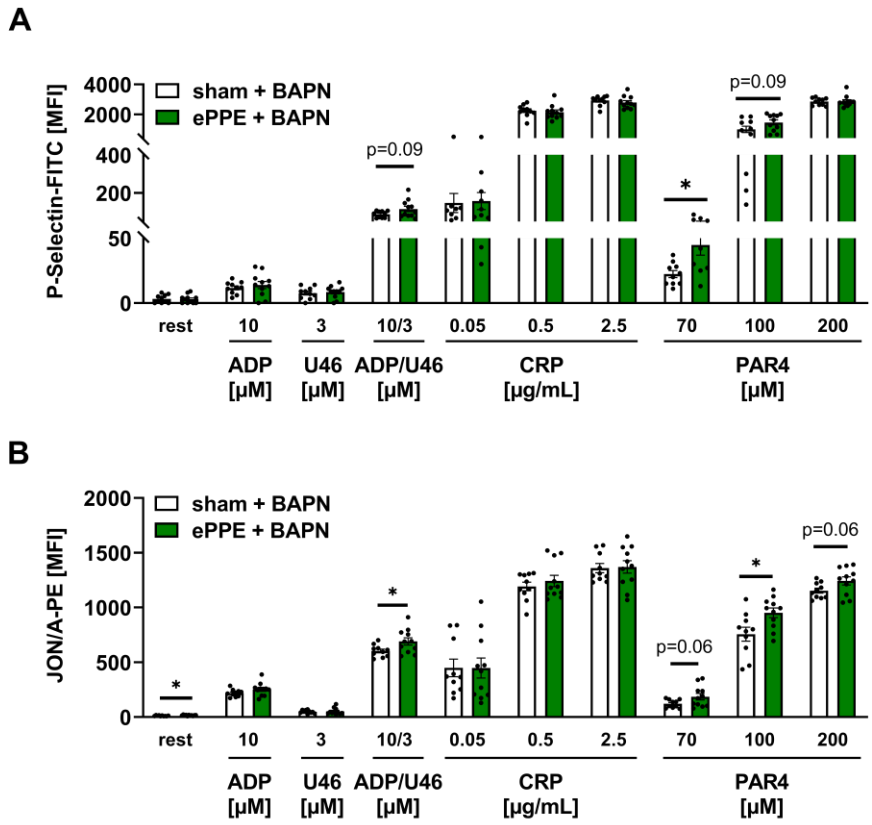

Figure 43. Platelet degranulation and activation were enhanced in ePPE-operated mice. (**A**) Platelet degranulation (P-selectin-FITC) and (**B**) integrin $\alpha_{IIb}\beta_3$ activation (JON/A-PE) were measured in whole blood samples of sham- and ePPE-operated mice with BAPN administration of 0.1% in drinking water using flow cytometry. Platelets were stimulated with indicated agonists (n = 10 – 11). Data are represented as mean ± SEM. Statistical significance was determined by (**A** and **B**) unpaired multiple t-tests. *p < 0.05. ADP = adenosine diphosphate; BAPN = β-aminopropionitrile; CRP = collagen-related peptide; ePPE = external porcine pancreatic elastase (application); MFI = mean fluorescence intensity; PAR4 = protease-activated receptor 4 activating peptide; U46619 (U46) = thromboxane A_2 analogue.

4.4.2 Shedding of GPVI and GPIb from the platelet surface correlated with aortic diameter upon aneurysm formation and progression

Next, the platelet surface exposure of integrin α_5, integrin β_3 and GPVI was measured by flow cytometry, revealing reduced exposure of GPVI on platelets from ePPE-operated mice (sham: 1899.6 ± 40.71 MFI; ePPE: 1754 ± 51.19 MFI; p = 0.043) (**Figure 44 A**). To investigate if the reduced GPVI expression on platelets is due to enhanced receptor shedding, the plasma concentration of soluble (s)GPVI was measured. As shown in **Figure 44 B**, an increased plasma concentration of sGPVI in plasma samples of ePPE-operated mice was detected (sham: 3.544 ± 0.31 ng/mL; ePPE: 4.71 ± 0.20 ng/mL; p = 0.0055). In addition, the plasma concentration was correlated with the surface expression of GPVI and the aneurysm diameter to determine possible correlations. Thereby, sGPVI was strongly negatively correlated

with the surface expression of GPVI with a high significance (r = - 0.78; *p* = 0.001) (**Figure 44 C**). In contrast, the correlation of sGPVI with aneurysm size showed a significant moderate positive relation (r = 0.47; *p* = 0.029) (**Figure 44 D**). As a result, an increase in sGPVI in plasma is accompanied by a decrease in GPVI on the platelet surface and an enlarged aneurysm diameter.

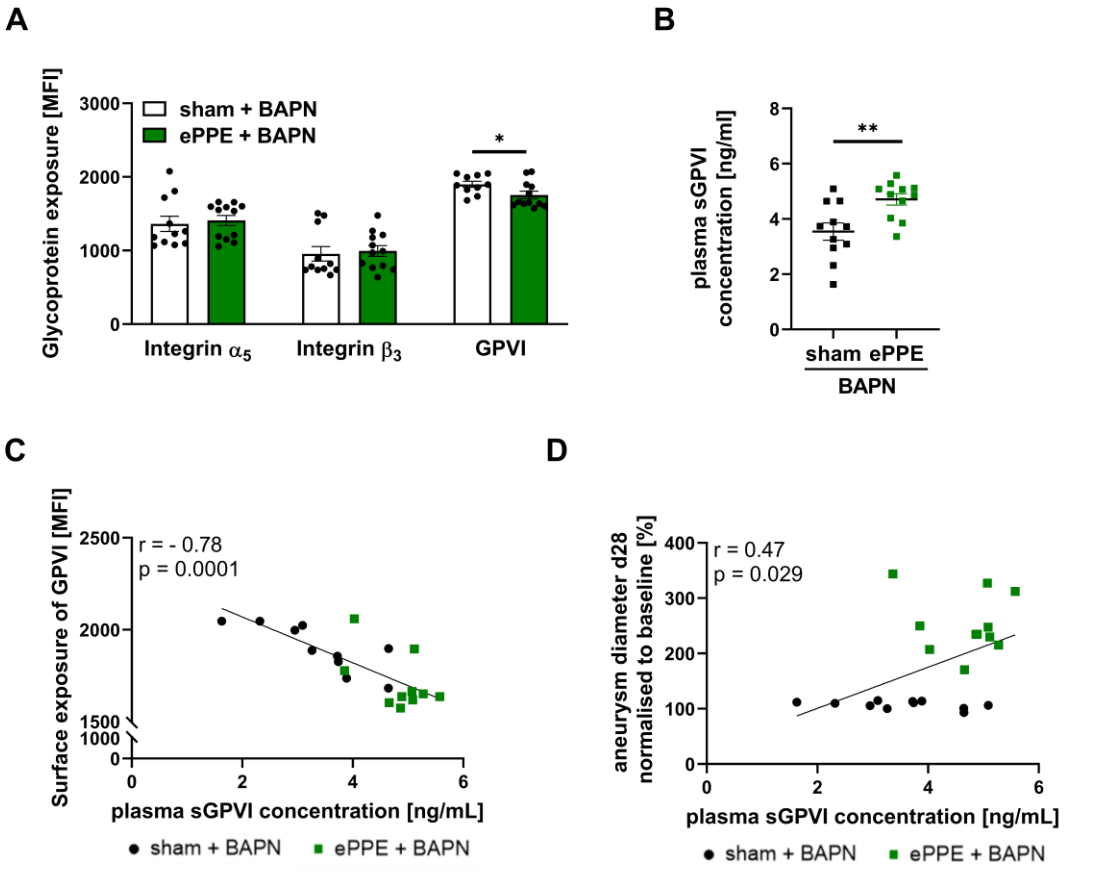

Figure 44. ePPE-operated mice showed reduced GPVI exposition on platelet surface and enhanced sGPVI in the plasma. (**A**) Surface exposure of integrin α_5, integrin β_3 and GPVI on platelets were measured in whole blood samples of sham- and ePPE-operated mice using flow cytometry (*n* = 10 – 12). (**B**) Plasma concentration of sGPVI were determined by ELISA (*n* = 11). Spearman's correlation between (**C**) surface exposure of GPVI and sGPVI plasma concentration (*n* = 10) as well as between (**D**) aneurysm size and sGPVI plasma concentration (*n* = 11). Data are represented as mean values ± SEM. Statistical significance was determined by (**A**) an unpaired multiple t-test and (**B**) unpaired student's t-test. **p* < 0.05, ***p* < 0.01. BAPN = β-aminopropionitrile; ePPE = external porcine pancreatic elastase (application); GP = glycoprotein; MFI = mean fluorescence intensity; sGPVI = soluble GPVI. Data partially published in Feige *et al.*, 2024. Layout changes have been made [127].

In addition, platelet surface glycoprotein GPIb, which is critical for haemostasis, was measured using flow cytometry showing no differences between sham- and ePPE-operated mice on day 28 after surgery (sham: 884.2 ± 81.75 MFI;

ePPE: 930 ± 72.56 MFI; *p* = 0.68) (**Figure 45 A**). Although no change in GPIb receptor exposition on the platelet surface was observed, plasma concentrations of the soluble form of GPIb, namely glycocalicin, were measured. Thereby, an increased plasma concentration of glycocalicin was found in ePPE-operated mice compared to sham controls (sham: 1.43 ± 0.038 µg/mL; ePPE: 1.71 ± 0.10 µg/mL; *p* = 0.029) (**Figure 45 B**). A correlation between the plasma concentration of glycocalicin and aneurysm size revealed a significant strong positive correlation between both parameters (r = 0.718; *p* = 0.0085). Thereby, an increase in aneurysm diameter is associated with elevated glycocalicin concentrations in the plasma of sham- and ePPE-operated mice (**Figure 45 C**).

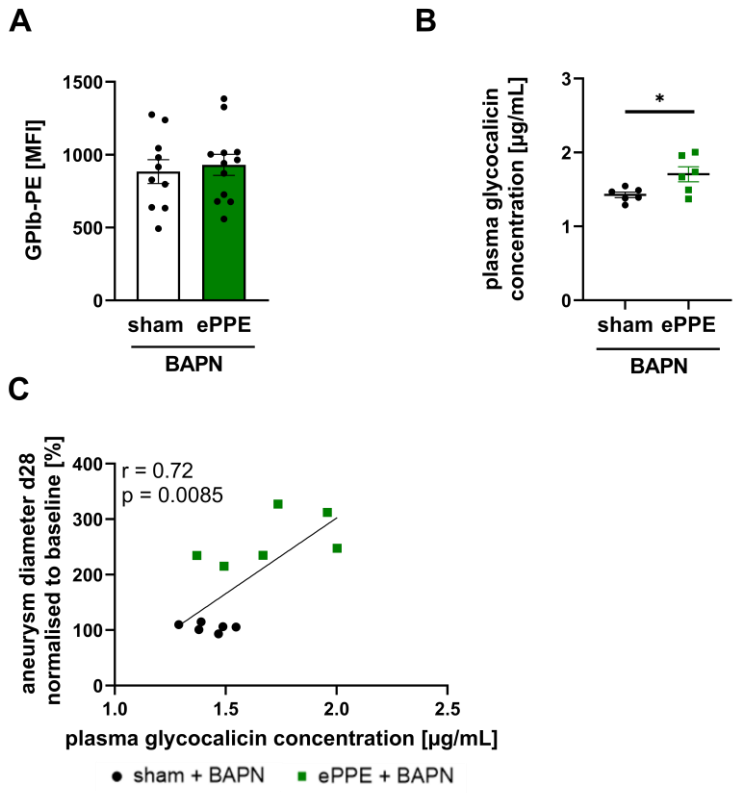

Figure 45. Plasma concentration of glycocalicin was increased in ePPE mice. Surface expression of (**A**) GPIb (*n* = 10 – 12) was measured in whole blood samples of sham- and ePPE-operated mice using flow cytometry (*n* = 5). (**B**) Measurement of plasma concentration of glycocalicin was performed via ELISA (*n* = 6). (**C**) Spearman's correlation between aneurysm size and glycocalicin plasma concentration (*n* = 6). Data are represented as mean values ± SEM. Statistical significance was determined by (**A** and **B**) unpaired student's t-tests. **p* < 0.05. BAPN = β-aminopropionitrile; ePPE = external porcine pancreatic elastase (application); GP = glycoprotein; MFI = mean fluorescence intensity.

4.4.3 Platelet pro-coagulant activity is increased in ePPE-operated mice

Flow cytometric analyses of AnnexinV-binding to platelets were performed to determine platelet pro-coagulant activity as an important factor in the process of thrombus formation. Thereby, no differences were observed under resting conditions or upon stimulation with the PAR4 agonist. In contrast, ePPE-operated mice showed an increased pro-coagulant activity upon CRP stimulation compared to sham controls (sham: 17.07 ± 2.9%; ePPE: 27.99 ± 4.4%; $p = 0.047$) (**Figure 46 A**). The correlation of CRP-induced AnnexinV-binding of platelets with the aneurysm size is moderate but significantly positive (r = 0.497; $p = 0.0045$) (**Figure 46 B**).

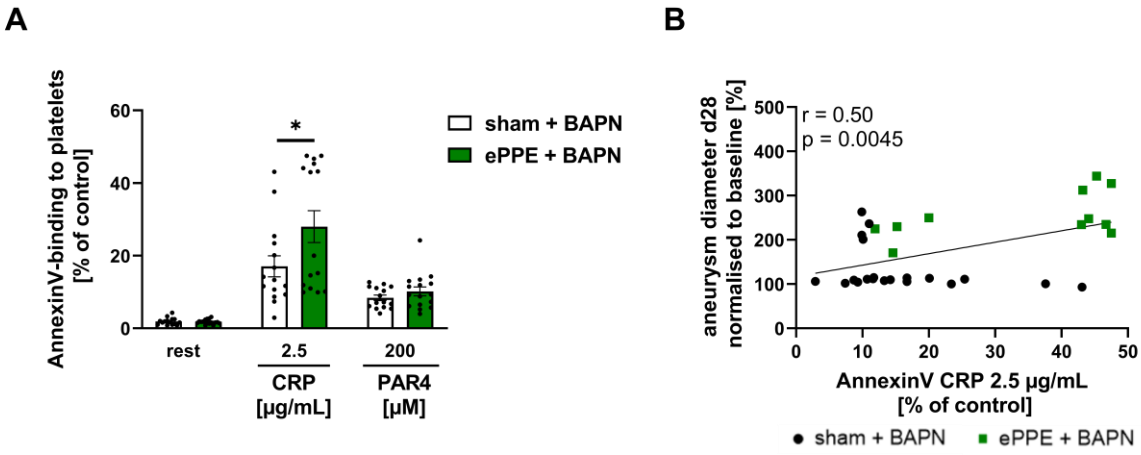

Figure 46. Platelet pro-coagulant activity was increased in ePPE-operated mice. (**A**) AnnexinV-binding to platelets (n = 15 – 16) was measured in whole blood samples of sham- and ePPE-operated mice using flow cytometry. Platelets were stimulated with indicated agonists. (**B**) Spearman's correlation between aneurysm size and AnnexinV-binding to platelets upon stimulation with CRP (n = 15 – 16). Data are represented as mean values ± SEM. Statistical significance was determined by (**A**) an unpaired multiple t-test. *p < 0.05. BAPN = β-aminopropionitrile; CRP = collagen-related peptide; ePPE = external porcine pancreatic elastase (application); PAR4 = protease-activated receptor 4 activating peptide.

4.4.4 Progressive aortic wall remodelling in the ePPE mouse model was characterised by thickening of the aortic media through cell proliferation and degradation of elastin

After analysing various platelet-specific parameters, aortic characteristics were also examined in sham- and ePPE-operated mice on day 28 after surgery. Important cellular features of the PPE model are the thinning of the vessel wall and the degradation of elastin fibres. These parameters were also examined in the ePPE mouse model. Therefore, H/E staining was used to analyse the general structure of

the aortic wall, while EvG staining was performed to investigate the grade of elastin degradation.

The histological H/E staining revealed a significantly increased intima/media thickness in ePPE-operated mice compared to sham controls (sham: 45.57 ± 1.64 µm; ePPE: 88.38 ± 9.13 µm; p = 0.0013) (**Figure 47 A** and **B**). The thickening of the vessel wall was strongly positively correlated with the aneurysm diameter (r = 0.83; p = 0.0005). This indicates that an enlargement of the aneurysm is accompanied by an increase of aortic wall thickness (**Figure 47 C**).

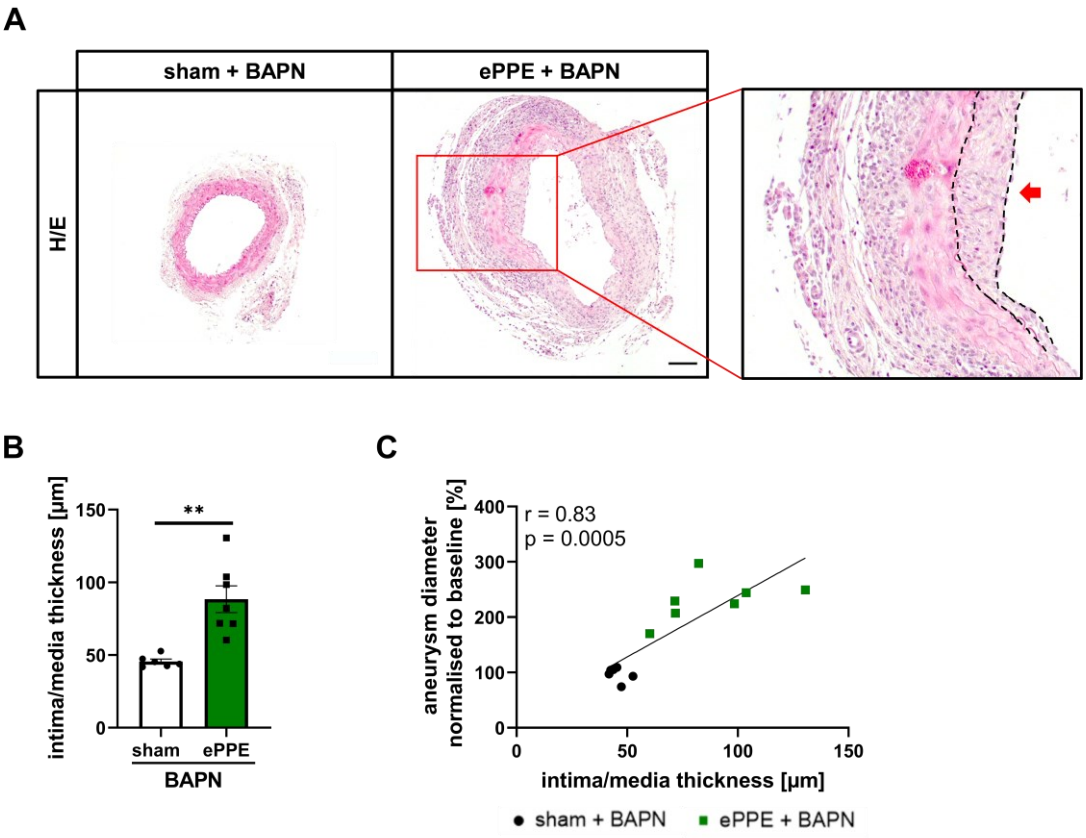

Figure 47. Elastase treatment during ePPE surgery led to a thickening of the aortic wall 28 days after surgery. (**A**) Representative images of histological H/E staining including (**B**) evaluated intima/media thickness (n = 6 – 7) and (**C**) Spearman's correlation between intima/media thickness and the aneurysm diameter (n = 6 – 7) at day 28 post ePPE surgery of sham- and ePPE-operated mice. Red arrow indicates proliferated tissue. Data are represented as mean ± SEM. Statistical significance was determined by (**B**) an unpaired student's t-test. **p < 0.01. Scale bar: 100 µm. BAPN = β-aminopropionitrile; ePPE = external porcine pancreatic elastase (application); H/E = haematoxylin-eosin.

Using the EvG staining, the elastin degradation grade was analysed in sham- and ePPE-operated mice. Thereby, an increased grade of elastin degradation was observed in ePPE-operated mice, while sham-operated mice showed no degradation (sham: 1 ± 0; ePPE: 2.57 ± 0.20; $p < 0.001$) (**Figure 48 A** and **B**). Correlating the elastin degradation grade with the aneurysm diameter revealed a very strong positive correlation (r = 0.90; $p = 0.001$), indicating that an increase in the aortic diameter is accompanied by enhanced elastin degradation (**Figure 48 C**).

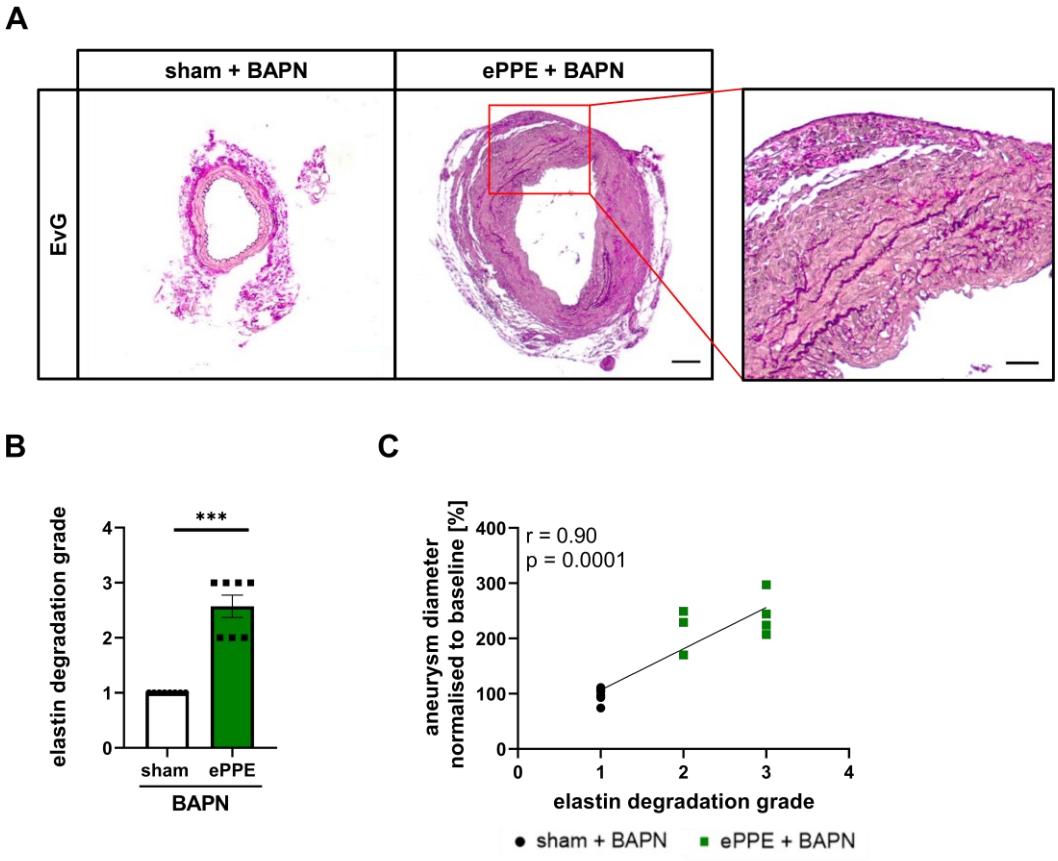

Figure 48. Elastin degradation was significantly enhanced in ePPE-operated mice. (**A**) Representative images of histological EvG staining with zoom in image including (**B**) evaluated elastin degradation grade ($n = 7 – 8$) and (**C**) Spearman's correlation between elastin degradation grade and the aneurysm diameter ($n = 7 – 8$) at day 28 post ePPE surgery of sham- and ePPE-operated mice. Elastin degradation grade was classified as described in **chapter 3.5.3**. Data are represented as mean values ± SEM. Statistical significance was determined by (**B**) an student's t-test. ***$p < 0.001$. Scale bar: 100 µm and 25 µm. BAPN = β-aminopropionitrile; ePPE = external porcine pancreatic elastase (application); EvG = Elastica-van-Gieson.

4.4.5 Aortic wall thickening in the ePPE mouse model is based on cell proliferation of α-SMA-positive cells

After analysing the basic aortic wall structure, including wall thickness and elastin degradation, immunofluorescence staining was used to investigate the cellular composition of the aortic wall and the surrounding tissue. Therefore, the content of alpha-smooth muscle cell actin (α-SMA) and caspase 3 (casp3) positive cells, as well as platelet (GPIbα positive cells) and macrophage (Mac3 positive cells) migration were analysed.

An important feature of aneurysm formation is the apoptosis of VSMCs which is also reflected in the PPE model. To analyse if the ePPE mouse model represents this characteristic feature of AAA as well, α-SMA positive cells were specifically stained in the aortic wall of sham- and ePPE-operated mice (**Figure 49 A**, *Appendix Figure 56)*. The analysis of the α-SMA content in the aortic wall revealed a higher α-SMA signal in ePPE-operated mice compared to sham controls (sham: 399.3 ± 39.71 MFI; ePPE: 632.8 ± 84.71 MFI; $p = 0.018$) (**Figure 49 B**). The increased α-SMA content indicates elevated VSMC proliferation and was consistent with the observation of a thickened aortic wall. Thus, this result let suggest that the newly formed tissue does not represent thrombus tissue as it was published by others recently. Correlating the α-SMA content with the aneurysm diameter showed a moderate positive correlation. This indicates that the enlargement of the aneurysm is accompanied by an increase in the α-SMA content in the aortic wall ($r = 0.52$; $p = 0.055$) (**Figure 49 C**).

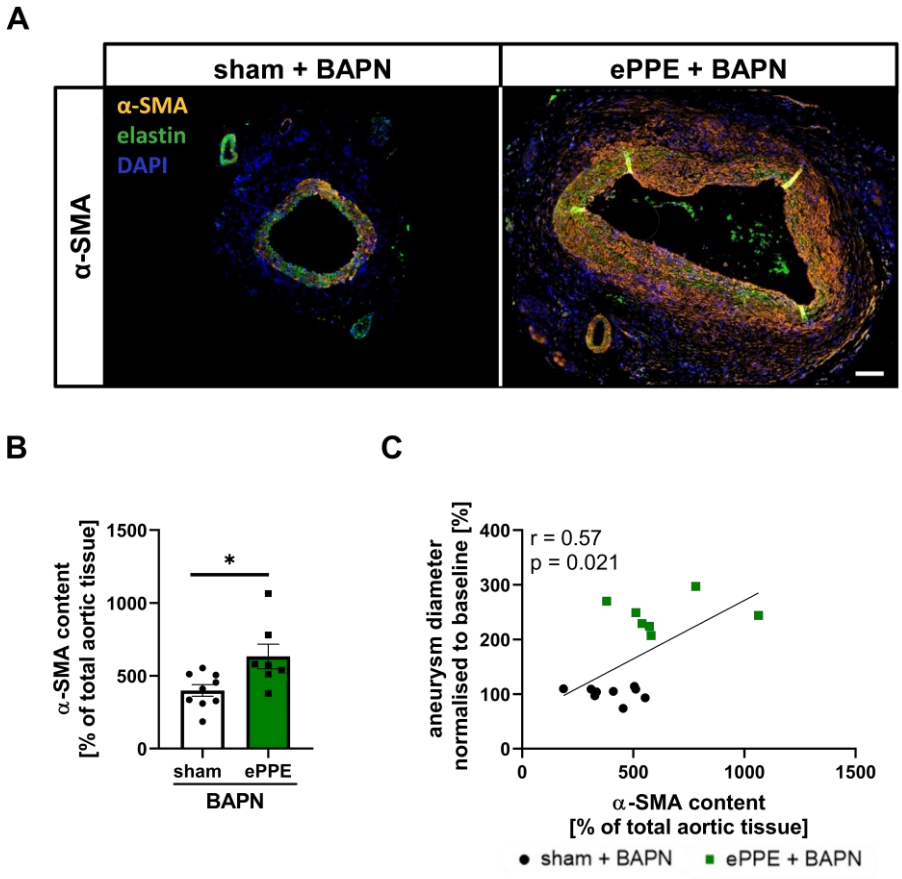

Figure 49. Content of α-SMA positive cells in the aortic wall correlated with the aneurysm diameter. (**A**) Representative images of immunofluorescence α-SMA staining including (**B**) quantification of α-SMA content in the aortic wall of sham- and ePPE-operated mice (*n* = 7 – 9). The aortic wall was specifically stained for α-SMA positive cells (anti- α-SMA, orange). Elastin (green) is demonstrated by autofluorescence, and nuclei were stained with DAPI (blue). (**C**) Spearman's correlation between α-SMA content and the aneurysm diameter (*n* = 7 – 9) at day 28 post ePPE surgery. Data are represented as mean values ± SEM. Statistical significance was determined by (B) an unpaired student's t-test. *p < 0.01. Scale bar: 100 µm. α-SMA = alpha smooth muscle cell actin; BAPN = β-aminopropionitrile; DAPI = 4′,6-Diamidin-2-phenylindol; ePPE = external porcine pancreatic elastase (application); GFP = green fluorescent protein.

Even though no thinning of the aortic wall due to reduced VSMCs was observed, the apoptosis of cells including VSMCs was analysed. Therefore, casp3 was specifically stained in the aortic wall tissue, revealing only a tendency to a higher content of casp3 in the ePPE-operated mice compared to sham-operated mice (sham: 155.2 ± 2.68 MFI; ePPE: 168.8 ± 20.17 MFI; p = 0.10) (**Figure 50 A** and **B**, *Appendix Figure 56*). Correlating the content of casp3 in the aortic wall with the aneurysm diameter showed a possible weak correlation (r = 0.32; p = 0.24) (**Figure 50 C**).

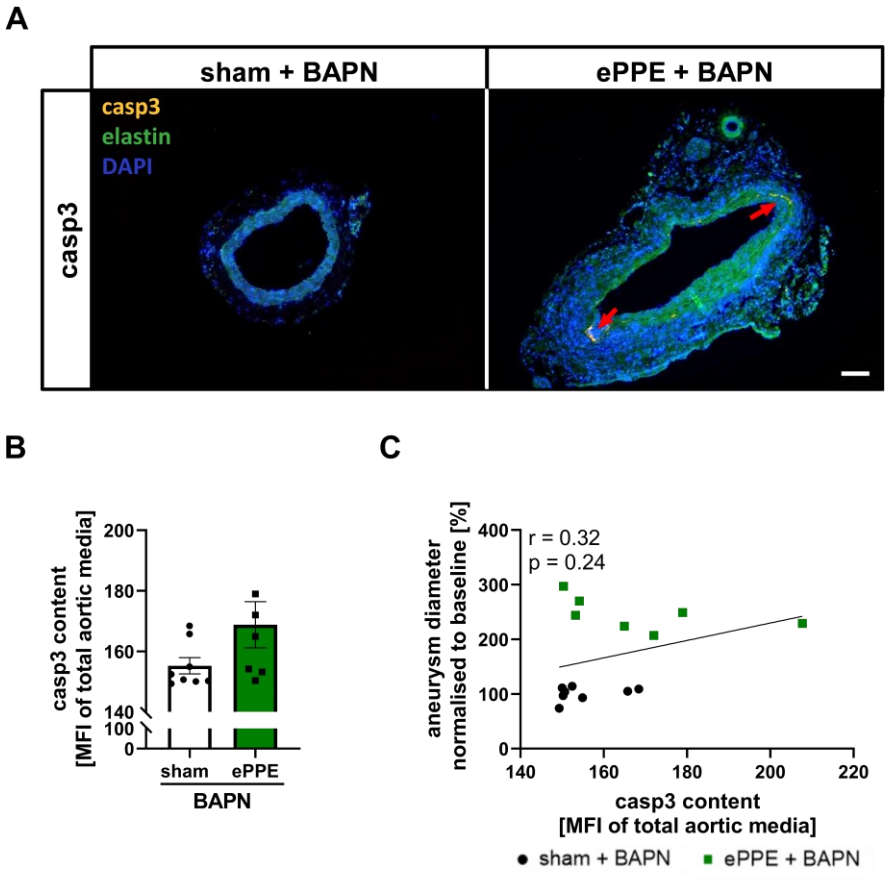

Figure 50. The content of caspase 3 positive cells was unaltered within the aortic wall of ePPE mice. (**A**) Representative images of immunofluorescence casp3 staining in aortic wall tissue, specifically stained for casp3 (anti-casp3, orange). Nuclei were stained with DAPI (blue) and elastin autofluorescence is shown in green. (**B**) Quantification of casp3 positive cells (n = 7 – 8) in sham- and ePPE-operated mice. (**C**) Spearman's correlation between the casp3 content and aneurysm diameter (n = 7 – 8) at day 28 post ePPE surgery of sham- and ePPE-operated mice. Data are represented as mean values ± SEM. Statistical significance was determined by (B) an unpaired student's t-test. Scale bar: 100 µm. BAPN = β-aminopropionitrile; casp3 = caspase 3; DAPI = 4′,6-Diamidin-2-phenylindol; ePPE = external porcine pancreatic elastase (application); GFP = green fluorescent protein.

4.4.6 Elevated inflammation in ePPE-operated mice

Next, the inflammatory response in ePPE mice was analysed. To this end, aggregate formation of platelets with different circulating inflammatory cell was investigated. As shown in **Figure 51**, no changes in aggregate formation were observed with $CD45^+$ leukocytes, $Ly6G^+$ neutrophils, $CD11^+$ or $CD14^+$ macrophages and granulocytes as well as $CD3^+$ T-cells.

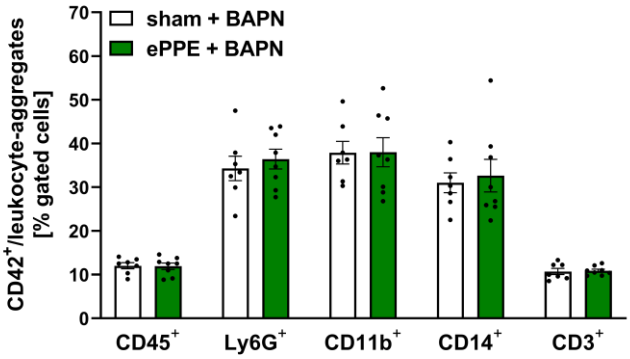

Figure 51. No differences in platelet-leukocytes aggregates in ePPE-operated mice. The formation of platelet-aggregates with inflammatory cells ($CD45^+$; $Ly6G^+$; $CD11b^+$; $CD14^+$; $CD3^+$) was measured in whole blood samples of sham- and ePPE-operated mice using flow cytometry (n = 7 – 8). Data are represented as percent of double-positive events for CD42b (platelet marker, GPIbα) and CD45 (leukocyte marker), Ly6G (neutrophil marker), CD11b (monocyte, macrophage and granulocyte marker), CD14b (monocyte and macrophage marker) and CD3 (T-cell marker). Statistical significance was determined by an unpaired multiple t-test. *p < 0.05. BAPN = β-aminopropionitrile; CD = cluster of differentiation; ePPE = external porcine pancreatic elastase (application); Ly6G = lymphocyte antigen 6 complex locus G.

In the PPE mouse model, platelet migration into the aortic wall was observed at early time points after elastase treatment [89]. Similarly, in the ePPE-operated mice, a significantly increased number of platelets (GPIbα) was found in aortic tissue 28 days after surgery compared to sham controls (sham: 235.1 ± 11.43 MFI; ePPE: 269.0 ± 9.39 MFI; p = 0.045) (**Figure 52 A** and **B**, *Appendix Figure 57*). When correlating the platelet content with the aortic diameter, a strong and significant positive correlation was detected (r = 0.77; p = 0.033). The increase of the aneurysm diameter was associated with an elevated content of GPIbα positive cells in the aortic wall (**Figure 52 C**).

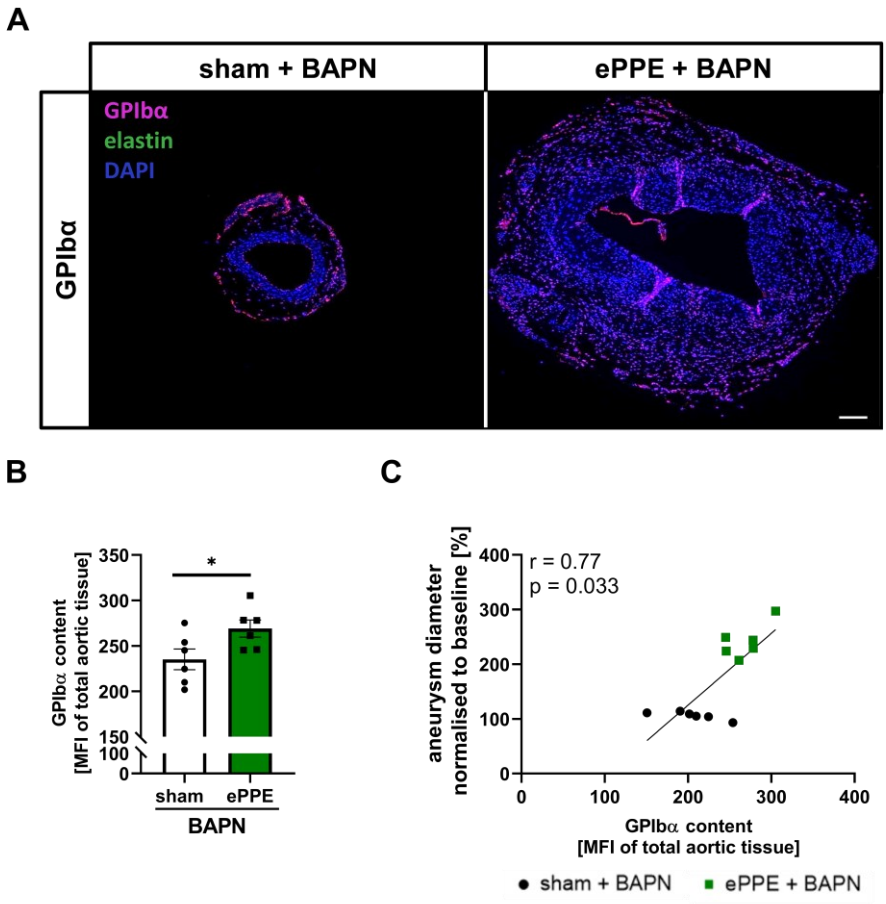

Figure 52. The platelet content was increased in the aortic wall of ePPE-operated mice. (**A**) Representative images of immunofluorescence GPIbα staining including (**B**) quantification (n = 6). Aortic tissue was specifically stained for platelets (anti- GPIbα, pink) and nuclei were stained with DAPI (blue). Elastin (green) is shown as well by autofluorescence. (**C**) Spearman's correlation between GPIbα content and the aneurysm diameter (n = 6) at day 28 post ePPE surgery of sham- and ePPE-operated mice. Data are represented as mean values ± SEM. Statistical significance was determined by (**B**) an unpaired student's t-test. *p < 0.05. Scale bar: 100 µm. BAPN = β-aminopropionitrile; DAPI = 4′,6-Diamidin-2-phenylindol; ePPE = external porcine pancreatic elastase (application); GFP = green fluorescent protein; GP = glycoprotein.

Finally, the content of infiltrating macrophages within the aneurysm segment was analysed (**Figure 53 A**, *Appendix Figure 57*). The migration of macrophages into the aortic wall of ePPE-operated mice was also increased compared to sham-operated mice (sham: 152.4 ± 1.46 MFI; ePPE: 172.3 ± 3.79 MFI; p = 0.0002) (**Figure 53 B**), revealing a strong positive correlation between the aneurysm diameter and the content of macrophages in the aortic wall (r = 0.87; p = 0.001) (**Figure 53 C**). In this context, it is important to mention that the amount of detectable Mac3 is basically marginal, since macrophages are cells of the acute inflammation, which is mainly part of the early stage of aneurysm formation.

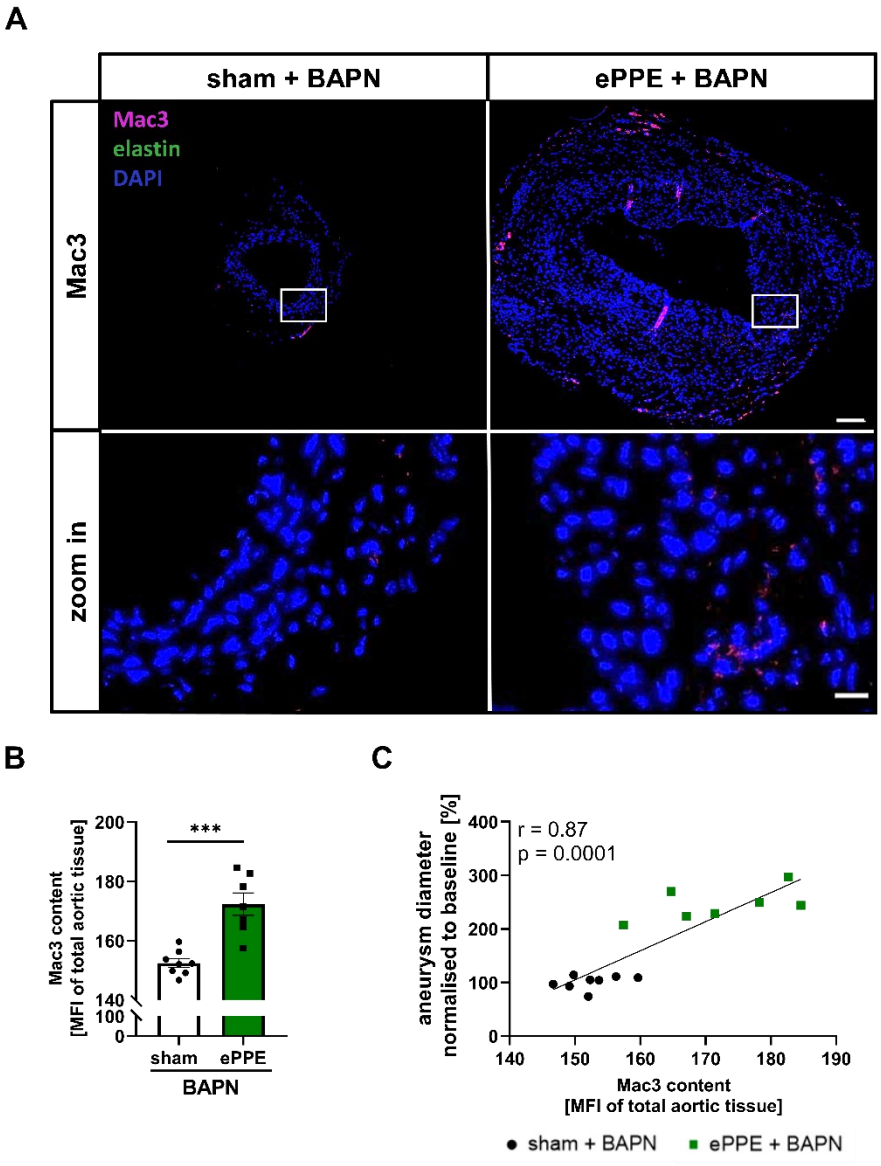

Figure 53. The migration of macrophages was significantly enhanced in ePPE-operated mice. (**A**) Representative images of immunofluorescence Mac3 staining, specifically stained for macrophages (anti- Mac3, pink), including zoom in images. Nuclei were stained with DAPI (blue) and elastin autofluorescence (green) is shown. (**B**) Quantification of Mac3 content (n = 7 – 8) in the aortic wall of sham- and ePPE-operated mice 28 days after surgery. (**C**) Spearman's correlation between Mac3 content and the aneurysm diameter (n = 7 – 8) at day 28 post ePPE surgery. Data are represented as mean values ± SEM. Statistical significance was determined by (**B**) an unpaired student's t-test. ***p < 0.001. Scale bar: 100 and 20 µm. BAPN = β-aminopropionitrile; DAPI = 4′,6-Diamidin-2-phenylindol; ePPE = external porcine pancreatic elastase (application); GFP = green fluorescent protein.

Taken together, the establishment of the ePPE mouse model, allows a more detailed characterisation of the role of platelets in experimental AAA, showing higher platelet activation as represented by elevated degranulation (P-selectin) and integrin $\alpha_{IIb}\beta_3$ activation (JON/A), increased shedding of GPVI and GPIb from the platelet surface

and higher pro-coagulant activity. Importantly, no ILT formation could be detected at day 28 as recently published by others. Instead, the proliferation of VSMCs was observed, leading to a thickening of the aortic wall.

5 Discussion

Platelets are known to play an important role in both, physiological and pathological processes. This includes CVDs such as atherosclerosis, arterial thrombus formation and AAA. As platelets are a driving force for the development of CVDs, they represent a primary target for their prevention. However, various retrospective clinical studies and meta-analyses demonstrated different effects of anti-platelet agents such as ASA on the progression and rupture of AAA [120, 128, 129]. Since there is no specific drug-based therapy for the treatment of AAA to date, platelets might represent a promising target in future. However, to date, anti-platelet therapies impair physiological functions of platelets, leading to prolonged bleeding times and therefore affect haemostasis. Thus, it is important to develop therapies for the treatment of AAA that do not affect haemostasis. Consequently, it is necessary to better understand how platelets contribute to the development and progression of AAA disease.

5.1 Platelets play a crucial role during aneurysm formation by modulating platelet activation and by affecting inflammation in AAA

Recently, Wagenhäuser *et al*. [89] published that platelets modulate chronic inflammation and progressive ECM degradation in the process of aneurysm formation. As a result, depletion of platelets led to reduced inflammation and ECM remodelling and consequently decreased aneurysm formation. The results of this thesis were partially published in Wagenhäuser *et al*. [89] and revealed that platelet activation and pro-coagulant activity might support AAA formation being shown in an experimental mouse model of aneurysm formation.

5.1.1 Aortic diameter in PPE-operated mice is significantly increased compared to sham-operated mice

After the confirmation of successful aneurysm formation over a time course of 28 days after PPE surgery by determining the size of the aortic diameter and AAA incidence (**Figure 14**), blood cell counts were measured 3, 10 and 28 days after intervention for a general overview (**Figure 15**). In this context, no differences could be observed in platelet count and size. This is consistent with data from the Ang II model, another AAA mouse model, where no differences in platelet count at day 28 could be observed [89]. However, these results are not in line with decreased platelet counts in AAA

patients as recently described in literature [89, 130]. As already known, 75% of AAA patients develop an intraluminal thrombus mainly consisting of platelets, erythrocytes and neutrophils [82, 92, 93]. Circulating platelets passing the aneurysm segment and the growing ILT might be activated and recruited to thrombus tissue [97], leading to reduced platelet counts in the circulation. In contrast, mice that underwent PPE surgery do not establish an ILT [106]. Also, Ang II-infused mice which were analysed in our research group that developed an aneurysm showed no thrombus formation (unpublished data). Here, it is important to mention that Ang II-infused mice may develop a thrombus, as shown by others. Nevertheless, this thrombus is not classified as an ILT, as it develops within the false lumen of the dissection induced in the Ang II mouse model. The absence of ILT formation in PPE-operated and Ang II-infused mice may help explain why these mice exhibit no significant differences in platelet counts compared to the control group. Mukaiyama *et al*. supported this hypothesis by providing evidence for the uptake of radiolabelled platelets into a mural thrombus in an AAA patient with reduced platelet counts [131].

5.1.2 Plasma concentration of glycocalicin is enhanced 28 days after aneurysm formation

By analysing the exposure of glycoproteins on platelets to characterise changes in the surface composition, no differences were observed in GPVI surface expression or the level of sGPVI in the plasma of mice 28 days after AAA induction (**Figure 17**). GPVI is the main collagen receptor at the platelet surface, playing a crucial role in platelet activation and adhesion [13]. According to the results in PPE-operated mice, Feige *et al*. reported that GPVI surface exposure was unchanged in AAA patients, whereas Benson *et al*. described an increased surface exposure of GPVI. Nevertheless, both found an increased concentration of sGPVI in the plasma of AAA patients that is in contrast to the results of PPE-operated mice [127, 132]. The opposing results of GPVI surface exposure as published by Feige *et al*. and Benson *et al*. may depend on the shear rates of AAA patients in the studied cohorts. In human AAA pathology, disturbed blood flow with high shear rates and enhanced wall shear stress can be observed in the dilated aorta [133, 134]. Al-Tamimi *et al.* could show that the ectodomain of the GPVI receptor on the platelet surface can be shed upon pathological shear rates, thus enhancing sGPVI levels in the plasma of AAA patients. The physiological shear rates in human vessels are in a range between 20-2,000 s^{-1}, declaring the increased level of sGPVI in plasma in patients with coronary stenosis with a mean shear rate of 2,935 s^{-1} (peak shear 19,224 s^{-1}) [135]. In PPE-operated mice, the development of flow velocity and shear rates in and after the aneurysm

segment, which change rapidly in human AAA and consequently becomes important for GPVI shedding, has not yet been published. Thus, it can be hypothesised that the increase of shear rates in the aorta of PPE-operated mice is not sufficient to promote shear-induced GPVI shedding from the platelet surface. Furthermore, there is no evidence of shear-induced GPVI shedding in mice to date. Therefore, measurements of shear rates using *e.g*. MRI within the aneurysm of PPE-operated mice could give a more detailed insight into the mechanisms of shear-induced GPVI shedding in mice.

Another important glycoprotein on the platelet surface is GPIb, the vWF receptor of platelets. By binding vWF, GPIb initiates platelet adhesion and activation in the process of haemostasis [8]. Analogous to GPVI, GPIb was analysed for its surface exposure and plasma concentration after PPE surgery. These analyses showed increased surface expression at an early time point of aneurysm formation and increased plasma concentrations at later time points in PPE-operated mice (**Figure 17**). In 2004, Bergmeier *et al*. were able to show that the metalloproteinase ADAM17 is a physiological sheddase of the GPIbα receptor in mice [136]. In general, the shedding of GPIbα from the platelet surface is a physiological process that constantly takes place in the circulation in a controlled process [137]. Upon activation of ADAM17, which binds to the Gly464 – Val465 peptide bond, GPIbα shedding can be upregulated [136, 138, 139]. In *in vitro* experiments with endothelial cells it was shown that shear stress accelerates the transport of mature ADAM17 to the cell surface [140]. Thus, we hypothesise that increased shear stress in the aneurysm segment of PPE-operated mice could induce the shedding of GPIb by ADAM17 and thus increase plasma glycocalicin levels. Furthermore, the results of enhanced glycocalicin levels in plasma of PPE-operated mice are consistent with glycocalicin levels being elevated in AAA patients compared to healthy controls and patients with symptomatic carotid disease [130]. In this context, the elevated glycocalicin level is not useful as a marker for AAA pathology, since this phenomenon can also be observed in other diseases such as cirrhosis and leukaemia [141].

5.1.3 Platelet activation and pro-coagulant activity are enhanced in late stages of aneurysm formation

The analysis of platelet activation is crucial for the investigation of their role in aneurysm formation as platelets can mediate various processes such as inflammation, ECM remodelling and ILT formation. The platelet activation profile is very important for the validation of the PPE model, especially when AAA pathology in

experimental mice is compared to the human pathology. Indicated by measurements of P-selectin exposure and integrin $\alpha_{IIb}\beta_3$ activation (JON/A), platelet activation was reduced upon stimulation with PAR4 in PPE-operated mice at an early stage of aneurysm formation. In contrast, at later time points, platelet activation was increased in PPE mice following CRP stimulation (**Figure 18**). A possible explanation for the initial reduction in platelet activation after PAR4 stimulation might be a temporary downregulation of the PAR4 receptor on the platelet surface. In an arterial thrombosis mouse model, Kawano and colleagues already showed that platelet reactivity can be reduced due to decreased platelet counts as well as due to the loss of platelet receptors [142]. Furthermore, it is known that the expression of the PAR4 receptor at the platelet surface can be negatively regulated at the post-transcriptional level by prostacyclin, which plays a regulatory role in the cardiovascular system and is known to be an important inflammatory mediator [143, 144]. Based on these studies, it can be speculated that the PAR4 receptor may be downregulated in PPE-operated mice at the beginning of aneurysm formation as induced by increased inflammation. Measurements of the prostacyclin level in plasma and the amount of the PAR4 receptor on the platelet surface using PAR4-specific antibodies in PPE mice may help to prove this hypothesis.

The analysis of platelet activation at later time points revealed an increase in the platelet activation of PPE-operated mice after stimulation of GPVI. This is consistent with human data, which show an increase in platelet activation in AAA patients compared to healthy controls [89]. Since vascular collagen fibres are exposed during aneurysm formation, we hypothesise that increased platelet reactivity upon stimulation of GPVI amplifies platelet activation in the circulation and thus supports further platelet recruitment to enhance aneurysm formation and progression. This hypothesis is supported by Feige *et al*., who recently published that GPVI is crucial for inflammation and aortic wall remodelling in the process of aneurysm formation by modulating different cellular processes including platelet migration, VSMC apoptosis and neutrophil infiltration. In another publication, Morrell *et al*. reported increased platelet reactivity upon stimulation of the thrombin receptors using the ePPE mouse model for AAA formation [145]. In contrast, in our research, we did not detect any differences in platelet reactivity when stimulating the PAR4 receptor. Of note, mouse platelets are known to express the thrombin receptors PAR3 and PAR4, and thrombin can bind to both receptors [146]. Thus, the discrepancy between our results and those of Morell *et al*. may arise from the agonists used to trigger platelet activation, but also from the choice of the mouse model for AAA. In still another mouse model of

aneurysm formation, the Ang II model, no increased platelet activation was observed at any of the time points of aneurysm formation that have been analysed [89]. These differences to the PPE and ePPE model can be explained by the fact that the Ang II model is rather a model for the analysis of aortic dissection than of aneurysm formation. However, in further studies from Owens and colleagues the inhibition of platelet activation revealed positive effects upon aneurysm formation. By administration of aspirin (ASA) and clopidogrel, they found reduced aortic diameter progression in Ang II-infused mice [128]. In another study, AZD6140, a $P2Y_{12}$ receptor antagonist, was found to inhibit platelet activation and to reduce aneurysm formation in a rat model of aneurysm formation. These results support our overall hypothesis that platelets play a crucial role in aneurysm formation and progression.

Moreover in this study, PS exposure was analysed as a marker for the pro-coagulant activity of platelets, a prominent cellular response of platelets in the process of thrombosis. Increased pro-coagulant activity was observed in PPE mice in late stages of aneurysm formation, which may account for increased platelet activity. In addition, a positive correlation between the aneurysm diameter and pro-coagulant activity was detected (**Figure 19**), supporting the hypothesis that PS exposure on platelets plays a crucial role in aneurysm formation. Pro-coagulant platelets are involved in the process of thrombin generation and in the activation and recruitment of further platelets to the injured vessel to stop bleeding [147, 148]. The observation of increased PS exposure at the platelet surface of PPE-operated mice is consistent with the results from AAA patients [89]. However, PS exposure is not a specific marker for AAA pathology, as pro-coagulant activity is also increased in other CVDs such the coronary artery disease [149].

5.1.4 Platelet-mediated inflammation is enhanced in PPE-operated mice during aneurysm formation

It is already known that AAA is associated with chronic inflammation. This chronic inflammation is characterised by the infiltration of inflammatory cells including macrophages, lymphocytes and leukocytes into the aortic wall [88, 150]. Studies with *in vivo* depletion of platelets in PPE-operated mice revealed a role of platelets in the inflammatory response and in aneurysm formation. In detail, Wagenhäuser and colleagues demonstrated that the aneurysm diameter, elastin fragmentation, the number of macrophages in the aortic tissue and gene expression of inflammatory genes including *IL-1B*, *IL-6*, *IL8*, *IL10*, *IL-12B*, *CCL2* and *TNFα* were reduced in

platelet-depleted PPE mice in an early stage of aneurysm formation. Furthermore, the expression of OPN, a matricellular protein which can also act as pro-inflammatory cytokine in its soluble form [151], was found to be decreased after platelet-depletion in PPE-operated mice at day 10 after PPE-surgery [89]. Similar results were shown by Liu *et al*. using another mouse model of AAA formation, namely the AngII mouse model. They demonstrated a reduction in inflammation and aneurysm progression after inhibition of platelets. Blocking of the platelet $P2Y_{12}$ receptor with clopidogrel resulted in reduced aortic diameter expansion, macrophage infiltration into the aneurysm tissue and monocyte chemotactic protein 1 (MCP1) content in the aortic wall [121]. In this thesis, OPN was found to be elevated in the aortic wall of PPE-operated mice, even at later stages of aneurysm formation (**Figure 21**). In addition, Wagenhäuser *et al*. provides evidence for a modulation of inflammatory gene expression in macrophages by the release of pro-inflammatory cytokines and growth factors from platelets *in vitro*. As a result, the *SPP1* gene (coding for OPN) and other important inflammatory genes such as *IL-1B*, *IL-6* and *IL-12B* were upregulated in macrophages after incubation with platelet releasates [89]. So we hypothesise that platelet are able to increase inflammation due to stimulation of migrated macrophages in aortic tissue.

Since chronic inflammation is characterised by the infiltration of various inflammatory cells into the aortic tissue, direct interaction of platelet with these inflammatory cells was analysed. Therefore, aggregate formation of platelets with circulating leukocytes, especially with neutrophils were measured, revealing increased platelet-neutrophil aggregates in the early stage of aneurysm formation (**Figure 20**). These results may support the previous hypothesis that increased inflammation induces downregulation of PAR4 leading to reduced platelet activation at early stages of aneurysm formation (see chapter **5.1.3**). In turn, Rigg *et al*. demonstrated a PAR4-specific decrease of platelet-leukocyte aggregate formation upon inhibition of the PAR4 receptor, indicating a correlation between both processes [152]. In summary, the here presented results clearly show that platelets play a role in the inflammatory process in AAA disease.

To summarise these findings, platelet activation and degranulation as well as increased pro-coagulant activity support aneurysm formation by the inflammatory response in early AAA formation. This is indicated by a hyperactive state of platelets in an early stage of AAA development, which in turn promotes the recruitment of pro-inflammatory cells as well as platelets into the aneurysm wall. The pro-inflammatory

environment within the aneurysm thereby fosters an enhanced pro-coagulant activity of circulating platelets. This pro-coagulant activity is crucial for local thrombin generation and thus ILT formation and progression. As the aortic diameter growth proceeds, enhanced luminal shear rates induce the shedding of GPIb from the platelet surface resulting in higher glycocalicin plasma levels.

5.2 The role of platelet-specific reelin in AAA formation and progression

Reelin is a large extracellular matrix protein that was originally found to be synthesised by Cajal-Retzius cells in the marginal zone of the developing cerebral cortex with a crucial role in brain development. Furthermore, reelin is expressed by various other cell types, including hepatic stellate cells in the liver and blood cells such as platelets, indicating its role in neurological as well as non-neurological functions [33, 34, 39]. Moreover, reelin can be released into the bloodstream by both, liver and blood cells, whereas liver cells represent the main source of circulating reelin [39]. Published data demonstrated that plasma reelin is able to directly influence the onset and progression of different CVDs by promoting vascular inflammation, platelet adhesion and activation, as well as thrombus formation [53, 60, 61]. In this context, Gowert *et al*. and Krueger *et al*. showed that the loss of reelin protects mice from arterial thrombosis by reducing platelet adhesion, which occurs through impaired GPIb-dependent inside-out activation of integrin $\alpha_{IIb}\beta_3$, as well as diminished reelin-induced GPVI activation and integrin $\alpha_{IIb}\beta_3$ outside-in signalling [53, 60]. After myocardial infarction, reelin, produced by lymphatic endothelial cells, exerts cardio protective effects, which is reflected by improved heart function [153]. Furthermore, Ding *et al*. demonstrated that the loss of reelin attenuates the development of atherosclerosis, as represented by a reduction in plaque size. This effect occurs through the inhibition of leukocyte-endothelial adhesion and macrophage accumulation via ApoER2, along with a decrease in the expression of endothelial adhesion molecules in mice [61]. Since AAA is an atherosclerotic cardiovascular disease [154, 155], we hypothesised that reelin may also contribute to the development and progression of AAA. Moreover, as the AAA pathology is characterised by a chronic inflammatory response as well as the formation of an ILT, reelin might represent a potential novel candidate for targeting AAA formation and progression. Therefore, a better mechanistically understanding how reelin affects the inflammatory response and ECM remodelling during AAA formation is crucial in order to identify suitable targets. However, to date there are no experimental or clinical data on the contribution of reelin and platelet-specific reelin to the formation and progression of AAA.

As platelets represent one source of circulating reelin the aim of this study was focused on the effect of platelet-derived reelin on platelet- and aortic-specific parameters during AAA progression. The analyses of Rln WT and Rln KO mice used in this study revealed contradictory results at different time points such as on day 7 and 28 (**Figure 22 – 37**). Further experiments demonstrated that reelin remains detectable in platelets of platelet-specific Rln KO mice (**Figure 38**). This indicates that platelets from Rln KO mice are capable to internalise reelin from the circulation, with liver cells or endothelial cells serving as the primary source of plasma reelin [39]. Based on this hypothesis, the discrepancy observed in the effect of platelet-derived reelin on AAA progression in platelet-specific Rln KO mice, collected 7 and 28 days post surgery, may be explained by the internalisation of different amounts of reelin. In detail, mice harvested at an early time point showed significant differences in aneurysm diameter, whereas those collected at the later time point displayed two populations, one with an increasing and the other with an almost unaltered aortic diameter compared to the baseline measurement. Thus, we assume that platelets from platelet-specific Rln KO mice might absorb reelin from circulation in different amounts that might be responsible for differences in aortic diameter progression. The capacity of platelets to internalise large proteins, such as glutamate or fibrinogen, from the circulation has already been shown both in humans and in mice (own unpublished data) [156-158]. D'Arcangelo *et al*. have already demonstrated that the reelin receptors ApoER2 and VLDL are capable of mediating reelin uptake into cells *in vitro* using COS-7 monkey fibroblast-like cells that were transfected with a VLDL receptor expression vector [50]. Duit *et al*. confirmed these findings for both receptors in murine embryonic NIH3T3 fibroblast cells expressing ApoER2 or VLDLR [159]. As these receptors are also expressed on the surface of platelets, the ApoER2- respectively VLDL-mediated endocytosis of reelin may represent a potential mechanism of reelin internalisation by reelin-deficient platelets. Therefore, further investigations are required in order to verify this potential mechanism of reelin internalisation in platelets.

Summarised this indicates that the analyses on the impact of platelet-derived reelin for AAA formation remain challenging. Nevertheless, the effect of global reelin in AAA disease could be investigated. In this context, PPE surgery could be performed in mice treated with the CR-50 antibody. Mechanistically, CR-50 prevents reelin oligomerisation and its subsequent receptor binding, and thereby effectively blocks reelin activity [45]. In former publications, it was demonstrated that targeting reelin by using the CR-50 antibody *in vivo* protects mice against atherosclerosis by reducing vascular adhesion of leukocytes and macrophage accumulation under pathological

conditions. As leukocytes and macrophages play a critical role in the formation and progression of AAA the use of the CR-50 antibody might be promising and a completely new approach for the treatment of AAA.

5.3 The ePPE mouse model shows no ILT formation 28 days after ePPE surgery

The PPE mouse model shows many characteristics of human AAA pathology. However, this does not include the process of ILT formation that is found in 75% of all AAA patients [66]. To date, the impact of ILT formation on AAA development and progression is highly debated and not clear yet. On the one hand, this ILT is a biological active entity that releases and transports molecules to the aortic wall and can thereby promote aneurysm formation [94, 97]. On the other hand, it can simultaneously reduce aortic wall stress and thus prevent ruptures [98, 160]. In this context, it is crucial to analyse the process of ILT formation in detail, along with the underlying mechanisms, to develop novel therapeutic approaches targeting AAA formation in future. For this reason, the ePPE mouse model, in which the formation of an ILT has been described by others [106], was established. Subsequently, platelet- and aortic-specific parameters as well as the formation of an ILT were analysed.

5.3.1 Administration of 0.1% BAPN shows mildest secondary effects

For the establishment of the ePPE mouse model, three different concentrations of BAPN were supplemented to the drinking water. As inhibitor of LOX, BAPN is able to prevent cross-linking of elastin and collagen [105, 106], supporting aneurysm development in elastase-treated mice. Interestingly, in young mice Ren *et al*. showed that BAPN is capable of causing aneurysm formation and following rupture without any other treatment such as elastase application [161]. Franklin *et al*. were able to demonstrate that the capability of BAPN alone to induce aneurysm formation in mice is diminished with increasing age, supporting the hypothesis of Sawada and colleagues. They assumed that BAPN has no effect on the cross-linking of already formed elastic fibres [162, 163]. In this way, only new elastin and collagen fibres are prevented from cross-linking during the repair process. Considering these findings, BAPN was added to the drinking water of sham- and elastase-treated mice in this thesis, in order to prevent simultaneous repair mechanisms. However, in *in vivo* experiments it has already been demonstrated that the BAPN concentration is crucial for the survival rate [164]. Therefore, different BAPN concentrations were tested to exclude potential side effects and to find the appropriate BAPN concentration with

regard to aortic diameter expansion. Analyses of survival, AAA incidence and aortic diameter progression over a time course of 28 days were performed. The results showed that the administration of BAPN affects the survival probability in our experiments due to ruptures. However, all elastase-treated mice developed an aneurysm independent of the BAPN concentration used (**Figure 39 – 41**). In ePPE-operated mice with an administration of 1% BAPN, RBC counts were reduced compared to ePPE-operated mice without an administration of BAPN. Furthermore, a reduction in WBC counts were observed in sham-operated mice with an administration of 1% BAPN compared to both other groups, indicating that the drop of circulating WBCs is due to BAPN treatment alone (**Figure 42**). WBCs play a crucial role in AAA formation, as shown by the migration of macrophages and neutrophils into the aortic wall and the release of cytokines and neutrophil elastase, contributing to increased inflammation [127]. Considering the secondary effects of the high BAPN concentration on WBCs, the administration of 1% of BAPN represented no appropriate concentration for the analysis of AAA formation and progression using the ePPE mouse model. To date, published data showing the influence of BAPN on inflammation were only obtained in the AAA mouse model of BAPN-induced aneurysm formation. In this mouse model, the inflammation was enhanced by the administration of BAPN in young mice. But this process of increased inflammation is probably linked to the formation of aneurysms, as the inhibition of aneurysm formation simultaneously reduces inflammation [165-169]. In order to gain further insights into the influence of BAPN on inflammatory cells, *in vitro* experiments with the treatment of BAPN on different blood cell types, including WBCs, could be performed. In contrast to mice administered with 1% BAPN, the administration of 0.1% BAPN showed no differences in the number of WBCs and RBCs compared to the group without BAPN administration (**Figure 42**). Since the aortic diameter in both groups with 0.1% and 1% BAPN treatment revealed similar progression, we decided to use 0.1% BAPN for further experiments.

5.3.2 Platelet activation and pro-coagulant activity might support AAA formation in ePPE-operated mice

After establishment of the ePPE mouse model, platelet-specific parameters at the end timepoint of 28 days were characterised. Regarding platelet activation, the results showed stronger activation upon stimulation with PAR4 and ADP in combination with U46 (**Figure 43**). As already mentioned, increased platelet activation in PPE mice is consistent with data obtained from AAA patients, since AAA patients showed enhanced platelet activation compared to healthy controls. In addition to the

pre-activated state detected in resting platelets, platelet degranulation and activation of integrin $\alpha_{IIb}\beta_3$ were increased upon stimulation of the $P2Y_{12}$ receptor and GPVI in AAA patients [89]. Moreover, the findings on platelet activation in ePPE-operated mice are consistent with recent data published by Morrell and colleagues. They detected increased platelet activation upon thrombin-mediated stimulation of platelets in the ePPE mouse model [145]. Nevertheless, in contrast to the PPE mouse model (**Figure 18 A**), platelet activation in the ePPE model revealed no changes in GPVI activation upon CRP stimulation. Further analyses revealed a reduction in GPVI expression on the platelet surface, accompanied by an increase in plasma levels of sGPVI and glycocalicin, both correlating with the aneurysm diameter (**Figure 44 – 45**). The reduced surface exposure of GPVI might explain the unaltered platelet activation in ePPE-operated mice following CRP stimulation. Furthermore, the decreased GPVI exposure might be due to enhanced GPVI shedding from the platelet surface, as sGPVI plasma levels were found to be elevated in ePPE-operated mice. The enhanced shedding of GPVI from the platelet surface can be mediated by high wall shear stress. The impact of pathological shear stress on the shedding process of platelet receptors was already discussed previously (see chapter **5.1.2**). Since mice undergoing ePPE surgery develop larger aneurysms, we hypothesise that they experience increased shear stress compared to PPE-operated mice, potentially exceeding the threshold necessary for GPVI shedding.

Furthermore, pro-coagulant activity of platelets in ePPE-operated mice was investigated using PS exposure as a marker (**Figure 46**). As observed in the PPE model (**Figure 16 – 20**), enhanced pro-coagulant activity in ePPE mice may result from increased platelet activity, potentially contributing to aneurysm formation. These results were already discussed in detail in chapter **5.1.4** in the context of analysis of the PPE-operated mice.

5.3.3 Aortic wall remodelling in ePPE-induced AAA formation is characterised by enhanced VSMC proliferation

In AAA patients, aneurysm formation is characterised by a progressive aortic wall remodelling including elastin degradation and thinning of the aortic wall due to enhanced VSMC apoptosis. Analysis of the aortic wall remodelling in ePPE mice revealed elevated elastin degradation in the thickened aortic wall of ePPE-operated mice 28 days after surgery. Moreover, additional tissue was detected growing from the aortic wall into the lumen (**Figure 47 – 48**). Further analyses indicated that this

additional tissue is no thrombus tissue composed of platelets, erythrocytes and WBCs, but a layer of proliferated VSMCs (**Figure 49**). These results are inconsistent with those shown in the review of Busch *et al*., where thrombus tissue was shown to be present in ePPE-operated mice 28 days after surgery. However, the additional tissue was only observed in H/E-stained aortic sections and postulated as ILT tissue [106] without further investigation. Although the AAA pathology is typically associated with thinning of the aortic wall, Lu *et al*. as well observed a thickening of the aortic wall and furthermore a disruption of the circular and longitudinal layer arrangement of VSMCs in ePPE-operated mice 28 days after surgery. This thickening of the tunica media was observed not only in the ePPE mouse model but also in another aneurysm mouse model with BAPN administration alone to induce aneurysm formation in young mice [108, 164]. In contrast, Wagenhäuser *et al*. were able to demonstrate a thinning of the murine aortic wall in the Ang II and PPE mouse models 28 days after surgery [89]. Since this characteristic is also found in AAA patients, results from the Ang II and PPE mouse model are more consistent with the human pathology. The main difference observed between the different mouse models may be linked to the addition of BAPN to the drinking water. As previously mentioned, BAPN is used as a LOX inhibitor to prevent cross-linking of collagen and elastin fibres. However, LOX is also expressed in VSMCs and has been shown to be associated with their migration and proliferation [170]. In this context, Varona *et al*. reported that LOX exerts anti-proliferative effects on VSMCs [171]. Therefore, inhibiting LOX using BAPN can also promote proliferation of VSMCs in the aortic wall of ePPE-operated mice, leading to thickening of the aortic wall. However, extended studies by Lu *et al*. revealed a thinning of the aortic wall due to loss of VSCMs and ILT formation over a time course of 100 days after surgery [108]. This indicates that the growth rate of the aneurysm, accompanied by a progressive destruction of the aortic wall, surpasses the proliferation rate of the VSMCs over time. To verify these findings and to establish ILT formation, mice should be analysed over a prolonged time period after ePPE surgery.

5.3.4 Inflammation contributes to aneurysm progression in ePPE-operated mice

In addition to the analyses of aortic wall remodelling experiments regarding platelet-mediated inflammation were performed, since both processes are typical features of aneurysm formation. In this context, platelets and macrophages were found in the aortic wall (**Figure 52 – 53**), indicating an enhanced migration promoting inflammation and aneurysm formation. Lu and colleagues showed macrophage infiltration into the aortic wall of ePPE-operated mice over a time course of 100 days. They found that

the number of infiltrated macrophages peaks at day 14 and decreases thereafter until day 28 [108]. These findings are consistent with the data presented in this study, as only a small amount of macrophages was detected in the aortic tissue of ePPE-operated mice at day 28 post surgery. Since macrophages are the most prominent cell type of acute inflammation, they appear immediately after a medical procedure and rapidly produce inflammatory cytokines [172]. Macrophage infiltration into aortic tissue has also been observed in other mouse models of aneurysm formation, including the PPE model. Published by Wagenhäuser *et al*. it was shown that platelet depletion in PPE-operated mice resulted in a reduced aortic diameter progression accompanied by a decreased macrophage infiltration into the aortic wall. Further, they hypothesised that infiltrated macrophages highly express the pro-inflammatory cytokine osteopontin, which appears to be a recruitment mechanism for platelets into the aortic tissue. Since platelets also release OPN from intracellular stores, they may amplify the recruitment signal for other platelets to infiltrate the aortic wall. This is supported by the finding that macrophages, platelets and osteopontin are co-localised in the aneurysm wall of AAA patients [89], indicating an interaction between those cells with a role for osteopontin.

5.4 Conclusion and outlook

During the last years, several potential candidates for a drug-based therapy in AAA were developed. However, a successful clinical implementation of these non-invasive therapies is still lacking to date. Thus, investigating the pathophysiological mechanisms underlying AAA is crucial for the identification of novel targets for drug-based therapies. In this context, the results of this thesis, showing increased platelet activation and pro-coagulant activity in two experimental mouse models of aneurysm formation, indicate that targeting specifically platelet activation and pro-coagulant activity may represent a new promising approach to reduce AAA formation and progression. Therefore, the novel experimental AAA mouse model “ePPE” was established within the scope of this work. The analysis of platelet-specific parameters in this experimental model revealed altered platelet function and characteristics, indicating their crucial role in AAA formation as mediated by platelet activation and pro-coagulant activity. Since ILT formation is described as unique feature of the ePPE mouse model, this AAA model provides opportunities to analyse the development of the ILT, including the impact of various platelet receptors in this process.

To date, the use of anti-platelet therapies including clopidogrel or ASA is already fully implemented into the clinical routine for decades, as they are used as secondary prophylaxis for the prevention of thromboembolic events following cardiovascular events [115-118]. However, several clinical studies on the effect of ASA on AAA formation revealed contrary outcomes which appear to be dependent on the initial size of the aneurysm in AAA patients. Thus, ASA failed as a potential candidate for the treatment of AAA as it could not effectively reduce growth rate of AAA irrespective of size [120, 173]. Therefore, it is of great interest to identify novel platelet-specific targets in order to develop new anti-platelet therapies. In this context, the impact of platelet-derived reelin on AAA formation was investigated in order to evaluate whether reelin-mediated platelet signalling represents a potential target. However, the analysis on the impact of platelet-derived reelin for AAA formation remains challenging, as recent studies of our working group revealed that platelets may be capable to internalise reelin from the circulation. This makes the analysis of platelet-specific reelin KO mice difficult because in these mice reelin is still present in the circulation and other cells beside platelets (own data unpublished). Thus, targeting reelin by inhibition of reelin dimerisation using the CR-50 antibody in an experimental AAA mouse model would represent a promising translational intervention although this will be a systemic approach that not only targets platelets but also endothelial cells and leukocytes. Nevertheless, applying the CR-50 antibody would provide the opportunity to analyse the underlying mechanisms of reelin-mediated signalling in the processes of inflammation, ECM remodelling and ILT formation and might evaluate a potential clinical outcome in AAA.

6 References

1. Linden, M.D., *Platelet physiology.* Methods in Molecular Biology, 2013. **992**.
2. Smyth, S.S., et al., *Platelet functions beyond hemostasis.* J Thromb Haemost, 2009. **7**(11): p. 1759-66.
3. Ribatti, D. and E. Crivellato, *Giulio Bizzozero and the discovery of platelets.* Leuk Res, 2007. **31**(10): p. 1339-41.
4. Ghoshal, K. and M. Bhattacharyya, *Overview of platelet physiology: its hemostatic and nonhemostatic role in disease pathogenesis.* ScientificWorldJournal, 2014. **2014**: p. 781857.
5. Schmitt, A., et al., *Of mice and men: comparison of the ultrastructure of megakaryocytes and platelets.* Exp Hematol, 2001. **29**(11): p. 1295-302.
6. Sbarouni, E., et al., *Significant changes in platelet count, volume and size in acute aortic dissection.* Int J Cardiol, 2013. **168**(4): p. 4349-50.
7. Wiwanitkit, V., *Plateletcrit, mean platelet volume, platelet distribution width: its expected values and correlation with parallel red blood cell parameters.* Clin Appl Thromb Hemost, 2004. **10**(2): p. 175-8.
8. Fredrickson, B.J., et al., *Shear-dependent rolling on von Willebrand factor of mammalian cells expressing the platelet glycoprotein Ib-IX-V complex.* Blood, 1998. **92**(10): p. 3684-93.
9. Calvete, J.J., *Platelet integrin GPIIb/IIIa: structure-function correlations. An update and lessons from other integrins.* Proc Soc Exp Biol Med, 1999. **222**(1): p. 29-38.
10. Payrastre B, M.K., Trumel C, Bodin S, Plantavid M, Chap H, *The integrin αIIb/β3 in human platelet signal transduction.* Biochemical Pharmacology, 2000. **60**.
11. Zeiler, M., M. Moser, and M. Mann, *Copy number analysis of the murine platelet proteome spanning the complete abundance range.* Mol Cell Proteomics, 2014. **13**(12): p. 3435-45.
12. Mohri H, O.T., *How Vitronectin Binds to Activated Glycoprotein IIb-IIIa Complex and Its Function in Platelet Aggregation.* American Journal of Clinical Pathology, 1991.
13. Sarratt, K.L., et al., *GPVI and alpha2beta1 play independent critical roles during platelet adhesion and aggregate formation to collagen under flow.* Blood, 2005. **106**(4): p. 1268-77.
14. Murugappa, S. and S.P. Kunapuli, *The role of ADP receptors in platelet function.* Front Biosci, 2006. **11**: p. 1977-86.
15. Pierce, K.L., R.T. Premont, and R.J. Lefkowitz, *Seven-transmembrane receptors.* Nat Rev Mol Cell Biol, 2002. **3**(9): p. 639-50.
16. Nakahata, N., *Thromboxane A2: physiology/pathophysiology, cellular signal transduction and pharmacology.* Pharmacol Ther, 2008. **118**(1): p. 18-35.
17. Hirano, K., *The roles of proteinase-activated receptors in the vascular physiology and pathophysiology.* Arterioscler Thromb Vasc Biol, 2007. **27**(1): p. 27-36.
18. Harrison, P. and E.M. Cramer, *Platelet alpha-granules.* Blood Rev, 1993. **7**(1): p. 52-62.

19. McNicol A, I.S., *Platelet Dense Granules: Structure, Function and Implications for Haemostasis.* Thrombosis Research, 1999.
20. Fukami, M., *Dense granule factors*. Platelets and their factors, ed. W.U. Bruchhausen F. 1997, New York: Springer. 419-432.
21. Reed, G.L., *Platelet secretory mechanisms.* Semin Thromb Hemost, 2004. **30**(4): p. 441-50.
22. Lefkovits, J., E.F. Plow, and E.J. Topol, *Platelet glycoprotein IIb/IIIa receptors in cardiovascular medicine.* N Engl J Med, 1995. **332**(23): p. 1553-9.
23. Chatterjee, M., et al., *Molecular Drivers of Platelet Activation: Unraveling Novel Targets for Anti-Thrombotic and Anti-Thrombo-Inflammatory Therapy.* Int J Mol Sci, 2020. **21**(21).
24. Li, Z., et al., *Signaling during platelet adhesion and activation.* Arterioscler Thromb Vasc Biol, 2010. **30**(12): p. 2341-9.
25. Varga-Szabo, D., I. Pleines, and B. Nieswandt, *Cell adhesion mechanisms in platelets.* Arterioscler Thromb Vasc Biol, 2008. **28**(3): p. 403-12.
26. Clemetson, K.J., *Platelets and primary haemostasis.* Thromb Res, 2012. **129**(3): p. 220-4.
27. Gale, A.J., *Current understanding of hemostasis.* Toxicol Pathol, 2011. **39**(1): p. 273-80.
28. Dahlback, B., *Blood coagulation.* Lancet, 2000. **355**(9215): p. 1627-32.
29. Shapira, S., et al., *The effect of storage on the expression of platelet membrane phosphatidylserine and the subsequent impacton the coagulant function of stored platelets.* Transfusion, 2000. **40**(10): p. 1257-63.
30. Huo, Y. and K.F. Ley, *Role of platelets in the development of atherosclerosis.* Trends Cardiovasc Med, 2004. **14**(1): p. 18-22.
31. Willoughby, S., A. Holmes, and J. Loscalzo, *Platelets and cardiovascular disease.* Eur J Cardiovasc Nurs, 2002. **1**(4): p. 273-88.
32. Committee, C.S., *A randomised, blinded, trial of clopidogrel versus aspirin in patients at risk of ischaemic events (CAPRIE). CAPRIE Steering Committee*. Lancet. Vol. 348. 1996. 1329-39.
33. Del Rio, J.A., et al., *A role for Cajal-Retzius cells and reelin in the development of hippocampal connections.* Nature, 1997. **385**(6611): p. 70-4.
34. Ogawa, M., et al., *The reeler gene-associated antigen on Cajal-Retzius neurons is a crucial molecule for laminar organization of cortical neurons.* Neuron, 1995. **14**(5): p. 899-912.
35. D'Arcangelo, G., et al., *A protein related to extracellular matrix proteins deleted in the mouse mutant reeler.* Nature, 1995. **374**(6524): p. 719-23.
36. Gilmore, E.C. and K. Herrup, *Cortical development: receiving reelin.* Curr Biol, 2000. **10**(4): p. R162-6.
37. Soriano, E. and J.A. Del Rio, *The cells of cajal-retzius: still a mystery one century after.* Neuron, 2005. **46**(3): p. 389-94.
38. Fatemi, S.H., *Reelin glycoprotein: structure, biology and roles in health and disease.* Mol Psychiatry, 2005. **10**(3): p. 251-7.
39. Smalheiser, N.R., et al., *Expression of reelin in adult mammalian blood, liver, pituitary pars intermedia, and adrenal chromaffin cells.* Proc Natl Acad Sci U S A, 2000. **97**(3): p. 1281-6.

40. Alexander, A., J. Herz, and L. Calvier, *Reelin through the years: From brain development to inflammation.* Cell Rep, 2023. **42**(6): p. 112669.

41. Falconer, D.S., *Two new mutants, 'trembler' and 'reeler', with neurological actions in the house mouse (Mus musculus L.).* J Genet, 1951. **50**(2): p. 192-201.

42. DeSilva, U., et al., *The human reelin gene: isolation, sequencing, and mapping on chromosome 7.* Genome Res, 1997. **7**(2): p. 157-64.

43. Curran, T. and G. D'Arcangelo, *Role of reelin in the control of brain development.* Brain Res Brain Res Rev, 1998. **26**(2-3): p. 285-94.

44. Knuesel, I., *Reelin-mediated signaling in neuropsychiatric and neurodegenerative diseases.* Prog Neurobiol, 2010. **91**(4): p. 257-74.

45. Utsunomiya-Tate, N., et al., *Reelin molecules assemble together to form a large protein complex, which is inhibited by the function-blocking CR-50 antibody.* Proc Natl Acad Sci U S A, 2000. **97**(17): p. 9729-34.

46. Lakatosova, S. and D. Ostatnikova, *Reelin and its complex involvement in brain development and function.* Int J Biochem Cell Biol, 2012. **44**(9): p. 1501-4.

47. Kohno, S., et al., *Mechanism and significance of specific proteolytic cleavage of Reelin.* Biochem Biophys Res Commun, 2009. **380**(1): p. 93-7.

48. Lambert de Rouvroit, C., et al., *Reelin, the extracellular matrix protein deficient in reeler mutant mice, is processed by a metalloproteinase.* Exp Neurol, 1999. **156**(1): p. 214-7.

49. Jossin, Y., et al., *The central fragment of Reelin, generated by proteolytic processing in vivo, is critical to its function during cortical plate development.* J Neurosci, 2004. **24**(2): p. 514-21.

50. D'Arcangelo, G., et al., *Reelin is a ligand for lipoprotein receptors.* Neuron, 1999. **24**(2): p. 471-9.

51. Hoe, H.S., et al., *Interaction of reelin with amyloid precursor protein promotes neurite outgrowth.* J Neurosci, 2009. **29**(23): p. 7459-73.

52. Bock, H.H. and J. Herz, *Reelin activates SRC family tyrosine kinases in neurons.* Curr Biol, 2003. **13**(1): p. 18-26.

53. Krueger, I., et al., *Reelin Amplifies Glycoprotein VI Activation and AlphaIIb Beta3 Integrin Outside-In Signaling via PLC Gamma 2 and Rho GTPases.* Arterioscler Thromb Vasc Biol, 2020. **40**(10): p. 2391-2403.

54. Stolt, P.C. and H.H. Bock, *Modulation of lipoprotein receptor functions by intracellular adaptor proteins.* Cell Signal, 2006. **18**(10): p. 1560-71.

55. Bock, H.H., et al., *Apolipoprotein E receptors are required for reelin-induced proteasomal degradation of the neuronal adaptor protein Disabled-1.* J Biol Chem, 2004. **279**(32): p. 33471-9.

56. Morimura, T., et al., *Disabled1 regulates the intracellular trafficking of reelin receptors.* J Biol Chem, 2005. **280**(17): p. 16901-8.

57. Dulabon, L., et al., *Reelin binds alpha3beta1 integrin and inhibits neuronal migration.* Neuron, 2000. **27**(1): p. 33-44.

58. Senzaki, K., M. Ogawa, and T. Yagi, *Proteins of the CNR family are multiple receptors for Reelin.* Cell, 1999. **99**(6): p. 635-47.

59. Tseng, W.L., et al., *Reelin is a platelet protein and functions as a positive regulator of platelet spreading on fibrinogen.* Cell Mol Life Sci, 2010. **67**(4): p. 641-53.

60. Gowert, N.S., et al., *Loss of Reelin protects mice against arterial thrombosis by impairing integrin activation and thrombus formation under high shear conditions.* Cell Signal, 2017. **40**: p. 210-221.

61. Ding, Y., et al., *Loss of Reelin protects against atherosclerosis by reducing leukocyte-endothelial cell adhesion and lesion macrophage accumulation.* Sci Signal, 2016. **9**(419): p. ra29.

62. Tseng, W.L., et al., *Impaired thrombin generation in Reelin-deficient mice: a potential role of plasma Reelin in hemostasis.* J Thromb Haemost, 2014. **12**(12): p. 2054-64.

63. Prisant LM, M.J., *Abdominal Aortic Aneurysm.* The Journal of Clinical Hypertension, 2004. **VI No. II**.

64. Lederle, F.A., et al., *Prevalence and associations of abdominal aortic aneurysm detected through screening. Aneurysm Detection and Management (ADAM) Veterans Affairs Cooperative Study Group.* Ann Intern Med, 1997. **126**(6): p. 441-9.

65. Scott, R.A., S.G. Bridgewater, and H.A. Ashton, *Randomized clinical trial of screening for abdominal aortic aneurysm in women.* Br J Surg, 2002. **89**(3): p. 283-5.

66. Di Achille, P.T., G.; Figueroa, C. A.; Humphrey, J. D., *A haemodynamic predictor of intraluminal thrombus formation in abdominal aortic aneurysms.* Proc. R. Soc. A, 2014. **470**.

67. Upchurch GR, S.T., *Abdominal Aortic Aneurysm.* Am Fam Physician, 2006. **73**.

68. Aggarwal, S., et al., *Abdominal aortic aneurysm: A comprehensive review.* Exp Clin Cardiol, 2011. **16**(1): p. 11-5.

69. Kniemeyer, H.W., et al., *Treatment of ruptured abdominal aortic aneurysm, a permanent challenge or a waste of resources? Prediction of outcome using a multi-organ-dysfunction score.* Eur J Vasc Endovasc Surg, 2000. **19**(2): p. 190-6.

70. Li, X., et al., *Prevalence and trends of the abdominal aortic aneurysms epidemic in general population--a meta-analysis.* PLoS One, 2013. **8**(12): p. e81260.

71. Vaduganathan, M., et al., *The Global Burden of Cardiovascular Diseases and Risk: A Compass for Future Health.* J Am Coll Cardiol, 2022. **80**(25): p. 2361-2371.

72. Krings, T., et al., *The aneurysmal wall. The key to a subclassification of intracranial arterial aneurysm vasculopathies?* Interv Neuroradiol, 2008. **14 Suppl 1**(Suppl 1): p. 39-47.

73. Jeyabalan, G., et al., *Comparison of modern open infrarenal and pararenal abdominal aortic aneurysm repair on early outcomes and renal dysfunction at one year.* J Vasc Surg, 2011. **54**(3): p. 654-9.

74. Komutrattananont, P., P. Mahakkanukrauh, and S. Das, *Morphology of the human aorta and age-related changes: anatomical facts.* Anat Cell Biol, 2019. **52**(2): p. 109-114.

75. Czerny, M., et al., *EACTS/STS Guidelines for diagnosing and treating acute and chronic syndromes of the aortic organ.* Eur J Cardiothorac Surg, 2024. **65**(2).

76. Gutterman, D.D., *Adventitia-dependent influences on vascular function.* Am J Physiol, 1999. **277**(4): p. H1265-72.

77. Sayantan, J., Mei, H.; Mengcheng, S.; Zamaneh K., *Extracellular matrix, regional heterogeneity of the aorta, and aortic aneurysm.* Experimental & Molecular Medicine, 2019. **51**.

78. Wagenseil, J.E. and R.P. Mecham, *Vascular extracellular matrix and arterial mechanics.* Physiol Rev, 2009. **89**(3): p. 957-89.

79. Robert, L., M.P. Jacob, and T. Fulop, *Elastin in blood vessels.* Ciba Found Symp, 1995. **192**: p. 286-99; discussion 299-303.

80. Lopez-Candales, A., et al., *Decreased vascular smooth muscle cell density in medial degeneration of human abdominal aortic aneurysms.* Am J Pathol, 1997. **150**(3): p. 993-1007.

81. Miller, F.J., Jr., et al., *Oxidative stress in human abdominal aortic aneurysms: a potential mediator of aneurysmal remodeling.* Arterioscler Thromb Vasc Biol, 2002. **22**(4): p. 560-5.

82. Vorp, D.A., et al., *Potential influence of intraluminal thrombus on abdominal aortic aneurysm as assessed by a new non-invasive method.* Cardiovasc Surg, 1996. **4**(6): p. 732-9.

83. Didangelos, A., et al., *Extracellular matrix composition and remodeling in human abdominal aortic aneurysms: a proteomics approach.* Mol Cell Proteomics, 2011. **10**(8): p. M111 008128.

84. Goodall, S., et al., *Enhanced invasive properties exhibited by smooth muscle cells are associated with elevated production of MMP-2 in patients with aortic aneurysms.* Eur J Vasc Endovasc Surg, 2002. **24**(1): p. 72-80.

85. Tsarouhas, K., et al., *Transcriptional regulation of TIMPs in ascending aorta aneurysms.* Thromb Res, 2010. **126**(5): p. 399-405.

86. Lesauskaite, V., et al., *Expression of matrix metalloproteinases, their tissue inhibitors, and osteopontin in the wall of thoracic and abdominal aortas with dilatative pathology.* Hum Pathol, 2006. **37**(8): p. 1076-84.

87. Satta, J., et al., *Increased turnover of collagen in abdominal aortic aneurysms, demonstrated by measuring the concentration of the aminoterminal propeptide of type III procollagen in peripheral and aortal blood samples.* J Vasc Surg, 1995. **22**(2): p. 155-60.

88. Lindholt, J.S. and G.P. Shi, *Chronic inflammation, immune response, and infection in abdominal aortic aneurysms.* Eur J Vasc Endovasc Surg, 2006. **31**(5): p. 453-63.

89. Wagenhauser, M.U., et al., *Crosstalk of platelets with macrophages and fibroblasts aggravates inflammation, aortic wall stiffening, and osteopontin release in abdominal aortic aneurysm.* Cardiovasc Res, 2024. **120**(4): p. 417-432.

90. Plana, E., et al., *Novel contributions of neutrophils in the pathogenesis of abdominal aortic aneurysm, the role of neutrophil extracellular traps: A systematic review.* Thromb Res, 2020. **194**: p. 200-208.

91. Pizzino, G., et al., *Oxidative Stress: Harms and Benefits for Human Health.* Oxid Med Cell Longev, 2017. **2017**: p. 8416763.

92. Folkesson, M., et al., *Protease activity in the multi-layered intra-luminal thrombus of abdominal aortic aneurysms.* Atherosclerosis, 2011. **218**(2): p. 294-9.

93. Harter, L.P., et al., *Ultrasonic evaluation of abdominal aortic thrombus.* J Ultrasound Med, 1982. **1**(8): p. 315-8.

94. Adolph, R., et al., *Cellular content and permeability of intraluminal thrombus in abdominal aortic aneurysm.* J Vasc Surg, 1997. **25**(5): p. 916-26.

95. O'Leary, S.A., et al., *The biaxial mechanical behaviour of abdominal aortic aneurysm intraluminal thrombus: classification of morphology and the determination of layer and region specific properties.* J Biomech, 2014. **47**(6): p. 1430-7.

96. Wilson, J.S., et al., *Biochemomechanics of intraluminal thrombus in abdominal aortic aneurysms.* J Biomech Eng, 2013. **135**(2): p. 021011.

97. Touat, Z., et al., *Renewal of mural thrombus releases plasma markers and is involved in aortic abdominal aneurysm evolution.* Am J Pathol, 2006. **168**(3): p. 1022-30.

98. Mower, W.R., W.J. Quinones, and S.S. Gambhir, *Effect of intraluminal thrombus on abdominal aortic aneurysm wall stress.* J Vasc Surg, 1997. **26**(4): p. 602-8.

99. Ponseti, I.V. and W.A. Baird, *Scoliosis and dissecting aneurysm of the aorta in rats fed with Lathyrus odoratus seeds.* Am J Pathol, 1952. **28**(6): p. 1059-77.

100. Bachhuber, T.E. and J.J. Lalich, *Effect of sweet pea meal on the rat aorta.* AMA Arch Pathol, 1955. **59**(2): p. 247-53.

101. Bachhuber, T.E., et al., *Lathyrus factor activity of beta-aminopropionitrile and related compounds.* Proc Soc Exp Biol Med, 1955. **89**(2): p. 294-7.

102. Golledge, J., S.M. Krishna, and Y. Wang, *Mouse models for abdominal aortic aneurysm.* Br J Pharmacol, 2022. **179**(5): p. 792-810.

103. Anidjar, S., et al., *Elastase-induced experimental aneurysms in rats.* Circulation, 1990. **82**(3): p. 973-81.

104. Pyo, R., et al., *Targeted gene disruption of matrix metalloproteinase-9 (gelatinase B) suppresses development of experimental abdominal aortic aneurysms.* J Clin Invest, 2000. **105**(11): p. 1641-9.

105. Bhamidipati, C.M., et al., *Development of a novel murine model of aortic aneurysms using peri-adventitial elastase.* Surgery, 2012. **152**(2): p. 238-46.

106. Busch, A., et al., *Translating mouse models of abdominal aortic aneurysm to the translational needs of vascular surgery.* JVS Vasc Sci, 2021. **2**: p. 219-234.

107. Busch, A., et al., *Extra- and Intraluminal Elastase Induce Morphologically Distinct Abdominal Aortic Aneurysms in Mice and Thus Represent Specific Subtypes of Human Disease.* J Vasc Res, 2016. **53**(1-2): p. 49-57.

108. Lu, G., et al., *A novel chronic advanced stage abdominal aortic aneurysm murine model.* J Vasc Surg, 2017. **66**(1): p. 232-242 e4.

109. Daugherty, A.M., M.W.; and C. L.A., *Angiotensin II promotes atherosclerotic lesions and aneurysms in apolipoprotein E–deficient mice.* J. Clin. Invest, 2000. **105**: p. 1605–1612.

110. Kanematsu, Y., et al., *Pharmacologically induced thoracic and abdominal aortic aneurysms in mice.* Hypertension, 2010. **55**(5): p. 1267-74.

111. Cooper, H.A., et al., *Targeting mitochondrial fission as a potential therapeutic for abdominal aortic aneurysm.* Cardiovasc Res, 2021. **117**(3): p. 971-982.

112. Chiou, A.C., B. Chiu, and W.H. Pearce, *Murine aortic aneurysm produced by periarterial application of calcium chloride.* J Surg Res, 2001. **99**(2): p. 371-6.

113. Lebas, H., et al., *Platelets Are at the Nexus of Vascular Diseases.* Front Cardiovasc Med, 2019. **6**: p. 132.

114. Sun, W., J. Zheng, and Y. Gao, *Targeting Platelet Activation in Abdominal Aortic Aneurysm: Current Knowledge and Perspectives.* Biomolecules, 2022. **12**(2).

115. Kim, S.P., et al., *Low-dose aspirin in the primary prevention of cardiovascular diseases: A retrospective, propensity score matched study.* Atherosclerosis, 2023. **371**: p. 54-60.

116. Michelson, A.D., *Antiplatelet therapies for the treatment of cardiovascular disease.* Nat Rev Drug Discov, 2010. **9**(2): p. 154-69.

117. Banerjee, S., et al., *Clopidogrel versus Other Antiplatelet Agents for Secondary Prevention of Vascular Events in Adults with Acute Coronary Syndrome or Peripheral Vascular Disease: Clinical and Cost-Effectiveness Analyses.* CADTH Technol Overv, 2012. **2**(1): p. e2102.

118. Golledge, J. and J.T. Powell, *Medical management of abdominal aortic aneurysm.* Eur J Vasc Endovasc Surg, 2007. **34**(3): p. 267-73.

119. Cameron, S.J., H.M. Russell, and A.P. Owens, 3rd, *Antithrombotic therapy in abdominal aortic aneurysm: beneficial or detrimental?* Blood, 2018. **132**(25): p. 2619-2628.

120. Lindholt, J.S., et al., *Low-dose aspirin may prevent growth and later surgical repair of medium-sized abdominal aortic aneurysms.* Vasc Endovascular Surg, 2008. **42**(4): p. 329-34.

121. Liu, O., et al., *Clopidogrel, a platelet P2Y12 receptor inhibitor, reduces vascular inflammation and angiotensin II induced-abdominal aortic aneurysm progression.* PLoS One, 2012. **7**(12): p. e51707.

122. Dai, J., et al., *Effect of blocking platelet activation with AZD6140 on development of abdominal aortic aneurysm in a rat aneurysmal model.* J Vasc Surg, 2009. **49**(3): p. 719-27.

123. Shifrin, M.M. and S.B. Widmar, *Platelet Inhibitors.* Nurs Clin North Am, 2016. **51**(1): p. 29-43.

124. J. Lysgaard Poulsen, J. Stubbe, and J.S. Lindholt, *Animal Models Used to Explore Abdominal Aortic Aneurysms: A Systematic Review.* European journal of vascular and endovascular surgery : the official journal of the European Society for Vascular Surgery.

125. Ho, Y.C., et al., *Heme oxygenase-1 deficiency exacerbates angiotensin II-induced aortic aneurysm in mice.* Oncotarget, 2016. **7**(42): p. 67760-67776.

126. Zwaal, R.F., P. Comfurius, and E.M. Bevers, *Surface exposure of phosphatidylserine in pathological cells.* Cell Mol Life Sci, 2005. **62**(9): p. 971-88.

127. Feige, T., et al., *GP VI-Mediated Platelet Activation and Procoagulant Activity Aggravate Inflammation and Aortic Wall Remodeling in Abdominal Aortic Aneurysm.* Arterioscler Thromb Vasc Biol, 2024.

128. Owens, A.P., 3rd, et al., *Platelet Inhibitors Reduce Rupture in a Mouse Model of Established Abdominal Aortic Aneurysm.* Arterioscler Thromb Vasc Biol, 2015. **35**(9): p. 2032-2041.

129. Wemmelund, H., et al., *Low-dose aspirin and rupture of abdominal aortic aneurysm.* J Vasc Surg, 2017. **65**(3): p. 616-625 e4.

130. Milne, A.A., et al., *Effects of asymptomatic abdominal aortic aneurysm on the soluble coagulation system, platelet count and platelet activation.* Eur J Vasc Endovasc Surg, 1999. **17**(5): p. 434-7.

131. Mukaiyama, H., et al., *Abdominal aortic aneurysm complicated with chronic disseminated intravascular coagulopathy: a case of surgical treatment.* J Vasc Surg, 1987. **6**(6): p. 600-4.

132. Benson, T.W., et al., *Soluble Glycoprotein VI Predicts Abdominal Aortic Aneurysm Growth Rate and is a Novel Therapeutic Target.* Blood, 2024.

133. Bernad, S.B., E.; Barbat, T.; Brisan, C.; Albulescu, V., *An analysis of blood flow dynamics in AAA*, in *Etiology, Pathogenesis and Pathophysiology of Aortic Aneurysms and Aneurysm Rupture*, R. Grundmann, Editor. 2011.

134. Boyd, A.J., et al., *Low wall shear stress predominates at sites of abdominal aortic aneurysm rupture.* J Vasc Surg, 2016. **63**(6): p. 1613-9.

135. Al-Tamimi, M., et al., *Pathologic shear triggers shedding of vascular receptors: a novel mechanism for down-regulation of platelet glycoprotein VI in stenosed coronary vessels.* Blood, 2012. **119**(18): p. 4311-20.

136. Bergmeier, W., et al., *Tumor necrosis factor-alpha-converting enzyme (ADAM17) mediates GPIbalpha shedding from platelets in vitro and in vivo.* Circ Res, 2004. **95**(7): p. 677-83.

137. Deng, W., et al., *Platelet clearance via shear-induced unfolding of a membrane mechanoreceptor.* Nat Commun, 2016. **7**: p. 12863.

138. Clemetson, K.J., H.Y. Naim, and E.F. Luscher, *Relationship between glycocalicin and glycoprotein Ib of human platelets.* Proc Natl Acad Sci U S A, 1981. **78**(5): p. 2712-6.

139. Gardiner, E.E., et al., *Controlled shedding of platelet glycoprotein (GP)VI and GPIb-IX-V by ADAM family metalloproteinases.* J Thromb Haemost, 2007. **5**(7): p. 1530-7.

140. Babendreyer, A., et al., *Differential Induction of the ADAM17 Regulators iRhom1 and 2 in Endothelial Cells.* Front Cardiovasc Med, 2020. **7**: p. 610344.

141. Beer, J.B., L.; Steiner B., *Glycocalicin: A New Assay—The Normal Plasma Levels and Its Potential Usefulness in Selected Diseases.* Blood, 1994. **83**: p. 691-702.

142. Kawano, T., et al., *Decreased Platelet Reactivity and Function in a Mouse Model of Human Pancreatic Cancer.* Thromb Haemost, 2023. **123**(5): p. 501-509.

143. Fender, A.C., et al., *Protease-Activated Receptor PAR-4: An Inducible Switch between Thrombosis and Vascular Inflammation?* Thromb Haemost, 2017. **117**(11): p. 2013-2025.

144. Stitham, J., et al., *Prostacyclin: an inflammatory paradox.* Front Pharmacol, 2011. **2**: p. 24.

145. Morrell, C.N., et al., *Platelet olfactory receptor activation limits platelet reactivity and growth of aortic aneurysms.* J Clin Invest, 2022. **132**(9).

146. Kahn, M.L., et al., *A dual thrombin receptor system for platelet activation.* Nature, 1998. **394**(6694): p. 690-4.

147. Monroe, D.M., M. Hoffman, and H.R. Roberts, *Platelets and thrombin generation.* Arterioscler Thromb Vasc Biol, 2002. **22**(9): p. 1381-9.

148. Chu, Y., et al., *Procoagulant platelets: Generation, characteristics, and therapeutic target.* J Clin Lab Anal, 2021. **35**(5): p. e23750.

149. Pasalic, L., et al., *Novel assay demonstrates that coronary artery disease patients have heightened procoagulant platelet response.* J Thromb Haemost, 2018. **16**(6): p. 1198-1210.

150. Yuan, Z., et al., *Abdominal Aortic Aneurysm: Roles of Inflammatory Cells.* Front Immunol, 2020. **11**: p. 609161.

151. Lund, S.A., C.M. Giachelli, and M. Scatena, *The role of osteopontin in inflammatory processes.* J Cell Commun Signal, 2009. **3**(3-4): p. 311-22.

152. Rigg, R.A., et al., *Protease-activated receptor 4 activity promotes platelet granule release and platelet-leukocyte interactions.* Platelets, 2019. **30**(1): p. 126-135.

153. Liu, X., et al., *Lymphoangiocrine signals promote cardiac growth and repair.* Nature, 2020. **588**(7839): p. 705-711.

154. Frostegard, J., *Immunity, atherosclerosis and cardiovascular disease.* BMC Med, 2013. **11**: p. 117.

155. Toghill, B.J., A. Saratzis, and M.J. Bown, *Abdominal aortic aneurysm-an independent disease to atherosclerosis?* Cardiovasc Pathol, 2017. **27**: p. 71-75.

156. Begni, B., et al., *Substrate-induced modulation of glutamate uptake in human platelets.* Br J Pharmacol, 2005. **145**(6): p. 792-9.

157. Handagama, P., et al., *Endocytosis of fibrinogen into megakaryocyte and platelet alpha-granules is mediated by alpha IIb beta 3 (glycoprotein IIb-IIIa).* Blood, 1993. **82**(1): p. 135-8.

158. Harrison, P., et al., *Uptake of plasma fibrinogen into the alpha granules of human megakaryocytes and platelets.* J Clin Invest, 1989. **84**(4): p. 1320-4.

159. Duit, S., et al., *Differential functions of ApoER2 and very low density lipoprotein receptor in Reelin signaling depend on differential sorting of the receptors.* J Biol Chem, 2010. **285**(7): p. 4896-908.

160. Thubrikar, M.J., et al., *Effect of thrombus on abdominal aortic aneurysm wall dilation and stress.* J Cardiovasc Surg (Torino), 2003. **44**(1): p. 67-77.

161. Ren, W., et al., *beta-Aminopropionitrile monofumarate induces thoracic aortic dissection in C57BL/6 mice.* Sci Rep, 2016. **6**: p. 28149.

162. Franklin, M.K., et al., *beta-aminopropionitrile Induces Distinct Pathologies in the Ascending and Descending Thoracic Aortic Regions of Mice.* bioRxiv, 2024.

163. Sawada, H., et al., *beta-Aminopropionitrile-induced aortic aneurysm and dissection in mice.* JVS Vasc Sci, 2022. **3**: p. 64-72.

164. Chen, T., et al., *BAPN-induced rodent model of aortic dissecting aneurysm and related complications.* J Thorac Dis, 2021. **13**(6): p. 3643-3651.

165. Ren, W., et al., *The Complement C3a-C3aR Axis Promotes Development of Thoracic Aortic Dissection via Regulation of MMP2 Expression.* J Immunol, 2018. **200**(5): p. 1829-1838.

166. Han, L., et al., *CD40L promotes development of acute aortic dissection via induction of inflammation and impairment of endothelial cell function.* Aging (Albany NY), 2018. **10**(3): p. 371-385.

167. Liu, C., et al., *Interleukin-3 stimulates matrix metalloproteinase 12 production from macrophages promoting thoracic aortic aneurysm/dissection.* Clin Sci (Lond), 2018. **132**(6): p. 655-668.

168. Wang, X., et al., *Dexamethasone reduces the formation of thoracic aortic aneurysm and dissection in a murine model.* Exp Cell Res, 2021. **405**(2): p. 112703.

169. Zhang, H., et al., *Asiatic acid alleviates vascular remodeling in BAPN-induced aortic dissection through inhibiting NF-kappaB p65/CX3CL1 signaling.* FASEB J, 2024. **38**(9): p. e23645.

170. Rodriguez, C., et al., *Regulation of lysyl oxidase in vascular cells: lysyl oxidase as a new player in cardiovascular diseases.* Cardiovasc Res, 2008. **79**(1): p. 7-13.

171. Varona, S., et al., *Lysyl oxidase (LOX) limits VSMC proliferation and neointimal thickening through its extracellular enzymatic activity.* Sci Rep, 2018. **8**(1): p. 13258.

172. Sheu, K.M. and A. Hoffmann, *Functional Hallmarks of Healthy Macrophage Responses: Their Regulatory Basis and Disease Relevance.* Annu Rev Immunol, 2022. **40**: p. 295-321.

173. Hariri, E., et al., *Antiplatelet Therapy, Abdominal Aortic Aneurysm Progression, and Clinical Outcomes.* JAMA Netw Open, 2023. **6**(12): p. e2347296.

7 Appendix

7.1 Appendix figures

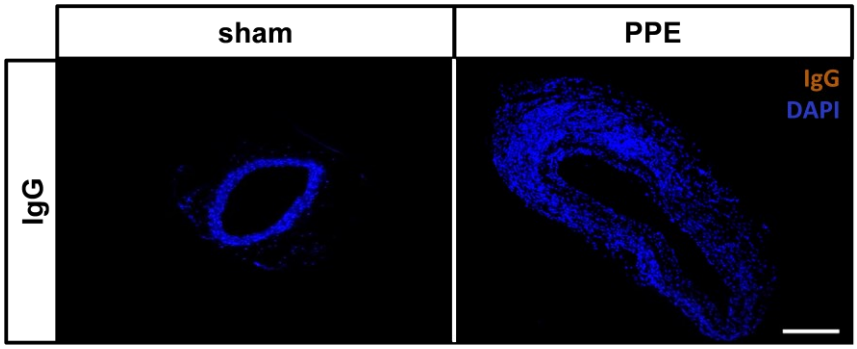

Figure 54. Inflammatory OPN was increased in aortic tissue of PPE-operated mice at late stage of aneurysm formation. Representative immunofluorescence images of IgG controls for OPN staining in aortic wall tissue from naive and PPE-operated mice 28 days after surgery. Scale bar: 100 µm. DAPI = 4′,6-diamidino-2-phenylindole; PPE = porcine pancreatic elastase (infusion).

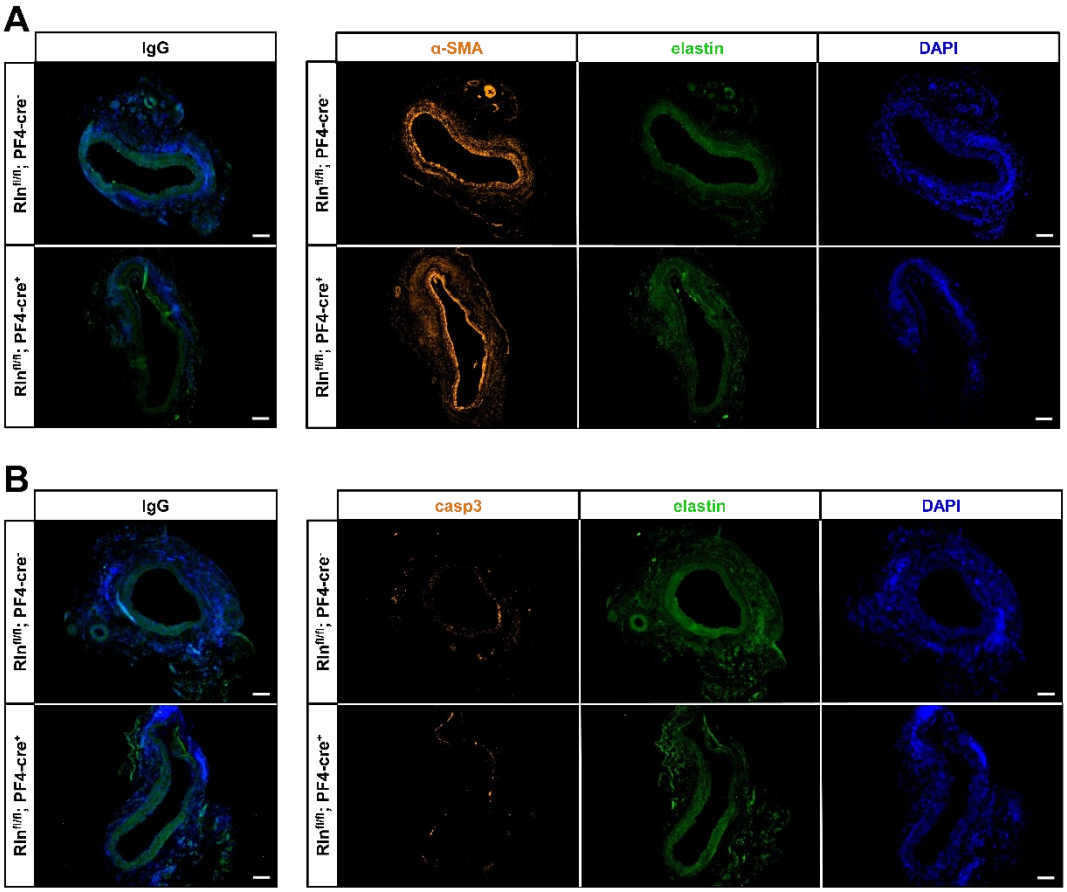

Figure 55. Platelet-specific reelin deficiency exhibited no effects on the aortic α-SMA and casp3 content at day 28 post PPE surgery. Representative single channel images and IgG controls of immunofluorescence stainings of (**A**) α-SMA and (**B**) casp3 in aortic wall of Rln WT (*Rln$^{fl/fl}$; PF4-cre^{-}*) and Rln KO (*Rln$^{fl/fl}$; PF4-cre^{+}*) mice 28 days after PPE surgery. Aortic tissue was specifically stained for (**A**) α-SMA (anti-α-SMA, orange) or (**B**) casp3 (anti-casp3, orange). Elastin (green) is demonstrated by autofluorescence, and nuclei were stained with DAPI (blue). Scale bar: 100 µm. α-SMA = alpha smooth muscle cell actin; DAPI = 4′,6-diamidino-2-phenylindole; KO = knockout; Rln = reelin; WT = wild-type.

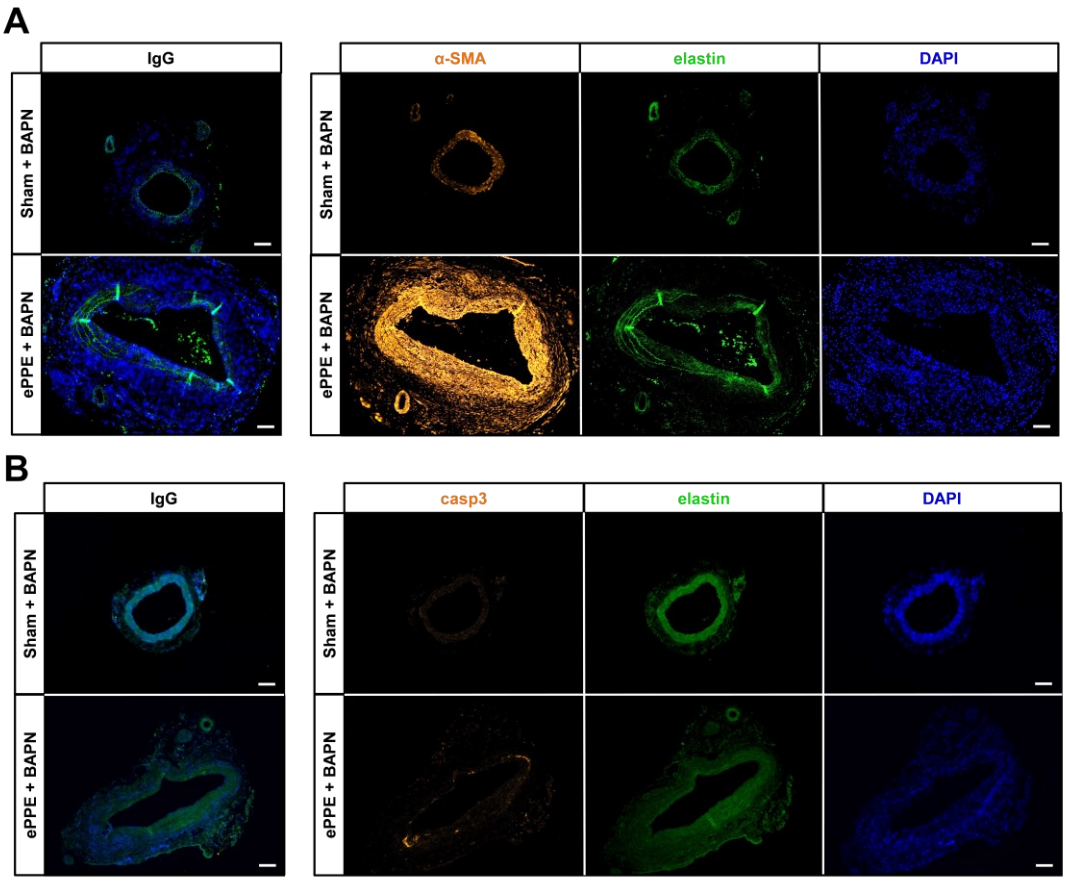

Figure 56. Content of α-SMA and casp3 positive cells in aortic wall of ePPE-operated mice. Representative single channel images and IgG controls of immunofluorescence stainings of (**A**) α-SMA and (**B**) casp3 positive cells in the aortic wall of sham- and ePPE-operated mice 28 days after surgery. Aortic tissue was specifically stained for (**A**) α-SMA (anti-α-SMA, orange) or (**B**) casp3 (anti-casp3, orange). Elastin (green) is presented by autofluorescence, and nuclei were stained with DAPI (blue). Scale bar: 100 µm. α-SMA = alpha smooth muscle cell actin; DAPI = 4′,6-diamidino-2-phenylindole; ePPE = external porcine pancreatic elastase (application).

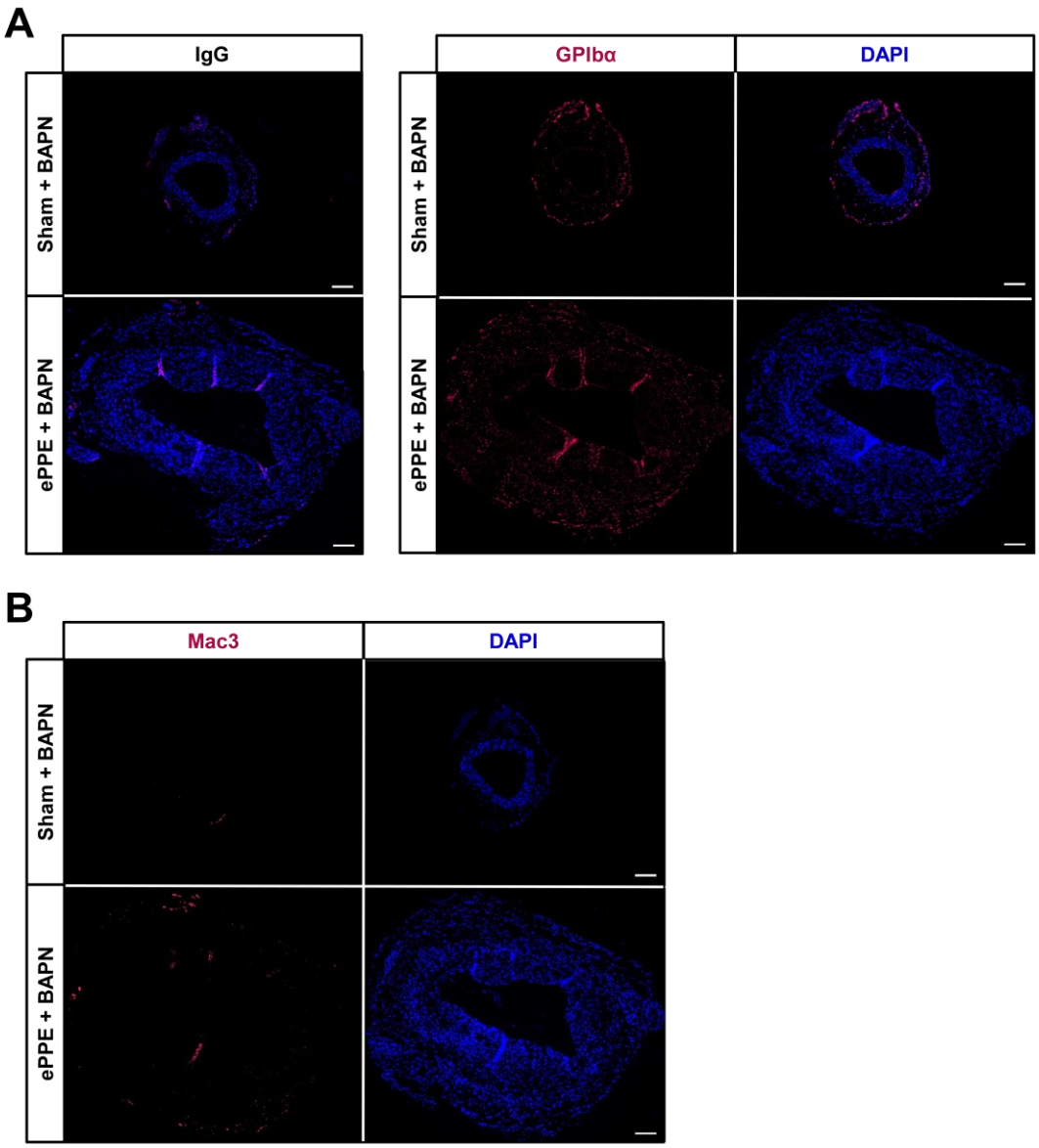

Figure 57. Content of platelets and macrophages was increased in the aortic wall of ePPE mice. Representative single channel images and IgG controls of immunofluorescence stainings of (**A**) GPIbα and (**B**) Mac3 in aortic wall of sham- and ePPE-operated mice 28 days after surgery. Aortic tissue was specifically stained for (**A**) GPIbα (anti- GPIbα, pink) or (**B**) Mac3 (anti- Mac3, pink). Nuclei were stained with DAPI (blue). IgG control, which is the same for both antibodies, was stained on one slide. Scale bar: 100 µm. DAPI = 4′,6-diamidino-2-phenylindole; ePPE = external porcine pancreatic elastase (application).

7.2 Reuse of figures from own publications

Wagenhäuser, M. U.*, Mulorz, J.*, Krott, K. J.*, **Bosbach, A.***, Feige, T., Rhee, Y. H., Chatterjee, M., Petzold, N., Böddeker, C., Ibing, W., Krüger, I., Popovic, A. M., Roseman, A., Spin, J. M., Tsao, P. S., Schelzig, H., & Elvers, M. (2024). Crosstalk of platelets with macrophages and fibroblasts aggravates inflammation, aortic wall stiffening, and osteopontin release in abdominal aortic aneurysm. *Cardiovascular research*, *120*(4), 417–432. https://doi.org/10.1093/cvr/cvad168

Permission: Order license ID link(s): 1565963-1

Feige, T.*, **Bosbach, A.***, Krott, K. J.*, Mulorz J., Chatterjee, M., Ortscheid, J., Krüger, E., Kürger, I., Salehzadeh, N., Goebel, S., Ibing, W., Grandoch, M., Münch, G., Wagenhäuser, M.U., Schelzig, H. & Elvers, M. (2024). GP VI-Mediated Platelet Activation and Procoagulant Activity Aggravate Inflammation and Aortic Wall Remodeling in Abdominal Aortic Aneurysm. *Arterioscler Thromb Vasc Biol*. https://doi.org/10.1161/ATVBAHA.123.320615

Permission: https://creativecommons.org/licenses/by-nc/4.0/

Some figures of this thesis are already published in the publications mentioned above. For each figure it is mentioned in the respective figure legend. Permission and license are received from CVR for the reuse of Figure 4 A, 5 A – G and S3 A – F, while ATVB has granted permission for the reuse of Figure 8 A – C.

7.3 Curriculum vitae

PERSONAL DETAILS

Name:	Agnes Bosbach, born Ehrenberg
Occupation:	PhD student
Date of birth:	29.08.1994, in Gladbeck
Nationality:	German
Place of residence:	[redacted]
Family status:	[redacted]

RESEARCH AND PROFESSIONAL EXPERIENCE

01/2020 – to date	PhD student in the group of Prof. Dr. Margitta Elvers at the Research Group Experimental Vascular Medicine, University Hospital of Duesseldorf, Germany
10/2017 – 06/2019	Master thesis, Institute of Anatomy, University Hospital Essen, Germany. Title of the master's thesis: ‘Charakterisierung neuer monoklonaler α-CEAxxx-Antikörper’. Prepared in the laboratory of PD Dr. Bernhard Singer.
10/2013 – 03/2017	Bachelor thesis, Institute of Virology, University Hospital Essen, Germany. Title of the bachelor's thesis: ‘Auswirkung von miR-502 und siRab1b auf die Replikation des Hepatitis-B-Virus’. Prepared in the laboratory of Prof. Dr. *rer. nat*. Mengji Lu.

EDUCATION

10/2017 – 06/2019	Studies in medical biology, University of Duisburg-Essen, Essen, Germany. Degree: Master of Science (M.Sc.)
10/2013 – 03/2017	Studies in medical biology, University of Duisburg-Essen, Essen, Germany. Degree: Bachelor of Science (B.Sc.)
08/2005 – 06/2013	A-level (Abitur), Heinrich-Heine-Gymnasium, Bottrop, Germany. Majors: english and mathematics

Duesseldorf, February 2025

7.4 List of publications

1. Chatterjee, M., **Ehrenberg, A.**, Toska, L. M., Metz, L. M., Klier, M., Krueger, I., Reusswig, F., & Elvers, M. (2020). Molecular Drivers of Platelet Activation: Unraveling Novel Targets for Anti-Thrombotic and Anti-Thrombo-Inflammatory Therapy. International journal of molecular sciences, 21(21), 7906. https://doi.org/10.3390/ijms21217906

2. Metz, L. M.*, Feige, T.*, de Biasi, L., **Ehrenberg, A.**, Mulorz, J., Toska, L. M., Reusswig, F., Quast, C., Gerdes, N., Kelm, M., Schelzig, H., & Elvers, M. (2023). Platelet pannexin-1 channels modulate neutrophil activation and migration but not the progression of abdominal aortic aneurysm. Frontiers in molecular biosciences, 10, 1111108. https://doi.org/10.3389/fmolb.2023.1111108

3. Wagenhäuser, M. U.*, Mulorz, J.*, Krott, K. J.*, **Bosbach, A.***, Feige, T., Rhee, Y. H., Chatterjee, M., Petzold, N., Böddeker, C., Ibing, W., Krüger, I., Popovic, A. M., Roseman, A., Spin, J. M., Tsao, P. S., Schelzig, H., & Elvers, M. (2024). Crosstalk of platelets with macrophages and fibroblasts aggravates inflammation, aortic wall stiffening, and osteopontin release in abdominal aortic aneurysm. *Cardiovascular research*, *120*(4), 417–432. https://doi.org/10.1093/cvr/cvad168

4. Feige, T.*, **Bosbach, A.***, Krott, K. J.*, Mulorz J., Chatterjee, M., Ortscheid, J., Krüger, E., Kürger, I., Salehzadeh, N., Goebel, S., Ibing, W., Grandoch, M., Münch, G., Wagenhäuser, M.U., Schelzig, H. & Elvers, M. (2024). GP VI-Mediated Platelet Activation and Procoagulant Activity Aggravate Inflammation and Aortic Wall Remodeling in Abdominal Aortic Aneurysm. *Arterioscler Thromb Vasc Biol.* https://doi.org/10.1161/ATVBAHA.123.320615

* The authors contributed equally to this work

7.5 International conferences

1. Poster presentation: *The role of GPVI-mediated platelet signalling in abdominal aortic aneurysm.* **66th Annual Meeting of the Society of Thrombosis and Haemostasis Research (GTH) 2022.** Virtual Congress.

2. Poster presentation: *The impact of platelets on inflammation and extracellular matrix remodelling in abdominal aortic aneurysm formation.* **Congress of the International Society on Thrombosis and Haemostasis (ISTH) 2023.** Montreal, Canada.

3. Oral presentation: *Analysis of the platelet activation profile in a novel experimental mouse model of AAA formation and progression.* **69th Annual Meeting of the Society of Thrombosis and Haemostasis Research (GTH) 2025.** Lausanne, Switzerland.

7.6 Danksagung

Zunächst möchte ich mich herzlich bei Prof. Dr. Elvers bedanken, dass sie mir die Gelegenheit gegeben hat, meine Doktorarbeit in ihrer Arbeitsgruppe für Experimentelle Vaskuläre Medizin in der Klinik für Vaskuläre und Endovaskuläre Chirurgie am Universitätsklinikum Düsseldorf anfertigen zu können.

Darüber hinaus möchte ich auch der ganzen Arbeitsgruppe für das angenehme Arbeitsklima, die unterhaltsamen gemeinsamen Mittagspausen und die wertvolle Unterstützung im Laboralltag danken. Ein ganz besonderer Dank geht dabei an Tobi und Kim - ich denke, dass wir uns in den letzten Jahren gemeinsam eine durchaus umfassende Expertise zum Thema AAA aufgebaut und zu einem unschlagbaren Team entwickelt haben. Ein ebenfalls ganz spezieller Dank geht auch an Martina, unseren Laborengel. Ohne dich wäre ich (und vermutlich auch jeder Andere in der Gruppe) in den letzten Jahren oft aufgeschmissen gewesen. Danke, Martina, dass du uns allen jederzeit mit Rat und Tat zur Seite stehst. :)

Neben meinen Arbeitskollegen möchte ich auch einigen Anderen ganz besonderen Personen meinen unendlichen Dank aussprechen. Zunächst meinen geliebten Eltern und Großeltern, die mich seit meiner Geburt in allen Lebensphasen begleitet, unterstützt und stets meinen Ehrgeiz gefordert und gefördert haben. Weiterhin natürlich meinen Geschwistern, die mich in meiner Entwicklung zu dem Menschen, der ich heute bin, maßgeblich geprägt haben. Auch wenn ihr nicht immer alles versteht, was ich tue – danke, dass ihr immer an meiner Seite steht. Ein riesiges Dankeschön und ganz viel Liebe an die beste Familie, die man sich wünschen kann.

Zum Schluss möchte ich meinem geliebten Ehemann und besten Freund meinen tiefsten Dank aussprechen. Danke, mein Schatz, dass du deine Familie zu meiner Familie gemacht hast und stets an meiner Seite bist. Seit meinem Bachelorstudium hast du meinen beruflichen Werdegang mitverfolgt und mich immer unterstützt – zunächst als bester Freund, dann als Partner und mittlerweile als Ehemann. Dabei ist unsere Liebe genauso gewachsen wie ich selber auch – aus der ehemals „kleinen“ Bachelorstudentin ist inzwischen fast eine Wissenschaftlerin mit Doktortitel geworden. Danke, dass du während all dieser Jahre zu mir gestanden hast.

Einfach Dankeschön! ♥

7.7 Affidavit

I declare in lieu of an oath, that the dissertation has been written by me independently and without unauthorised outside help, in compliance with the "Principles for Ensuring Good Scientific Practice at the Heinrich-Heine-University of Duesseldorf". Furthermore, I confirm, that this thesis has not yet been submitted as part of an-other examination process neither in identical nor in similar.

Duesseldorf, February 2025 _____

7.8 Eidesstaatliche Erklärung

Ich versichere an Eides Statt, dass die Dissertation von mir selbständig und ohne unzulässige fremde Hilfe unter Beachtung der „Grundsätze zur Sicherung guter wissenschaftlicher Praxis an der Heinrich-Heine-Universität Düsseldorf“ erstellt worden ist. Ich erkläre außerdem, dass die Dissertation weder in gleicher noch in ähnlicher Form bereits in einem anderen Prüfungsverfahren vorgelegen hat.

Düsseldorf, Februar 2025 _____